ISSN 2095-8137 CN 53-1229/Q
Volume 38 Issue 3
18 May 2017

ZR

Zoological Research

Creating animal models,
why not use the Chinese tree shrew?

Science Press
CODEN: DOYADI
www.zoores.ac.cn

ZOOLOGICAL RESEARCH

Volume 38, Issue 3 18 May 2017

CONTENTS

Cover image: Transgenic Chinese tree shrew with the enhanced green fluorescent protein. Photo by Xiao-Feng Ma **Cover design:** Lin Lei

Reconsidering the distribution of gray wolves

When attempting to understand where domestic plants and animals were domesticated, it is essential to consider the geographic distribution of the wild ancestor. Many domestic taxa now inhabit just about every continent thanks to their human-mediated dispersal which began soon after they were incorporated into the human niche. But just because sheep are now crucial to the economy of New Zealand and Wales, for example, does not mean that they were domesticated there. In fact, they could not have been since the wild ancestors of sheep were geographically restricted to a relatively small portion of Western Eurasia (Pedrosa et al., 2005).

Similarly, chickens, rabbits and camels are now found across the planet. Though wild populations of all three have also been moved by people and thrive in their new environments, it is only within the pre-historic natural ranges of the wild species that they could have been domesticated (Larson et al., 2014; Larson & Fuller, 2014; Wang et al., 2014).

The geographic origins of dogs have been contentious for several reasons, not the least of which is the widespread distribution of wolves across the Northern Hemisphere. The ability of wolves to colonise such a tremendous range from Portugal to Newfoundland means that, at least theoretically, dog domestication could have taken place anywhere (or more than once) across these longitudes.

Since 2002, multiple genetic studies of modern samples have suggested that dogs were domesticated in Southern East Asia (e.g., Wang et al., 2016a), though other studies have suggested alternative scenarios (e.g., Botigué et al., 2016; Frantz et al., 2016; Shannon et al., 2015). According to several canonical maps of wolf distribution, however, wolf populations never existed in this region. If true, then the conclusions based upon the genetic studies will have failed at the first hurdle since it would be impossible to domesticate a population that did not exist.

In order to establish the veracity of the commonly accepted maps, and to establish whether wolves were ever present in China, a new study conducted by Wang et al. (2016b) systematically searched for evidence for the presence of wolves. They began with a comprehensive literature search, but not content to rely on the testimony of others, they also visited three natural history museums and obtained 26 skins collected across China. Lastly, they identified 25 archaeological sites including wolf remains.

Taken in isolation, these individual lines of evidence could be questioned. The weight of all three together, however, suggests that at least historically, and most likely in pre-history as well, grey wolves maintained populations across China. An email exchange with the authors of the primary source that claimed wolves were absent from most of China revealed that the southern borders of the wolf distribution map were a great deal more equivocal than the boundary led readers to believe.

This result demonstrates the pitfalls of taking species distribution maps at face value. In this case, the line demarking the southern boundary of the grey wolf distribution has enormous ramifications. If wolves were present in central and southern China as recently as the second half of the 20th century, they were likely present in the preceding millennia and thus, they could have been the source of a domestication process in East Asia. This is not to say that dogs were definitively domesticated in China, but this result does at least remove a major hurdle that had been undermining that contention.

More generally, Wang et al. (2016b) demonstrates the power of a comprehensive due diligence to clarify what had been a long-standing, though ultimately insubstantial claim. In addition, this approach is key for ground-truthing and illuminating western scientists about the literature and records that have historically been difficult to penetrate. A great deal more information is sitting just under the surface and with collaborations between Eastern and Western scientist, the entire scientific community will benefit enormously, and answers to long-standing questions will be forthcoming.

Greger Larson*

Palaeogenomics & Bio-Archaeology Research Network, Research Laboratory for Archaeology and History of Art, University of Oxford, UK

*Corresponding author, E-mail: greger.larson@arch.ox.ac.uk

REFERENCES

Botigué LR, Song SY, Scheu A, Gopalan S, Pendleton AL, Oetjens M, Taravella AM, Seregély T, Zeeb-Lanz A, Arbogast RM, Bobo D, Daly K, Unterländer M, Burger J, Kidd JM, Veeramah KR. 2016. Ancient European dog genomes reveal continuity since the Early Neolithic. *bioRxiv*, doi: 10.1101/068189.

Frantz LA, Mullin VE, Pionnier-Capitan M, Lebrasseur O, Ollivier M, Perri A,

Received: 28 April 2017; Accepted: 04 May 2017
DOI: 10.24272/j.issn.2095-8137.2017.021

Linderholm A, Mattiangeli V, Teasdale MD, Dimopoulos EA, Tresset A, Duffraisse M, McCormick F, Bartosiewicz L, Gál E, Nyerges ÉA, Sablin MV, Bréhard S, Mashkour M, Bălăşescu A Gillet B, Hughes S, Chassaing O, Hitte C, Vigne JD, Dobney K, Hänni C, Bradley DG, Larson G. 2016. Genomic and archaeological evidence suggest a dual origin of domestic dogs. *Science,* **352**(6290): 1228-1231.

Larson G, Piperno DR, Allaby RG, Purugganan MD, Andersson L, Arroyo-Kalin M, Barton L, Vigueira CC, Denham T, Dobney K, Doust AN, Gepts P, Gilbert MT, Gremillion KJ, Lucas L, Lukens L, Marshall FB, Olsen KM, Pires JC, Richerson PJ, de Casas RR, Sanjur OI, Thomas MG, Fuller DQ. 2014. Current perspectives and the future of domestication studies. *Proceedings of the National Academy of Sciences of the United States of America*, **111**(17): 6139-6146.

Larson G, Fuller DQ. 2014. The evolution of animal domestication. *Annual Review of Ecology, Evolution, and Systematics*, **45**: 115-136.

Pedrosa S, Uzun M, Arranz JJ, Gutiérrez-Gil B, San Primitivo F, Bayón Y. 2005. Evidence of three maternal lineages in near eastern sheep supporting multiple domestication events. *Proceedings of the Royal Society B: Biological Sciences*, **272**(1577): 2211-2217.

Shannon LM, Boyko RH, Castelhano M, Corey E, Hayward JJ, McLean C, White ME, Abi Said M, Anita BA, Bondjengo NI, Calero J, Galov A, Hedimbi M, Imam B, Khalap R, Lally D, Masta A, Oliveira KC, Pérez L, Randall J, Tam NM, Trujillo-Cornejo FJ, Valeriano C, Sutter NB, Todhunter RJ, Bustamante CD, Boyko AR. 2015. Genetic structure in village dogs reveals a Central Asian domestication origin. *Proceedings of the National Academy of Sciences of the United States of America,* **112**(44): 13639-13644.

Wang GD, Xie HB, Peng MS, Irwin D, Zhang YP. 2014. Domestication genomics: evidence from animals. *Annual Review of Animal Biosciences,* **2**: 65-84.

Wang GD, Zhai WW, Yang HC, Wang L, Zhong L, Liu YH, Fan RX, Yin TT, Zhu CL, Poyarkov AD, Irwin DM, Hytönen MK, Lohi H, Wu CI, Savolainen P, Zhang YP. 2016a. Out of southern East Asia: the natural history of domestic dogs across the world. *Cell Research,* **26**(1): 21-33.

Wang L, Ma YP, Zhou QJ, Savolainen P, Wang GD. 2016b. The geographical distribution of grey wolves (*Canis Lupus*) in China: a systematic review. *Zoological Research,* **37**(6): 315-326.

Genes for the high life: New genetic variants point to positive selection for high altitude hypoxia in Tibetans

People living on the high plateaus of the world have long fascinated biological anthropologists and geneticists because they live in “thin air” and epitomize an extreme of human biological adaptation. Far from posing obstacles to human habitation, the hypoxic conditions of the Tibetan Plateau, the Andean highlands, and the Amhara Plateau of Ethiopia have served as the contexts for natural experiments in human adaptability (Beall, 2014). To the studies of the high-altitude human phenotype of the latter half of the twentieth century have been added studies of the complementary high-altitude genotype in the first decades of the twenty first century. Studies of genetic adaptation in Tibetans have commanded great interest because humans there live at altitudes around 4 000 m above sea level, breathe air that has an oxygen concentration about 40% lower and experience ultraviolet radiation about 30% higher than at sea level. An extreme habitat indeed.

Among the most dramatic adaptations to hypobaric hypoxia seen in high-altitude-dwelling Tibetans are the higher levels of the vasodilator, nitric oxide, in their exhaled breath and blood. Regulation of the pulmonary vascular response to hypoxia has been recognized as a key feature of the high altitude adaptation of Tibetans, but until recently little was known of the genetic basis of this phenomenon. Two recent papers in this journal from the laboratory of Bing Su, by Guo et al. (2017) and Zheng et al. (2017), now shed light on this. These papers reveal that the *GCH1* (GTP-cyclohydrolase I) gene and the *EP300* (histone acetyltransferase p300) gene, which are both involved in maintaining nitric oxide synthetase (NOS) function and normal blood pressure, harbor potentially adaptive variants in Tibetans. Both genes show high allelic divergence between Tibetan and lowland-dwelling Han Chinese, with signals of positive selection in the Tibetans.

These discoveries add to the extensive catalogue of evidence indicating that the Tibetan genome has undergone natural selection at multiple loci concerned with distinct aspects of blood-related phenotypes, including regulation of hemoglobin phenotype (Beall, 2014) and folate metabolism (Yang et al., 2017). Humans have been traversing the Tibetan Plateau for more than 30 000 years and have been permanent residents there for at least 6 000 years (Qiu, 2015). The true evolutionary significance of the unique genetic variants carried by Tibetans still remains to be established through “ground truthing” of human survival and reproduction (Beall, 2014), but this new genetic information provides further important and suggestive evidence that natural selection along with culture shaped humanity’s adaptations to some of the planet’s most extreme environments.

Nina G. Jablonski*

The Pennsylvania State University, University Park, PA 16902, USA

*Corresponding author, E-mail: ngj2@psu.edu

REFERENCES

Beall CM. 2014. Adaptation to high altitude: Phenotypes and genotypes. *Annual Review of Anthropology,* **43**(1): 251-272.

Guo YB, He YX, Cui CY, Ouzhuluobu, Baimakangzhuo, Duojizhuoma, Dejiquzong, Bianba, Peng Y, Bai CJ, Gonggalanzi, Pan YY, Qula, Kangmin, Cirenyangji, Baimayangji, Guo W, Yangla, Zhang H, Zhang XM, Zheng WS, Xu SH, Chen H, Zhao SG, Cai Y, Liu SM, Wu TY, Qi XB, Su B. 2017. *GCH1* plays a role in the high-altitude adaptation of Tibetans. *Zoological Research*, **38**(3): 155-162.

Qiu J. 2015. Who are the Tibetans? *Science,* **347**(6223): 708-711.

Yang J, Jin ZB, Chen J, Huang XF, Li XM, Liang YB, Mao JY, Chen X, Zheng ZL, Bakshi A, Zheng DD, Zheng MQ, Wray NR, Visscher PM, Lu F, Qu J. 2017. Genetic signatures of high-altitude adaptation in Tibetans. *Proceedings of the National Academy of Sciences of the United States of America,* **114**(16): 4189-4194.

Zheng WS, He YX, Cui CY, Ouzhuluobu, Dejiquzong, Peng Y, Bai CJ, Duojizhuoma, Gonggalanzi, Bianba, Baimakangzhuo, Pan YY, Qula, Kangmin, Cirenyangji, Baimayangji, Guo W, Yangla, Zhang H, Zhang XM, Guo YB, Xu SH, Chen H, Zhao SG, Cai Y, Liu SM, Wu TY, Qi XB, Su B. 2017. *EP300* contributes to high-altitude adaptation in Tibetans by regulating nitric oxide production. *Zoological Research*, **38**(3): 163-170.

Received: 10 May 2017; Accepted: 11 May 2017

DOI: 10.24272/j.issn.2095-8137.2017.031

Creating animal models, why not use the Chinese tree shrew (*Tupaia belangeri chinensis*)?

Yong-Gang Yao[1,2,*]

[1] *Key Laboratory of Animal Models and Human Disease Mechanisms*, *Kunming Institute of Zoology*, *Chinese Academy of Sciences*, *Kunming Yunnan* 650223, *China*

[2] *Kunming Primate Research Center of the Chinese Academy of Sciences*, *Kunming Institute of Zoology*, *Chinese Academy of Sciences*, *Kunming Yunnan* 650223, *China*

ABSTRACT

The Chinese tree shrew (*Tupaia belangeri chinensis*), a squirrel-like and rat-sized mammal, has a wide distribution in Southeast Asia, South and Southwest China and has many unique characteristics that make it suitable for use as an experimental animal. There have been many studies using the tree shrew (*Tupaia belangeri*) aimed at increasing our understanding of fundamental biological mechanisms and for the modeling of human diseases and therapeutic responses. The recent release of a publicly available annotated genome sequence of the Chinese tree shrew and its genome database (www.treeshrewdb.org) has offered a solid base from which it is possible to elucidate the basic biological properties and create animal models using this species. The extensive characterization of key factors and signaling pathways in the immune and nervous systems has shown that tree shrews possess both conserved and unique features relative to primates. Hitherto, the tree shrew has been successfully used to create animal models for myopia, depression, breast cancer, alcohol-induced or non-alcoholic fatty liver diseases, herpes simplex virus type 1 (HSV-1) and hepatitis C virus (HCV) infections, to name a few. The recent successful genetic manipulation of the tree shrew has opened a new avenue for the wider usage of this animal in biomedical research. In this opinion paper, I attempt to summarize the recent research advances that have used the Chinese tree shrew, with a focus on the new knowledge obtained by using the biological properties identified using the tree shrew genome, a proposal for the genome-based approach for creating animal models, and the genetic manipulation of the tree shrew. With more studies using this species and the application of cutting-edge gene editing techniques, the tree shrew will continue to be under the spot light as a viable animal model for investigating the basis of many different human diseases.

Keywords: Chinese tree shrew; Genome biology; Animal model; Gene editing; Innate immunity

INTRODUCTION

As human beings, our knowledge about ourselves, especially about how our brain works, how a disease develops, and the discovery of many efficient therapeutic agents, has largely come from studies using animals. The higher the similarity between an animal species and the human, the more we can obtain helpful and precise information concerning the fundamental biology, disease mechanism, and safety, efficiency and predictability of therapeutic agents (Franco, 2013; McGonigle & Ruggeri, 2014). Because of ethical concerns and restrictions, chimpanzees and large primates have been forbidden from being used in the creation of most animal models and in many types of drug tests, albeit they remain the best animals for studying human physiology (Bennett & Panicker, 2016; Knight, 2008). Monkeys have played a critical role in medical research (Zhang et al., 2014), but their costs are relatively high. Rodents are more commonly used in biomedical research, however, the results are sometimes difficult to extrapolate due to species disparity, methodological flaws and other reasons (van der Worp et al., 2010). The search for a suitable animal that is close to the human, but with a modest cost-efficiency, for use as a model for the study of disease is a long pursued task. On the other hand, each species has its own unique features, and we need to understand more about the particular species before we can attempt to use it in biomedical research.

Received: 08 Feburary 2017; Accepted: 10 April 2017

Foundation items: This study was supported by the grant of the National Natural Science Foundation of China (NSFC U1402224) and the Chinese Academy of Sciences (CAS zsys-02)

*Corresponding author, E-mail: yaoyg@mail.kiz.ac.cn

DOI: 10.24272/j.issn.2095-8137.2017.032

The tree shrew (*Tupaia belangeri*) is a squirrel-like and rat-sized mammal that is widely distributed in Southeast Asia, South and Southwest China. It has a small body size (100-150 g), a low-cost of maintenance, a short reproductive cycle (~ 6 weeks) and life span (6-8 years), a high brain-to-body mass ratio, and a close relationship to primates (Peng et al., 1991; Zheng et al., 2014). In the past few decades, the tree shrew has been used in biomedical research to increase our understanding of the fundamental biological and pathological mechanisms of life and disease (Amako et al., 2010; Cao et al., 2003; Fitzpatrick, 1996; Fuchs, 2005; Muly & Fitzpatrick, 1992; Peng et al., 1991; Su et al., 1987; Xu et al., 2013b; Yan et al., 1996; Zhao et al., 2002; Zheng et al., 2014). There is a proposal for using the tree shrew to replace primates in biomedical research (Cao et al., 2003; Peng et al., 1991), albeit there is still a long way to go.

THE CLOSE GENETIC RELATIONSHIP OF THE TREE SHREW TO PRIMATES

The phylogenetic relationship of the tree shrew in the Euarchontoglires has been debated for a long time and a clarification of the genetic relationship of the tree shrew to primates will provide a firm basis for using the tree shrew as an alternative to primates in biomedical research. Previous studies have reported different clustering patterns regarding the phylogenetic affinity of the tree shrew to primates, lagomorphs and rodents on the basis of various kinds of genetic data (Fan et al., 2013; Lin et al., 2014; O'Leary et al., 2013; Song et al., 2012; Xu et al., 2012, 2013a; Zhou et al., 2015). The recent comparative genome analysis of the Chinese tree shrew (*Tupaia belangeri chinensis*) and related vertebrate species (including primates) has provided sufficient evidence to resolve this question and has showed that the tree shrew has a much closer affinity to primates than that of rodents (Fan et al., 2013; Lin et al., 2014; Xu et al., 2013a). Note that a recent phylogenomic analysis of 1 912 exons from 22 representative mammals claimed that the position of tree shrews within the Euarchonta is unstable (Zhou et al., 2015). Leaving aside the technical problems and the usage of different datasets, the current taxonomical status of tree shrew in the Order Scandentia is well supported (Fan et al., 2013; Xu et al., 2013a).

COMMON AND UNIQUE GENETIC PROPERTIES OF THE TREE SHREW

Despite the closer affinity of the tree shrew to primates as compared to that of rodents to primates, the estimated divergence time between the tree shrew and primates has been estimated to be around 90.9 million years ago (Fan et al., 2013). This lengthy period of time has resulted in the evolution of a number of unique genetic features in the tree shrew, whilst many other genetic features have continued to be present in both the tree shrew and in primates.

Common genetic properties between the tree shrew and human

Our previous comparative genome analysis of the tree shrew and human identified 28 genes previously considered to be primate-specific in the tree shrew genome, and there was a high sequence identity between the tree shrew and human for the majority of those genes/pathways involved in neuropsychiatric disorders and infectious diseases (Fan et al., 2013). For instance, we found all the human neurotransmitter transporters in the tree shrew genome, and these gene sequences were highly conserved between the tree shrew and human (Fan et al., 2013). Neuropeptidomics of the brain tissue of tree shrews showed that the identified neuropeptides have a significantly higher degree of homology to the equivalent sequences in humans than those in rodents (Petruzziello et al., 2012). This genetic pattern was compatible with the usage of the tree shrew as an experimental model for studying psychosocial stress and antidepressant drug effect (Fuchs, 2005; Pryce & Fuchs, 2017). The genes in the Aβ production and neurofibrillary tangles formation pathways, which produce the two hallmarks of Alzheimer's disease (AD), also had a generally higher sequence identity with human (unpublished data). In particular, the Aβ42 peptide sequence of tree shrew was the same as that of human, whereas mouse and rat all differed from human by three residues (Pawlik et al., 1999). The gene expression pattern of the AD-related genes in the Chinese tree shrew also resembled that of rhesus monkey (*Macaca mulatta*) and human, but differed remarkably from that of mouse (unpublished data). These observations have suggested that the tree shrew has the genetic basis for being used to create an AD model, and could also explain previous observations for an early stage of amyloid accumulation in the brains of aged tree shrews (Yamashita et al., 2010, 2012). The majority of the autism-related genes also shared a high level of sequence identity (with less than 5% of variance compared to human) between the tree shrew and human (Fan & Yao, 2014). An analysis for common candidate drug targets, such as kinases, G-protein-coupled receptors, ion channel proteins, nuclear receptors, immune-related proteins, neuropeptides, proteases and inhibitors, in the Chinese tree shrew showed that half of the predicted drug targets had a higher sequence similarity to human targets than found in the mouse (Zhao et al., 2014). Also, proteomic characterization of tree shrew liver and muscle tissues demonstrated that nearly half of the identified proteins were highly similar to those of humans, whereas only 25% of them were highly similar to rats or mice, suggesting that the tree shrew is closer to the human than to the mouse and rat (Li et al., 2012). All these pieces of evidence of a high level of similarity in gene sequences, pathway components and proteomic characteristics between the tree shrew and the human have laid the foundation for an essential genetic basis to use the tree shrew in the creation of a viable animal model to study these related diseases.

Unique genetic differences between the tree shrew and human

The unique genetic features of the tree shrew provide a good opportunity for us to understand the specific physiobiology of the tree shrew and to explore the biological implications of adaptation and evolution. For instance, among the 209 known visually related human genes, the tree shrew only lacked the

OPN1MW (opsin 1 (cone pigments), medium-wave-sensitive) and *OPN1NW2* (opsin 1 (cone pigments), medium-wave-sensitive 2) genes. The lack of these two cone photoreceptor genes, as well as other unique features in the rod photoreceptor rhodopsin (Fan et al., 2013), are compatible with the diurnal pattern of behavior and dichromacy of the tree shrew (Hunt et al., 1998). The evolutionary comparison of 407 locomotion system related genes in human, monkey, tree shrew, dog, rat and mouse showed that 29 genes had undergone positive selection, including *HOXA6* (homeobox A6) and *AVP* (arginine vasopressin) that affected skeletal morphogenesis or muscle contraction (Fan et al., 2014b). This observation is compatible with the tree shrew's ability to move fast and jump strongly (Fan et al., 2014b).

The absence of certain genes (relative to human) from the tree shrew genome provides a model to understand specific pathways that were mediated by these lost genes. In the previous analysis, we have provided a list of 11 examples of (potential) gene loss and 144 pseudo-genes in the tree shrew genome (Fan et al., 2013); and these are now undergoing further validation and characterization studies. Among these genes, loss of the important antiviral gene *RIG-I* (retinoic acid-inducible gene I, also known as DDX58) in the Chinese tree shrew lineage has provided us a rare opportunity to understand the evolutionary adaptation and functional diversity of antiviral activity in vertebrates. Moreover, this might be one of the principal genetic reasons for the tree shrew's suitability as an animal model for studying viral infections. Previous intensive studies of innate immunity showed that after viral challenge, the pattern recognition receptors (PRRs) had a rapid response, leading to the subsequent production of antiviral cytokines such as type-I interferons (IFNs), inflammatory factors and complements (Takeuchi & Akira, 2010). These cytosolic PRRs, including Toll-like receptors (TLRs), NOD-like receptors (NLRs), RIG-I-like receptors (RLRs) and cytosolic DNA receptors, are actively involved in the host innate immunity response against invasion by pathogens (Barbalat et al., 2011). The RLRs contains three members, RIG-I, MDA5 (melanoma differentiation factor 5, also known as IFIH1), and LGP2 (laboratory of genetics and physiology 2, also known as DHX58), which are found in the cytosol of most types of mammalian cells and act as PRRs to response to viral RNA (Barbalat et al., 2011; Takeuchi & Akira, 2010). The loss of RIG-I in the Chinese tree shrew has raised several interesting questions concerning the unique genetic features of the innate immune response in this animal and the evolution of innate immunity in mammals: why can the *RIG-I* gene be lost in this animal? Is there a functional replacement for this key factor in the tree shrew immune system? What are the biological implications concerning this evolutionary event of the antiviral innate immunity in mammals? An understanding of the biological effects of the loss of RIG-I in the Chinese tree shrew will undoubtedly offer insights into the origin and development of the innate immunity in mammals. Recently, we attempted to answer these questions and deciphered the mechanisms underlying the loss of *RIG-I* in the Chinese tree shrew (Xu et al., 2016). We first confirmed the absence of *RIG-I* in the tree shrew lineage by analyzing a group of tree shrews collected from different regions and by comparing them to the Malayan flying lemur (which had a close relationship to the tree shrew). Further viral infection tests showed that the loss of this gene did not impair *IFNB1* induction in the tree shrew primary renal cells in response to a variety of RNA viruses, indicating that there is a functional substitute or a compensation of the response network for the loss of RIG-I in sensing viral RNAs in the tree shrew. Alongside the loss of *RIG-I*, both *MDA5* (*tMDA5*) and *LGP2* (*tLGP2*) had undergone strong positive selection in the tree shrew. Moreover, tMDA5 or tMDA5/tLGP2 could sense Sendai virus (a RNA virus used as a RIG-I agonist) by inducing IFN, though conventional RIG-I and MDA5 were thought to recognize distinct RNA structures and viruses. tMDA5 also acquired an ability to interact with adaptor tMITA (STING/TMEM173/ERIS), which was reported to bind only with RIG-I. Further functional analysis showed that the positively selected sites (PSSs) in tMDA5 endowed the substitute function for the lost RIG-I (Xu et al., 2016). The evolutionary interpretation of the potential function of the PSSs in the tree shrew was further supported by a gain-of-function analysis, in which we introduced the positively selected variants at the equivalent positions in human MDA5. These artificially made human MDA5 mutants showed an enhanced antiviral function (Xu et al., 2016). As a consequence of working on the evolutionary event of *RIG-I* loss in the tree shrew, we were able to uncover a previously unknown evolutionary signal in response to RIG-I loss in the tree shrew (Xu et al., 2016). This special case provided insights into the functional conservation and divergence of RLRs in innate immunity (Figure 1).

To give another example of the genetic uniqueness of the tree shrew immune system, we recently characterized the evolution of the tTLRs in the Chinese tree shrew. We found that the tree shrew had 13 putative TLRs (including 12 orthologs of mammalian *TLR1-TLR9* and *TLR11-TLR13*, and a pseudogenized *TLR10*). Moreover, the tree shrew *TLR8* and *TLR9* genes had undergone positive selection, possibly due to the adaptation of the pathogen challenge (Yu et al., 2016). The expression of the TLRs varied in response to viral infection. The pseudogenization of *TLR10* in the tree shrew and the positive selection signal in the *TLR8* and *TLR9* genes deserve extensive analyses (Yu et al., 2016). In a similar way to the RLRs, further characterization of the tree shrew's unique pattern of TLRs will help us to understand more about this important innate immune pathway and the antiviral response in the context of creating animal models to investigate infections.

TREE SHREWS AS MODELS FOR STUDYING FUNDAMENTAL BIOLOGICAL FUNCTIONS AND DISEASE MECHANISMS

For decades, there have been many efforts to promote the tree shrew as an experimental animal and for it to replace primates in the study of fundamental biological functions and human diseases (Amako et al., 2010; Cao et al., 2003; Fang et al., 2016; Fitzpatrick, 1996; Fuchs, 2005; Khani & Rainer, 2012; Lee et al., 2016; MacEvoy et al., 2009; Nair et al., 2014; Peng et al., 1991; Pryce & Fuchs, 2017; Su et al., 1987; Veit et al.,

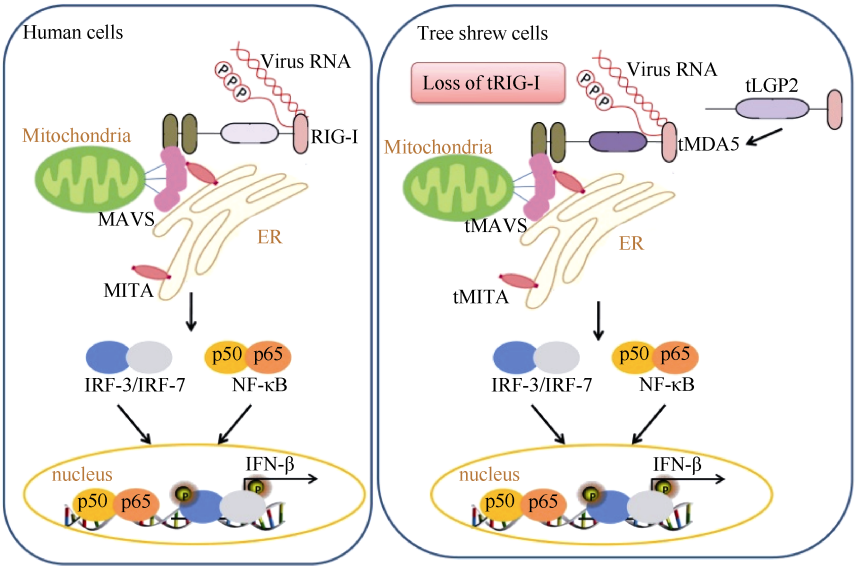

Figure 1 Schematic profile of the antiviral response in the Chinese tree shrew (right) and human (left)

In human cells, RLRs detect viral RNAs in the cytoplasm and activate downstream signaling. Among the three RLR family members, RIG-I mainly recognizes viral RNA containing a 5' triphosphate (5' ppp) through MAVS (also known as IPS-1/VISA/Cardiff), which leads to the activation of the IRF3/IRF7 and NF-κB signaling pathways. The activated transcription factors are subsequently translocated to the nucleus and coordinate the cytokine expression including IFNs to restrict viral propagation. In the Chinese tree shrew, RIG-I is absent in the genome. The loss of RIG-I had an evolutionary consequence, and tree shrew MDA5 (tMDA5) had a functional replacement in the antiviral pathway. tMDA5, together with tLGP2, can sense viral RNA. Meanwhile, tMDA5 interacts with tMITA (STING/TMEM173/ERIS), which was reported to bind only with RIG-I (Xu et al., 2016).

2011, 2014; Xu et al., 2013b; Yan et al., 1996; Zhao et al., 2002; Zheng et al., 2014). Indeed, tree shrews have many characteristics that make it a good laboratory animal, such as small body size, low-cost of maintenance, short reproductive cycle and life span, and most importantly, its close relationship to primates (Fan et al., 2013; Zheng et al., 2014). Also, the ethical concerns of using the tree shrew in biomedical research are less controversial than engendered by the use of primates. Here I would like to highlight several areas where studies using the tree shrew have advanced our knowledge about fundamental biological functions and disease mechanisms, as a way of showing the developing importance of the tree shrew.

Study of tree shrew visual cortex (striate cortex)

Increasing our fundamental knowledge of brain function, including brain circuits and networks, neural mechanism and information processing underlying cognitive function, is one of the core goals of global brain initiatives (Grillner et al., 2016). The tree shrew has great potential for its use as a suitable animal for studying the function of the visual cortex, as previous studies have revealed a close homology between the tree shrew and the macaque (and human) in the area of visual cortex at both the neuroanatomical and the neurophysiological levels (Fitzpatrick, 1996; Muly & Fitzpatrick, 1992; Van Hooser et al., 2013; Veit et al., 2011, 2014). Thanks to the great efforts by Fitzpatrick and colleagues since 1990s, we now have a better understanding of the morphological basis and functional organization of local circuits and connections in the tree shrew visual cortex, and a better understanding of the response properties of neurons in this region (Fitzpatrick, 1996; Lee et al., 2016; Mooser et al., 2004; Muly & Fitzpatrick, 1992; Van Hooser et al., 2013). In particular, a study of the receptive fields of layer 2/3 neurons in the tree shrew visual cortex revealed the distinct arrangement of ON (light-responsive) and OFF (dark-responsive) pathways, with specific topographic constraints of each representation, to construct orderly columnar representations of stimulus orientation and visual space (Lee et al., 2016). These results derived from using tree shrew visual cortex will undoubtedly assist the fundamental research into brain function and disease.

Other interesting aspects from a comparative point of view are the superior memory-related capabilities of the tree shrew as compared to that of rodents, as has been seen for example in performance of novelty preference tasks (Khani & Rainer, 2012; Nair et al., 2014). The recent studies of the presence and distribution of neuropeptides in tree shrew brain and comparative analyses with other species (Ni et al., 2014, 2015; Petruzziello et al., 2012) has laid the biochemical basis for us to learn more about the specific and common features of tree shrew brain. It is very important to highlight all of these diverse and interesting aspects of the tree shrew, in order to promote the acceptance of this animal more widely in neurobehavioral studies.

Tree shrew disease models

There are two main kinds of tree shrew disease models at present, the induced model and the spontaneous model. For the induced tree shrew model of disease, surgical and/or

chemical approaches are used to induce the onset of disease symptoms in the context of similar phenotypes, similar pathological mechanism, and similar clinical efficacy (McGonigle & Ruggeri, 2014; Yao et al., 2015). Hitherto, the tree shrew has been reported to be used successfully as an animal model for a variety of diseases, such as breast cancer (Ge et al., 2016; Xia et al., 2014), alcohol-induced (Xing et al., 2015) or non-alcoholic fatty liver diseases (Zhang et al., 2015, 2016), hepatitis B virus (HBV) infection (Su et al., 1987; Walter et al., 1996; Yan et al., 1996), hepatitis C virus (HCV) infection (Amako et al., 2010; Xu et al., 2007; Zhao et al., 2002), and herpes simplex virus type 1 (HSV-1) infection (Darai et al., 1978; Li et al., 2016), to name a few, albeit some results need further studies to elucidate the underlying mechanism. In previous review papers, there are ample descriptions and literature surveys of the tree shrew disease models (Cao et al., 2003; Xu et al., 2013b). In a recent book entitled "*Basic Biology and Disease Models of Tree Shrews*", which is the second monograph about the tree shrew in this field, there are also many descriptions of tree shrew models of human diseases, including depression, drug addiction, bacterial infection, breast cancer, glioblastoma, and thrombosis. Some of these models were first described there (see Zheng et al. (2014)). To iterate every detail of each tree shrew model is beyond the scope and space of the current opinion paper, and there is indeed no need to do so. However, I would like to highlight the use of the tree shrew as a model for breast cancer to exemplify the benefits and differences of tree shrew models as compared to current rodent models.

The tree shrew has a similar mammary gland to that of the human based on the morphology and structure (Xia et al., 2014) and this has provided the basis for creating a model of breast cancer. The description of spontaneous breast cancer in the tree shrew dates back to the 1960s when it was reported by Elliot and coworkers (Elliot et al., 1966), that a breast cancer was found in a female tree shrew (*Tupaia glis*) belonging to a different species within the genus *Tupaia*. This animal was in a late stage of pregnancy and had a nodular lesion beneath the skin of the right thoracic breast near the nipple (Elliot et al., 1966). Subsequent studies showed that tree shrews are prone to spontaneous breast tumor, with a frequency of around 1% (Xia et al., 2012, 2014). The spontaneous breast cancer reported by Xia and coworkers (Xia et al., 2012) was an intraductal papilloma, in which epithelium cells grow papillarily with an intact basal membrane. This tumor was positive for progesterone receptor (PR), but negative for human epidermal growth factor receptor 2 (HER2, also named as erb-b2 receptor tyrosine kinase 2 (ERBB2)). It had a high frequency of Ki-67 positive staining and few cleaved caspase-3 positive staining cells, suggesting that the malignant cells are highly proliferative and less apoptotic. The further analysis of 18 spontaneous breast cancers (including the one described by (Xia et al., 2012)) showed that these tumors could be classified as intraductal papilloma (22.2%), papillary carcinoma (55.6%), and invasive ductal carcinoma (22.2%) with or without lung metastasis (Xia et al., 2014). Moreover, tree shrew breast cancerous tissue has frequently been shown to have mutations in the *PTEN/PIK3CA* genes, with a mutation spectrum resembling a subset of human breast cancers with the PTEN/PIK3CA mutations, whereas currently no mouse breast cancer model shows this type of cancer. The *PTEN/PIK3CA* genes mutation status was also correlated with the expression of pAKT in the tree shrew tumorous tissue (Xia et al., 2014).

Besides spontaneously developing breast cancer, the tree shrew could be induced to develop breast cancer by using carcinogen treatment (Xia et al., 2014) and lentivirus expressing the polyomavirus middle T antigen (PyMT) oncogene (Ge et al., 2016). Administration of 7,12-dimethylbenz(a)anthracene (DMBA) induced a breast tumor in around 12% of tree shrews, whereas co-administration of DMBA and medroxyprogesterone acetate had an even higher success rate for inducing tumor (up to 50%) (Xia et al., 2014). However, the shortcoming of this carcinogen-induced breast tumor was also apparent, with a relatively low frequency and a long latency (around 7 months), but this could be overcome by introducing the lentivirus expressing the PyMT oncogene into the mammary ducts (Ge et al., 2016). The latter lentivirus-mediated approach induced mammary tumors within seven weeks in all tree shrews, with the major tumor type being papillary carcinoma. Further analysis of the PyMT-induced mammary tumors showed elevated levels of phosphorylated AKT, ERK and STAT3 in 41%-68% of tumors. Moreover, growth of the mammary tumors was sensitive to Cisplatin and Epidoxorubicin treatment (Ge et al., 2016). All these efforts showed that tree shrews are capable of developing breast cancer by a variety of approaches, including the spontaneous approach, the surgically and chemically induced approach, and the surgically and lentivirus-mediated oncogene induced approach. The tree shrew breast cancer model best demonstrated a subset of human breast cancer with the PTEN/PIK3CA mutations (Xia et al., 2014). The tree shrew breast cancer model can now be used for the testing of drug efficacy and safety and for elucidating the pathogenesis of mammary tumors.

From the above example of tree shrew breast cancer, it is quite obvious that using the tree shrew could overcome some of the shortcomings of the available rodent models for certain diseases. Tree shrew models of human diseases have been shown to have many benefits, albeit some of the models need further improvement for repeatability, stability, and uniformity. Moreover, analysis of tree shrew disease models will also provide a novel molecular basis to study individual human diseases, such as the susceptibility to stress (Fang et al., 2016). However, it should be mentioned that so far, the present tree shrew models have not demonstrated a unique advantage in drug development or succeeded in leading to any significant scientific discovery. The only exception to this may possibly come from the identification of sodium taurocholate cotransporting polypeptide as a functional receptor for HBV and hepatitis D virus (HDV) infection (Yan et al., 2012), which was triggered by the observation that the tree shrew and its hepatocytes could be infected by HBV (Su et al., 1987; Walter et al., 1996; Yan et al., 1996). I expect that a genome-based approach may be more helpful for the design of tree shrew models of human diseases. Namely, based on the characterization of the tree

shrew's unique genetic features and common genes and pathways, instead of "trial and error", will be a more efficient method to create a new model of tree shrew and to predict the validity of the model. A convenient way to start is by looking at the genes and pathways of the tree shrew by searching the tree shrew genome database (www.treeshrewdb. org) (Fan et al., 2014a) to find items which have a close similarity to their human counterparts. But to overcome the complications of the heterogeneous genetic background of various captured wild tree shrews and to achieve a uniform response of each animal during the creation of animal models and drug tests, there is a pressing need to establish tree shrew inbred lines.

Genome editing of tree shrew

The recent advances in genetic manipulation techniques, in particular CRISPR/Cas9 technology (Cong et al., 2013; Hsu et al., 2014; Luo et al., 2016; Mei et al., 2016; Shao et al., 2016), have provided methods whereby it is possible to perform genome editing of any non-model animal and to make genetically modified animal models. Due to the lack of knowledge about the reproductive biology and assisted reproduction technologies in the tree shrew (Yan et al., 2016), gene editing methods using one-cell embryos or embryonic stem cells, which are commonly used in rodents (Wang et al., 2015) and primates (Guo & Li, 2015; Niu et al., 2014), have hitherto been unavailable for the tree shrew. This limitation has also hindered the wide acceptance of the tree shrew as an important laboratory animal. This disadvantage was luckily resolved by our recent success based on the isolation of tree shrew spermatogonial stem cells (SSCs) and the establishment of a culture system for these SSCs (Li et al., 2017). In this pioneer study, we solved the two key technical obstacles for establishing a line of SSC: identification of the necessary supplements for the culture medium and the isolation of suitable feeder cells for producing SSCs. In brief, we used the thymus cell antigen 1 (Thy1$^+$) to enrich tree shrew SSCs, followed by transcriptomic analysis to massively identify the activated signaling pathways during the differentiation of cultured SSCs. We then attempted to optimize the culture medium by supplying additional protein that plays a role in the activated signaling pathway, such as Wnt3a protein in the Wnt/β-catenin signaling pathway. This strategy was very successful in maintaining the survival of tree shrew primary SSCs. The other technical trick involves the use of tree shrew Sertoli cells, but not mouse embryonic fibroblasts, as feeder for the expansion and long-term culture of tree shrew SSCs. The expanded SSCs could then be transfected with the lentiviral vector containing the enhanced green fluorescent protein (EGFP), and the positive SSC clone was expanded and transplanted into the testes of sterilized adult male recipients, which were created by treating adult male tree shrews with Busulfan to eliminate the pre-existing germ cells. The expanded SSCs were capable of continuous spermatogenesis after transfection with EGFP-expressing virus and transplantation into recipient males, and EGFP-tagged sperms generated viable transgenic tree shrews (Figure 2) (Li et al., 2017). By way of example, we showed that these SSCs were suitable for the CRISPR/Cas9-mediated knockout of the *APP* (amyloid beta precursor protein) gene, with a reasonably high efficiency in single SSC cells (17/70=24.3%) (Li et al., 2017), although no living offspring have as yet been created at the time of publishing our paper. This is the first study of a successful genetic manipulation of tree shrew. We believe that more genetically modified tree shrews will be produced in the near future by using this SSC-based gene editing strategy. Currently, we are working on the creation of transgenic tree shrews with human APP and PSEN1 mutations that are causal for AD. We expect that the tree shrew AD model will be superior to the currently available rodent AD models.

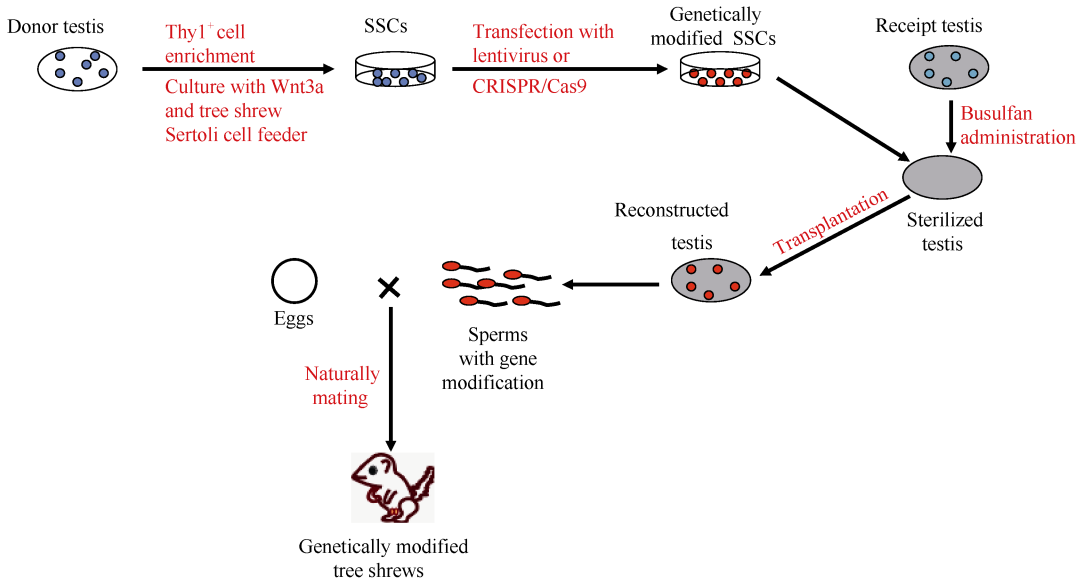

Figure 2 Schematic procedure for making a transgenic tree shrew by using the spermatogonial stem cells based on the study by Li et al. (2017)

FUTURE PERSPECTIVE FOR TREE SHREW USAGE IN BIOMEDICAL RESEARCH

Based on the above descriptions, it is no doubt of the tree shrew's superiority over rodents for studying certain human diseases and understanding the neural mechanism of brain function resulting from specific aspects of genetic makeup or lifestyle. In particular, the tree shrew has the top three benefits of our human/monkey research partnerships in biomedical research: safety, efficacy, and greater predictability. The more we know about tree shrew, the more success we can expect to have. The recent release of the tree shrew genome database (www.treeshrewdb.org) has provided for easy access to the tree shrew genome data (Fan et al., 2014a). We are currently re-sequencing more tree shrew individuals, in particular from inbred lines, with the intention of refining the quality of the tree shrew genome and improving our understanding of the genomic diversity of this animal. The re-sequencing data will be deposited into the tree shrew genome database. We have also collected and compiled the available transcriptomic data from the tree shrew, and will frequently update the information at the webserver. Following the genome-based approach to retrieve more information regarding the genetic makeup of tree shrew, especially for the nervous and immune systems, it would be easier and safer to make a valid design of a tree shrew model of human diseases and to uncover the underlying mechanisms.

With the successful gene manipulation of the tree shrew (Li et al., 2017) and by the use of cutting-edge techniques, e.g., two-photon imaging of GCaMP6 calcium signals for neurons in visual cortex (Lee et al., 2016), there is only one big obstacle remaining for a wider usage of tree shrew, that is, the establishment of inbred lines. At present we are attempting to create the tree shrew inbred lines at the Kunming Institute of Zoology (KIZ), Chinese Academy of Science (CAS), and we have successfully achieved F4 offspring by sibling mating although the population size is still very small. We have every reason to believe that the tree shrew, with a tag of "made in China" or "created in China", will become reality in the coming years.

ACKNOWLEDGEMENTS

I thank Ian Logan (22 Parkside Drive, Exmouth, Devon, UK), Wai-Yee Chan (The Chinese University of Hong Kong) and three anonymous reviewers for helpful comments on the early version of the manuscript. I thank Ping Zheng (KIZ, CAS) for helping with the preparation of Figure 2, Ling Xu and Dan-Dan Yu (KIZ, CAS) for making Figure 1. The opinions expressed in this paper represent my personal views. I would like to apologize to those colleagues whose work was not mentioned or elaborately represented in this opinion paper as I was not making a comprehensive literature survey for all tree shrew studies and/or because of my ignorance and negligence.

REFERENCES

Amako Y, Tsukiyama-Kohara K, Katsume A, Hirata Y, Sekiguchi S, Tobita Y, Hayashi Y, Hishima T, Funata N, Yonekawa H, Kohara M. 2010. Pathogenesis of hepatitis C virus infection in *Tupaia belangeri*. *Journal of Virology,* **84**(1): 303-311.

Barbalat R, Ewald SE, Mouchess ML, Barton GM. 2011. Nucleic acid recognition by the innate immune system. *Annual Review of Immunology,* **29**(1): 185-214.

Bennett AJ, Panicker S. 2016. Broader impacts: international implications and integrative ethical consideration of policy decisions about US chimpanzee research. *American Journal of Primatology,* **78**(12): 1282-1303.

Cao J, Yang EB, Su JJ, Li Y, Chow P. 2003. The tree shrews: adjuncts and alternatives to primates as models for biomedical research. *Journal of Medical Primatology,* **32**(3): 123-130.

Cong L, Ran FA, Cox D, Lin SL, Barretto R, Habib N, Hsu PD, Wu XB, Jiang WY, Marraffini LA, Zhang F. 2013. Multiplex genome engineering using CRISPR/Cas systems. *Science,* **339**(6121): 819-823.

Darai G, Schwaier A, Komitowski D, Munk K. 1978. Experimental infection of *Tupaia belangeri* (tree shrews) with herpes simplex virus types 1 and 2. *Journal of Infectious Diseases,* **137**(3): 221-226.

Elliot OS, Elliot MW, Lisco H. 1966. Breast cancer in a tree shrew (*Tupaia glis*). *Nature,* **211**(5053): 1105.

Fan Y, Huang ZY, Cao CC, Chen CS, Chen YX, Fan DD, He J, Hou HL, Hu L, Hu XT, Jiang XT, Lai R, Lang YS, Liang B, Liao SG, Mu D, Ma YY, Niu YY, Sun XQ, Xia JQ, Xiao J, Xiong ZQ, Xu L, Yang L, Zhang Y, Zhao W, Zhao XD, Zheng YT, Zhou JM, Zhu YB, Zhang GJ, Wang J, Yao YG. 2013. Genome of the Chinese tree shrew. *Nature Communications,* **4**: 1426.

Fan Y, Yao YG. 2014. Chapter 3. Characteristics of the genome of the Chinese tree shrew. *In*: Zheng YT, Yao YG, Xu L. Basic Biology and Disease Models of Tree Shrews. Kunming: Yunnan Science and Technology Press, 32-75. (in Chinese)

Fan Y, Yu D, Yao YG. 2014a. Tree shrew database (TreeshrewDB): a genomic knowledge base for the Chinese tree shrew. *Scientific Reports,* **4**: 7145.

Fan Y, Yu DD, Yao YG. 2014b. Positively selected genes of the Chinese tree shrew (*Tupaia belangeri chinensis*) locomotion system. *Zoological Research,* **35**(3): 240-248.

Fang H, Sun YJ, Lv YH, Ni RJ, Shu YM, Feng XY, Wang Y, Shan QH, Zu YN, Zhou JN. 2016. High activity of the stress promoter contributes to susceptibility to stress in the tree shrew. *Scientific Reports,* **6**: 24905.

Fitzpatrick D. 1996. The functional organization of local circuits in visual cortex: insights from the study of tree shrew striate cortex. *Cerebral Cortex,* **6**(3): 329-341.

Franco NH. 2013. Animal experiments in biomedical research: a historical perspective. *Animals,* **3**(1): 238-273.

Fuchs E. 2005. Social stress in tree shrews as an animal model of depression: an example of a behavioral model of a CNS disorder. *CNS Spectrums,* **10**(3): 182-190.

Ge GZ, Xia HJ, He BL, Zhang HL, Liu WJ, Shao M, Wang CY, Xiao J, Ge F, Li FB, Li Y, Chen CS. 2016. Generation and characterization of a breast carcinoma model by PyMT overexpression in mammary epithelial cells of tree shrew, an animal close to primates in evolution. *International Journal of Cancer,* **138**(3): 642-651.

Grillner S, Ip N, Koch C, Koroshetz W, Okano H, Polachek M, Poo MM, Sejnowski TJ. 2016. Worldwide initiatives to advance brain research. *Nature Neuroscience,* **19**(9): 1118-1122.

Guo XY, Li XJ. 2015. Targeted genome editing in primate embryos. *Cell Research,* **25**(7): 767-768.

Hsu PD, Lander ES, Zhang F. 2014. Development and applications of CRISPR-Cas9 for genome engineering. *Cell,* **157**(6): 1262-1278.

Hunt DM, Dulai KS, Cowing JA, Julliot C, Mollon JD, Bowmaker JK, Li WH, Hewett-Emmett D. 1998. Molecular evolution of trichromacy in primates. *Vision Research,* **38**(21): 3299-3306.

Khani A, Rainer G. 2012. Recognition memory in tree shrew (*Tupaia belangeri*) after repeated familiarization sessions. *Behavioural Processes,* **90**(3): 364-371.

Knight A. 2008. The beginning of the end for chimpanzee experiments? *Philosophy, Ethics, and Humanities in Medicine,* **3**: 16.

Lee KS, Huang XY, Fitzpatrick D. 2016. Topology of ON and OFF inputs in visual cortex enables an invariant columnar architecture. *Nature,* **533**(7601): 90-94.

Li CH, Yan LZ, Ban WZ, Tu Q, Wu Y, Wang L, Bi R, Ji S, Ma YH, Nie WH, Lv LB, Yao YG, Zhao XD, Zheng P. 2017. Long-term propagation of tree shrew spermatogonial stem cells in culture and successful generation of transgenic offspring. *Cell Research,* **27**(2): 241-252.

Li LH, Li ZR, Wang EL, Yang R, Xiao Y, Han HB, Lang FC, Li X, Xia YJ, Gao F, Li QH, Fraser NW, Zhou JM. 2016. Herpes simplex virus 1 infection of tree shrews differs from that of mice in the severity of acute infection and viral transcription in the peripheral nervous system. *Journal of Virology,* **90**(2): 790-804.

Li RX, Xu W, Wang Z, Liang B, Wu JR, Zeng R. 2012. Proteomic characteristics of the liver and skeletal muscle in the Chinese tree shrew (*Tupaia belangeri chinensis*). *Protein & Cell,* **3**(9): 691-700.

Lin JN, Chen GF, Gu L, Shen YF, Zheng MZ, Zheng WS, Hu XJ, Zhang XB, Qiu Y, Liu XQ, Jiang CZ. 2014. Phylogenetic affinity of tree shrews to Glires is attributed to fast evolution rate. *Molecular Phylogenetics and Evolution,* **71**: 193-200.

Luo X, Li M, Su B. 2016. Application of the genome editing tool CRISPR/Cas9 in non-human primates. *Zoological Research,* **37**(4): 214-219.

MacEvoy SP, Tucker TR, Fitzpatrick D. 2009. A precise form of divisive suppression supports population coding in the primary visual cortex. *Nature Neuroscience,* **12**(5): 637-645.

McGonigle P, Ruggeri B. 2014. Animal models of human disease: challenges in enabling translation. *Biochemical Pharmacology,* **87**(1): 162-171.

Mei Y, Wang Y, Chen HQ, Sun ZS, Ju XD. 2016. Recent progress in CRISPR/Cas9 technology. *Journal of Genetics and Genomics,* **43**(2): 63-75.

Mooser F, Bosking WH, Fitzpatrick D. 2004. A morphological basis for orientation tuning in primary visual cortex. *Nature Neuroscience,* **7**(8): 872-879.

Muly EC, Fitzpatrick D. 1992. The morphological basis for binocular and ON/OFF convergence in tree shrew striate cortex. *Journal of Neuroscience,* **12**(4): 1319-1334.

Nair J, Topka M, Khani A, Isenschmid M, Rainer G. 2014. Tree shrews (*Tupaia belangeri*) exhibit novelty preference in the novel location memory task with 24-h retention periods. *Frontiers in Psychology,* **5**: 303.

Ni RJ, Shu YM, Wang J, Yin JC, Xu L, Zhou JN. 2014. Distribution of vasopressin, oxytocin and vasoactive intestinal polypeptide in the hypothalamus and extrahypothalamic regions of tree shrews. *Neuroscience,* **265**: 124-136.

Ni RJ, Shu YM, Luo PH, Fang H, Wang Y, Yao L, Zhou JN. 2015. Immunohistochemical mapping of neuropeptide Y in the tree shrew brain. *Journal of Comparative Neurology,* **523**(3): 495-529.

Niu YY, Shen B, Cui YQ, Chen YC, Wang JY, Wang L, Kang Y, Zhao XY, Si W, Li W, Xiang AP, Zhou JK, Guo XJ, Bi Y, Si CY, Hu B, Dong GY, Wang H, Zhou ZM, Li TQ, Tan T, Pu XQ, Wang F, Ji SH, Zhou Q, Huang XX, Ji WZ, Sha JH. 2014. Generation of gene-modified cynomolgus monkey via Cas9/RNA-mediated gene targeting in one-cell embryos. *Cell,* **156**(4): 836-843.

O'Leary MA, Bloch JI, Flynn JJ, Gaudin TJ, Giallombardo A, Giannini NP, Goldberg SL, Kraatz BP, Luo ZX, Meng J, Ni X, Novacek MJ, Perini FA, Randall ZS, Rougier GW, Sargis EJ, Silcox MT, Simmons NB, Spaulding M, Velazco PM, Weksler M, Wible JR, Cirranello AL. 2013. The placental mammal ancestor and the post-K-Pg radiation of placentals. *Science,* **339**(6120): 662-667.

Pawlik M, Fuchs E, Walker LC, Levy E. 1999. Primate-like amyloid-β sequence but no cerebral amyloidosis in aged tree shrews. *Neurobiology of Aging,* **20**(1): 47-51.

Peng YZ, Ye ZZ, Zou RJ, Wang YX, Tian BP, Ma YY, Shi LM. 1991. Biology of Chinese Tree Shrews. Kunming: Yunnan Science and Technology Press. (in Chinese)

Petruzziello F, Fouillen L, Wadensten H, Kretz R, Andren PE, Rainer G, Zhang XZ. 2012. Extensive characterization of *Tupaia belangeri* neuropeptidome using an integrated mass spectrometric approach. *Journal of Proteome Research,* **11**(2): 886-896.

Pryce CR, Fuchs E. 2017. Chronic psychosocial stressors in adulthood: studies in mice, rats and tree shrews. *Neurobiology of Stress,* **6**: 94-103.

Shao M, Xu TR, Chen CS. 2016. The big bang of genome editing technology: development and application of the CRISPR/Cas9 system in disease animal models. *Zoological Research,* **37**(4): 191-204.

Song S, Liu L, Edwards SV, Wu SY. 2012. Resolving conflict in eutherian mammal phylogeny using phylogenomics and the multispecies coalescent model. *Proceedings of the National Academy of Sciences of the United States of America,* **109**(37): 14942-14947.

Su JJ, Yan QR, Gan YQ, Zhou DN, Huang DR, Huang GH. 1987. Experimental infection of human hepatitis B virus (HBV) in adult tree shrews. *Chinese Journal of Pathology,* **16**(2): 103-106. (in Chinese)

Takeuchi O, Akira S. 2010. Pattern recognition receptors and inflammation. *Cell,* **140**(6): 805-820.

van der Worp HB, Howells DW, Sena ES, Porritt MJ, Rewell S, O'Collins V, Macleod MR. 2010. Can animal models of disease reliably inform human studies? *PLoS Medicine,* **7**(3): e1000245.

Van Hooser SD, Roy A, Rhodes HJ, Culp JH, Fitzpatrick D. 2013. Transformation of receptive field properties from lateral geniculate nucleus to superficial V1 in the tree shrew. *Journal of Neuroscience,* **33**(28): 11494-11505.

Veit J, Bhattacharyya A, Kretz R, Rainer G. 2011. Neural response dynamics of spiking and local field potential activity depend on CRT monitor refresh rate in the tree shrew primary visual cortex. *Journal of Neurophysiology,* **106**(5): 2303-2313.

Veit J, Bhattacharyya A, Kretz R, Rainer G. 2014. On the relation between receptive field structure and stimulus selectivity in the tree shrew primary visual cortex. *Cerebral Cortex,* **24**(10): 2761-2771.

Walter E, Keist R, Niederöst B, Pult I, Blum HE. 1996. Hepatitis B virus infection of tupaia hepatocytes *in vitro* and *in vivo*. *Hepatology,* **24**(1): 1-5.

Wang LR, Shao YJ, Guan YT, Li L, Wu LJ, Chen FR, Liu MZ, Chen HQ, Ma YL, Ma XY, Liu MY, Li DL. 2015. Large genomic fragment deletion and functional gene cassette knock-in via Cas9 protein mediated genome editing in one-cell rodent embryos. *Scientific Reports,* **5**: 17517.

Xia HJ, Wang CY, Zhang HL, He BL, Jiao JL, Chen CS. 2012. Characterization of spontaneous breast tumor in tree shrews (*Tupaia belangeri chinenesis*). *Zoological Research,* **33**(1): 55-59.

Xia HJ, He BL, Wang CY, Zhang HL, Ge GZ, Zhang YX, Lv LB, Jiao JL, Chen CS. 2014. *PTEN/PIK3CA* genes are frequently mutated in spontaneous and medroxyprogesterone acetate-accelerated 7, 12-dimethylbenz(a)anthracene-induced mammary tumours of tree shrews. *European Journal of Cancer,* **50**(18): 3230-3242.

Xing HJ, Jia K, He J, Shi CZ, Fang MX, Song LL, Zhang P, Zhao Y, Fu JN, Li SJ. 2015. Establishment of the tree shrew as an alcohol-induced Fatty liver model for the study of alcoholic liver diseases. *PLoS One,* **10**(6): e0128253.

Xu L, Chen SY, Nie WH, Jiang XL, Yao YG. 2012. Evaluating the phylogenetic position of Chinese tree shrew (*Tupaia belangeri chinensis*) based on complete mitochondrial genome: implication for using tree shrew as an alternative experimental animal to primates in biomedical research. *Journal of Genetics and Genomics,* **39**(3): 131-137.

Xu L, Fan Y, Jiang XL, Yao YG. 2013a. Molecular evidence on the phylogenetic position of tree shrews. *Zoological Research,* **34**(2): 70-76. (in Chinese)

Xu L, Zhang Y, Liang B, Lü LB, Chen CS, Chen YB, Zhou JM, Yao YG. 2013b. Tree shrews under the spot light: emerging model of human diseases. *Zoological Research,* **34**(2): 59-69. (in Chinese)

Xu L, Yu DD, Fan Y, Peng L, Wu Y, Yao YG. 2016. Loss of RIG-I leads to a functional replacement with MDA5 in the Chinese tree shrew. *Proceedings of the National Academy of Sciences of the United States of America,* **113**(39): 10950-10955.

Xu XP, Chen HB, Cao XM, Ben KL. 2007. Efficient infection of tree shrew (*Tupaia belangeri*) with hepatitis C virus grown in cell culture or from patient plasma. *Journal of General Virology,* **88**(9): 2504-2512.

Yamashita A, Fuchs E, Taira M, Hayashi M. 2010. Amyloid beta (Aβ) protein- and amyloid precursor protein (APP)-immunoreactive structures in the brains of aged tree shrews. *Current Aging Science,* **3**(3): 230-238.

Yamashita A, Fuchs E, Taira M, Yamamoto T, Hayashi M. 2012. Somatostatin-immunoreactive senile plaque-like structures in the frontal cortex and nucleus accumbens of aged tree shrews and Japanese macaques. *Journal of Medical Primatology,* **41**(3): 147-157.

Yan H, Zhong GC, Xu GW, He WH, Jing ZY, Gao ZC, Huang Y, Qi YH, Peng B, Wang HM, Fu LR, Song M, Chen P, Gao WQ, Ren BJ, Sun YY, Cai T, Feng XF, Sui JH, Li WH. 2012. Sodium taurocholate cotransporting polypeptide is a functional receptor for human hepatitis B and D virus. *eLife,* **1**: e00049.

Yan LZ, Sun B, Lyu LB, Ma YH, Chen JQ, Lin Q, Zheng P, Zhao XD. 2016. Early embryonic development and transplantation in tree shrews. *Zoological Research,* **37**(4): 252-258.

Yan RQ, Su JJ, Huang DR, Gan YC, Yang C, Huang GH. 1996. Human hepatitis B virus and hepatocellular carcinoma I. Experimental infection of tree shrews with hepatitis B virus. *Journal of Cancer Research and Clinical Oncology,* **122**(5): 283-288.

Yao YG, Chen YB, Liang B. 2015. The 3rd symposium on animal models of primates-the application of non-human primates to basic research and translational medicine. *Journal of Genetics and Genomics,* **42**(6): 339-341.

Yu DD, Wu Y, Xu L, Fan Y, Peng L, Xu M, Yao YG. 2016. Identification and characterization of toll-like receptors (TLRs) in the Chinese tree shrew (*Tupaia belangeri chinensis*). *Developmental & Comparative Immunology,* **60**: 127-138.

Zhang LQ, Zhang ZG, Li YH, Liao SS, Wu XY, Chang Q, Liang B. 2015. Cholesterol induces lipoprotein lipase expression in a tree shrew (*Tupaia belangeri chinensis*) model of non-alcoholic fatty liver disease. *Scientific Reports,* **5**: 15970.

Zhang LQ, Wu XY, Liao SS, Li YH, Zhang ZG, Chang Q, Xiao RY, Liang B. 2016. Tree shrew (*Tupaia belangeri chinensis*), a novel non-obese animal model of non-alcoholic fatty liver disease. *Biology Open,* **5**(10): 1545-1552.

Zhang XL, Pang W, Hu XT, Li JL, Yao YG, Zheng YT. 2014. Experimental primates and non-human primate (NHP) models of human diseases in China: current status and progress. *Zoological Research,* **35**(6): 447-464.

Zhao F, Guo XL, Wang YJ, Liu J, Lee WH, Zhang Y. 2014. Drug target mining and analysis of the Chinese tree shrew for pharmacological testing. *PLoS One,* **9**(8): e104191.

Zhao XP, Tang ZY, Klumpp B, Wolff-Vorbeck G, Barth H, Levy S, von Weizsäcker F, Blum HE, Baumert TF. 2002. Primary hepatocytes of *Tupaia belangeri* as a potential model for hepatitis C virus infection. *Journal of Clinical Investigation,* **109**(2): 221-232.

Zheng YT, Yao YG, Xu L. 2014. Basic Biology and Disease Models of Tree Shrews. Kunming: Yunnan Science and Technology Press, 1-475. (in Chinese)

Zhou XM, Sun FM, Xu SX, Yang G, Li M. 2015. The position of tree shrews in the mammalian tree: comparing multi-gene analyses with phylogenomic results leaves monophyly of Euarchonta doubtful. *Integrative Zoology,* **10**(2): 186-198.

Tree shrew (*Tupaia belangeri*) as a novel laboratory disease animal model

Ji Xiao[1,2], Rong Liu[2], Ce-Shi Chen[2,*]

[1] *Medical Faculty of Kunming University of Science and Technology*, *Kunming Yunnan* 650500, *China*

[2] *Key Laboratory of Animal Models and Human Disease Mechanisms of the Chinese Academy of Sciences and Yunnan Province*, *Kunming Institute of Zoology*, *Chinese Academy of Sciences*, *Kunming Yunnan* 650223, *China*

ABSTRACT

The tree shrew (*Tupaia belangeri*) is a promising laboratory animal that possesses a closer genetic relationship to primates than to rodents. In addition, advantages such as small size, easy breeding, and rapid reproduction make the tree shrew an ideal subject for the study of human disease. Numerous tree shrew disease models have been generated in biological and medical studies in recent years. Here we summarize current tree shrew disease models, including models of infectious diseases, cancers, depressive disorders, drug addiction, myopia, metabolic diseases, and immune-related diseases. With the success of tree shrew transgenic technology, this species will be increasingly used in biological and medical studies in the future.

Keywords: Tree shrew (*Tupaia belangeri*); Animal model; Transgenic; Disease

INTRODUCTION

Animal models are used to simulate complex biological phenomena and human disease characteristics. Laboratory animal models are essential for addressing complicated biological problems, understanding the mechanisms of human diseases, and testing the efficacies of therapeutics. To date, *Drosophila*, zebrafish (*Brachydanio rerio*), frog (*Xenopus laevis*), mouse (*Mus musculus*), rat (*Rattus norvegicus*), rabbit (*Oryctolagus cuniculus*), dog (*Canis lupus familiaris*), pig (*Sus scrofa domesticus*), and rhesus macaque (*Macaca mulatta*) have been applied as animal models in the simulation of human cancers, as well as cardiovascular, neurological, metabolic, infectious, and autoimmune diseases (Buchholz, 2015; Jiang et al., 2011; Kazama, 2016; Xu, 2011; Xue et al., 2014). While mature animal models have propelled medical research considerably, no perfect model for human disease currently exists. Each animal model has its own unique advantages and disadvantages. Mice, e.g., have been widely applied due to their small size and clear genetic background; however, the significant genetic differences between rodents and humans mean that such models are unsatisfactory for certain diseases, such as hepatitis and AIDS (Glebe & Bremer, 2013). Compared with other experimental animals, non-human primates are genetically close to humans, allowing for the relatively accurate simulation of human pathology and physiology. However, their high cost and low reproductivity severely limit their use as experimental models. Therefore, the development of novel animal models to balance the advantages and disadvantages for specific disease research is critical.

The tree shrew (*Tupaia belangeri*) belongs to Mammalia, Scandentia, and Tupaiidae (Wang, 1987). It lives mainly in Southeast Asia and is characterized by short reproductive and life cycles, high reproductivity (4–6 months from birth to adulthood, with 2–6 offspring born each time), moderate size (adult weight 120–150 g), and easy feeding. The physiological features of the tree shrew, such as anatomy, neurodevelopment, and psychological stress, are highly similar to those of primates, including humans. For example, based on their mixed insectivorous and frugivorous diets, tree shrews are adept at climbing and moving with ease. Furthermore, tree shrews have a relatively well developed and arranged visual thalamus, resulting in acute visual and color discrimination abilities (Ranc et al., 2012). The primary visual cortex branch of the tree shrew is similar to that of primates, but not of rats, indicating that their visual system is closer to that of primates than that of rodents (Caspi et al., 2003; Veit et al., 2011, 2014; Wang et al., 2013b). The amygdaloid nucleus/hippocampus rate of tree shrews is much greater than that of rodents, allowing tree shrews to more easily accomplish memory tasks (Khani & Rainer, 2012; Nair et al., 2014; Wang et al., 2013b). Because of these advantages, a

Received: 14 March 2017; Accepted: 03 May 2017

Foundation items: This study was supported by the National Nature Science Foundation of China (81325016, U1602221, 81322038 and U1502222)

*Corresponding author, E-mail: chenc@mail.kiz.ac.cn

DOI: 10.24272/j.issn.2095-8137.2017.033

growing number of tree shrew disease models have been created (Xu et al., 2013). In 2012, the Kunming Institute of Zoology of the Chinese Academy of Sciences (KIZ, CAS) completed genome sequencing of the Chinese tree shrew, which showed that the nervous, immune, and metabolic systems of the tree shrew were very close to those of humans (Fan et al., 2013). The tree shrew database website (http://www.treeshrewdb.org/) was built based on the tree shrew genome sequence data (Fan et al., 2014). In addition, 3 482 tree shrew proteins have been predicted to be drug targets for cancer chemotherapy, depression, and cardiovascular diseases (Zhao et al., 2014). These studies have greatly facilitated the application of the Chinese tree shrew as an animal model in biomedical research. To date, 1 136 papers related to the tree shrew have been published.

INFECTIOUS DISEASES MODELS

Hepatitis virus infection models

Hepatitis is a serious health problem worldwide (Gravitz, 2011; Thun et al., 2010; Yan et al., 2012). However, it is difficult to identify suitable animal models for hepatitis research. In recent decades, studies have shown the tree shrew to be a practical small-animal model for experimental studies on the hepatitis virus, including hepatitis B, C, D, and E. Su (1987) and Pang et al. (1981) inoculated HBV into wild tree shrews and were able to detect the integrated HBV DNA, suggesting that HBV infection could be established in tree shrew models. Walter et al. (1996) also detected HBV DNA replication and viral protein expression in HBV-infected tree shrew liver. Experimental chronic hepatitis B infection in neonatal tree shrews further improved the efficiency of infection and more accurately simulated human chronic HBV infection (Liang et al., 2006; Wang et al., 2012a; Yang et al., 2009). Neonatal tree shrews can be persistently infected with HBV, and hepatic histopathological changes observed in chronically HBV-infected animals are similar to those observed in HBV-infected humans (Ruan et al., 2013). Additionally, chronic HBV infection combined with aflatoxin B1 has been shown to induce liver cancer in tree shrews (Li et al., 1999b; Yang et al., 2015). Furthermore, tumor necrosis factor α (TNFα) can inhibit hepatitis B virus replication in *Tupaia* hepatocytes (Xu et al., 2011). Sodium taurocholate co-transporting polypeptide (NTCP) has also been identified as a functional receptor for HBV and HDV based on a tree shrew model (Yan et al., 2012; Zhong et al., 2013).

Hepatitis C virus (HCV) is responsible for 150–200 million chronic infections and more than 350 000 deaths worldwide every year (Gravitz, 2011). Although chimpanzees and monkeys are considered natural infection hosts (Li et al., 2011), HCV has also been shown in tree shrews, with infected animals exhibiting intermittent viremia, high levels of ALT during the acute phase of infection, chronic hepatitis, liver steatosis, cirrhotic nodules, and accompanying tumorigenesis in the late stage (Amako et al., 2010). Irradiation has also been shown to increase the proportion of HCV infection in tree shrews (Xie et al., 1998). In addition, HCV can infect the primary hepatocytes of tree shrews (Amako et al., 2010; Zhao et al., 2002), with HCV receptors CD81, scavenger receptor BI (SR-BI), claudin-1, and occludin found to be essential factors for HCV entry and infection cycle in the primary hepatocytes of *Tupaia belangeri* (Tong et al., 2011).

Previous research successfully established HDV/HBV double infection in adult tree shrews to study virus pathogenesis and treatment (Li et al., 1995). In addition, tree shrews have been found to be susceptible to HEV when intravenously injected with swine genotype 4 HEV, with HEV RNA subsequently detected in the feces, liver, spleen, kidneys, and bile of infected tree shrews (Yu et al., 2016).

As one of only a few hepatitis susceptible animals, tree shrews can be infected with almost all hepatitis viruses, and can exhibit symptoms similar to those observed in humans. This makes the tree shrew an ideal animal for hepatitis disease research.

Bacterial infection models

Pathogenic bacteria, such as *Staphylococcus aureus*, *Escherichia coli*, and *Pseudomonas aeruginosa*, can cause hundreds of thousands of deaths every year. Li et al. (2012) found that tree shrews are susceptible to *Staphylococcus aureus* and *Pseudomonas aeruginosa*. Zhan et al. (2014) infected Chinese tree shrews with *Mycobacterium tuberculosis* and found that infected animals developed serious symptoms similar to the clinical signs of active tuberculosis observed in humans. These studies indicate that tree shrews can be used to establish bacterial infection models.

Other virus infection models

Other human viruses can also infect tree shrews. Herpes Simplex Virus type I (HSV-1) and type 2 (HSV-2) can latently infect peripheral nervous system sensory neurons, and their reactivation can lead to recurring cold sores in tree shrews (Han et al., 2011). HSV-1 infection in the tree shrew trigeminal ganglion following ocular inoculation differs significantly from mice in the expression of key HSV-1 genes, including ICP0, ICP4, and latency-associated transcript (LAT), providing a valuable alternative model to study HSV-1 infection and pathogenesis (Han et al., 2011; Li et al., 2016a, b). As an important human pathogen of hand-foot-mouth disease (HFMD), Coxsackie virus A16 (CA16) has been successfully used to infect tree shrews to investigate its pathogenesis (Li et al., 2014). Foamy virus can naturally infect *Tupaia belangeri chinensis* and is highly related to simian foamy virus in *Macaca mulatta* (Huang et al., 2013a). Human H1N1 influenza-infected tree shrews have been shown to display mild to moderate systemic and respiratory symptoms and pathological changes in respiratory tracts (Yang et al., 2013). *Tupaia belangeri chinensis* has also been positively infected with enterovirus 71 (EV71) via oral administration, nasal dripping, and tail intravenous injection (Wang et al., 2012b).

Immune-related disease models

Tree shrews can be used as an alternative to primates for studying immune-related diseases. The homology of the interleukin-2 (IL-2) protein sequence between tree shrews and

humans is reportedly as high as 80% (Huang et al., 2013b). Although retinoic acid induction gene protein I (RIG-I) has been lost in the Chinese tree shrew lineage, melanoma differentiation-associated protein 5 (MDA5) replaces its role in innate antiviral activity (Xu et al., 2016). In addition, chemokines in tree shrews might play similar roles as those in humans (Chen et al., 2014). Intraperitoneal injection of pristane and LPS (lipopolysaccharide) can induce systemic lupus erythematosus (SLE) (Ruan et al., 2016). Major histocompatibility complex (MHC) class I and II cell surface proteins are crucial for the self/non-self-discrimination of the adaptive immune system, with the MHC class I gene recently characterized in the tree shrew successfully (Zhang et al., 2013).

CANCER MODELS

Hepatocellular carcinoma (HCC) models

Hepatocellular carcinoma is one of the most common malignancies worldwide (Raphael et al., 2012). Tree shrews can develop spontaneous HCC (Hofmann et al., 1981), but it can also be induced by aflatoxin B1 application (Reddy et al., 1976). The incidence of HCC has also been found to significantly increase when animals are infected with HBV and exposed to AFB1 (52.94%) compared with those solely infected with HBV (11.11%) or solely exposed to AFB1 (12.50%) (Yan et al., 1996). Alterations in *p53* and *p21* genes have also been detected in tree shrew HCCs induced by human HBV and/or AFB1 (Park et al., 2000; Su et al., 2003, 2004).

Breast cancer models

Breast cancer is a common malignant tumor in women (Tong et al., 2014). Elliot et al. (1966) reported the first observed spontaneous breast cancer in tree shrew in the 1960s. Xia et al. (2012) further characterized a second case of spontaneous breast papillary tumor, with additional research showing that 50% of female tree shrews developed mammary tumors with long latency (about 7 months) following oral administration of carcinogens 7,12-dimethylbenz(a)anthracene plus medroxyprogesterone acetate (DMBA and MPA). Interestingly, the *PTEN/PIK3CA* genes, but not the *TP53* gene, were frequently mutated in both the spontaneous and DMBA plus MPA-induced tree shrew mammary tumors (Xia et al., 2014; Xu et al., 2015). Overexpression of the *PyMT* oncogene by lentivirus can also efficiently induce mammary tumors in tree shrews within a month (Ge et al., 2016). Furthermore, KLF5, an important transcription factor in breast cancer initiation and development, is reported to be highly conserved between tree shrews and humans (Shao et al., 2017).

Lung cancer models

Pulmonary cancer has the highest incidence and mortality in the world (Torre et al., 2016). The first spontaneous lung tumor in the tree shrew was reported in 1996 (Brack et al., 1996). The administration of DHPN (2,2'-dihydroxy-di-n-propylnitrosamine) at a weekly dose of 250 mg/kg body weight subcutaneous for 80 weeks resulted in 78%–89% of animals developing pulmonary adenomas between 65 and 102 weeks (Rao & Reddy, 1980). In 2013, we administered a single dose of 4-(methylnitrosamino)-1-(3-pyridyl)-1-butanone (NNK, 100 mg/kg) via intraperitoneal injection to induce lung cancer in tree shrews, but did not find any lesions in the lungs after one year (unpublished data). Furthermore, PM10 (particulate matter with diameters of 10 μm or less) from Xuanwei bituminous coal dust was found to induce bronchial epithelial hyperplasia in tree shrews, although animals died within a week of prefusion (Chen et al., 2015). Most recently, tree shrews receiving iodized oil suspensions of 3-methylcholanthrene (3-MC) and diethylnitrosamine (DEN) via endotracheal instillation for 11 weeks developed bronchial epithelial atypical hyperplasia and carcinoma *in situ*, although all experimental animals died (Ye et al., 2016).

Other tumor models

Spontaneous lymphoma was first observed in tree shrews in 1996 (Brack et al., 1996). Overexpression of H-Ras (human) and shP53 (tree shrew) by lentivirus for 139 days was shown to induce glioma tumors in tree shrews (Tong et al., 2017). Compared with corresponding mouse gliomas, tree shrew gliomas are more similar to human glioblastomas in terms of gene expression profile (Tong et al., 2017).

METABOLIC DISEASE MODELS

Diabetes models

Diabetes along with hyperglycemia is a metabolic disease. There are about 285 million diabetic patients worldwide (Shaw et al., 2010). Rabb et al. (1966) reported that spontaneous diabetes with the same ketosis, alopecia, and cataract phenotypes as observed in human diabetes was also found in the Philippine tree shrews (*Urogale everetti)*. Several research groups have successfully induced type 1 diabetes in tree shrews using streptozotocin (STZ) (Ishiko et al., 1997; Xian et al., 2000), which is widely used to establish diabetic animal models by selectively killing β cells (Srinivasan & Ramarao, 2007). Li et al. (2010) used a high-glucose-fat-diet in combination with dexamethasone to induce type 2 diabetes in tree shrews (Li et al., 2010). Wu et al. (2013) also established similar type 2 diabetes in tree shrews using different doses of STZ (60, 70, and 80 mg/kg). Furthermore, a diabetic nephropathy tree shrew model was successfully induced by a high-sugar and high-fat diet and four injections of STZ, with bone-marrow mesenchymal stem cell transplantation also demonstrated to improve insulin resistance (Pan et al., 2014).

Fatty liver disease models

With economic development and an increase in the standard of living, fatty liver disease has become increasingly common (Qian et al., 2007). Tree shrews treated with alcohol solutions (10% and 20%) for two weeks were found to develop fatty liver-like pathological changes and alterations (Xing et al., 2015), while Meng et al. (2003) found that Rosiglitazone could prevent fatty liver development in the tree shrew. Using a high fat, cholesterol, and cholate diet, Zhang et al. (2015, 2016) successfully established non-alcoholic non-obese fatty liver disease (NAFLD) in tree shrews; interestingly, the inhibition of

lipoprotein lipase by Poloxamer 407 improved the severity of steatosis and reduced inflammation (Zhang et al., 2015). Additionally, 20% sucrose and 1% cholesterol added to their standard diet resulted in massive gallstones in the tree shrew (Schwaier, 1979). Compared with the mouse fatty liver disease model, the tree shrew model shows a shorter onset time and more obvious symptoms (Zhang et al., 2015).

Blood vascular disease models

Tree shrews are regarded as an animal model resistant to atherosclerosis. Liu et al. (2010) showed that tree shrews are resistant to atherosclerosis because of low cholesteryl ester transfer protein expression and low phospholipid transfer protein activities. Li et al. (1999a) induced thrombotic cerebral ischemia in tree shrews using a photochemical approach, with Feng et al. (2011) showing that cerebral ischemia caused a predominant increase in TLR4 protein expression in the tree shrew hippocampus. A blood stasis syndrome model was also successfully established in tree shrews with high-dose carrageen glue (Zhang et al., 2016)

MENTAL DISEASE MODELS

Depression models

Depression, a common mental disease, influences about 20% of people worldwide (Nestler et al., 2002). Tree shrews are diurnal animals, which can be advantageous in certain research compared with using nocturnal animals such as rodents. Previous studies have shown a variety of physiological changes, such as constantly elevated levels of urinary cortisol and norepinephrine and reduced body weight, in subordinate, but not dominant males (Fuchs et al., 1995; Magariños et al., 1996). Fuchs & Flügge (2002) described the physiology, brain function, and behaviors of subordinate tree shrews. Coexistence of two males with visual and olfactory contact led to a stable dominant/subordinate relationship, with the subordinate showing obvious changes in behavior, neuroendocrine, and central nervous activity similar to the symptoms observed in depression patients (Van Kampen et al., 2002). Clomipramine treatment has also been shown to counteract the behavioral and endocrine effects of chronic psychosocial stress in tree shrews (Fuchs, 2005; Fuchs et al., 1996), whereas diazepam has no beneficial effects on stress-induced behavioral and endocrine changes in male tree shrews (Van Kampen et al., 2000). Wang et al. (2011) examined two male tree shrews for one hour of direct conflict (fighting) and 23 hours of indirect influence (e.g., smell, visual cues) per day for 21 days and found that the subordinate tree shrews showed alterations in body weight, locomotion, avoidance behavior, and urinary cortisol levels in the final week of social conflict. Schmelting et al. (2014) reported that agomelatine normalized the core body temperature in psychosocially stressed male tree shrews. Moreover, chronic clomipramine treatment reversed symptoms of depression, such as weight loss, anhedonia, fluctuations in locomotor activity, sustained urinary cortisol elevation, irregular cortisol rhythms, and deficient hippocampal long-term potentiation (LTP) in subordinate tree shrews (Wang et al., 2013a). These findings all suggest that tree shrews are suitable for studying depression.

Drug addiction models

Drug addiction is a chronic and relapsing brain disease. Tree shrews are useful animal models for the study of human drug addiction pathogenesis due to their well-developed central nervous system. Opitz & Weischer (1988) observed that non-deprived, unstressed tree shrews preferred nicotine solution over water in a free-choice situation. In addition, Wiens et al. (2008) revealed that wild tree shrews naturally preferred alcohol. Morphine, an effective analgesic, induces tolerance and addiction in animals. Sun et al. (2012) injected tree shrews with morphine for 7 days and induced conditioned place aversion (CPA) along with withdrawal symptoms. Intramuscular injection of morphine (5 or 10 mg/kg) has been shown to significantly increase the locomotor activity of tree shrews, with morphine-conditioned tree shrews exhibiting place preference in the morphine-paired chamber and naloxone-precipitated withdrawal inducing place aversion in chronic morphine-dependent tree shrews (Wang et al., 2012a). Cocaine and amphetamine regulated transcript peptides are also reported to show similar expression patterns in tree shrews and primates (Ábrahám et al., 2005). These findings suggest that tree shrews are suitable for studying human drug addiction.

NERVE RELATED DISEASES

Myopia models

Chickens and monkeys are the most commonly used animal models for myopia study; however, tree shrews might be better candidates due to their low cost, short experiment cycle, small size, and similar eye development to humans. Axial myopia has been reliably produced in tree shrews raised with eyelid closure (Marsh-Tootle & Norton, 1989) and following the application of agents to block collagen crosslinking (McBrien & Norton, 1994). Dark treatment has also resulted in a shift toward myopia in tree shrews (Norton et al., 2006). Tree shrews demonstrated significant scleral thinning and tissue loss, particularly at the posterior pole of the eye, after monocular deprivation of pattern vision (McBrien et al., 2001). The scleral gene expression levels are regulated by the visual environment during the development of myopia and recovery (Guo et al., 2014; He et al., 2014; Siegwart & Norton, 2002). The use of positive lenses has been shown to inhibit myopia in tree shrews, suggesting that daily intermittent positive lens wear might effectively prevent myopia progression in children (McBrien et al., 2012; Siegwart & Norton, 2010). Taken together, tree shrews appear to be ideal animal models for studying myopia.

Alzheimer's disease (AD) models

Alzheimer's disease is one of the most common neurodegenerative diseases. The central pathological feature of AD is the profuse deposition of amyloid-β protein (Aβ) in the brain parenchyma and vessel walls. The sequence of the tree shrew Aβ protein has very high homology (92% identity) with the human Aβ protein (Pawlik et al., 1999). Fan et al. (2013) revealed that genes related to AD in tree shrews share a high degree of homology with human beings. Yamashita et al. (2012) observed

senile plaque-like structures in the frontal cortex and nucleus accumbens of aged tree shrews. He et al. (2013) induced AD in tree shrews by intracerebroventricular injection of Aβ. Lin et al. (2016) injected Aβ1-40 into the tree shrew hippocampus and induced cognitive lesions associated with neuronal apoptosis. Thus, tree shrews are a potentially effective animal for studying AD.

Transgenic tree shrews

Transgenesis is an important technology for the establishment of disease models. To date, site-directed gene editing has been applied to generate transgenic animals (Capecchi, 2005). Additionally, the development of CRISPR/Cas9 technology has made transgenesis more extensively applicable (Mali et al., 2013). Li et al. (2017) found a culture system for the long-term expansion of tree shrew spermatogonial stem cells without the loss of stem cell properties and successfully generated transgenic offspring by transplanting enhanced green fluorescent protein (EGFP) into sterilized adult male tree shrew testes. Such research has greatly consolidated the position of the tree shrew in the field of disease animal models.

CONCLUSIONS AND PERSPECTIVES

The tree shrew is more closely related to humans than to rodents in evolution and offers distinct advantages in breeding (Fan et al., 2013). This species has garnered increasing attention in China and worldwide in terms of its use as a novel animal model for a variety of human diseases. To date, tree shrews have shown unique advantages in the study of hepatitis, depression, drug addiction, and myopia. The successful application of transgenic techniques in tree shrews (Li et al., 2017) will broaden the choices for researchers in selecting appropriate animal models for studying human diseases.

However, several hurdles still exist in this field. To date, there are no tree shrew strains with a pure genetic background. Scientists at KIZ, CAS have worked very hard to establish tree shrew strains in recent years, but have only obtained fourth generation offspring by inbreeding so far. Additionally, gene knockout techniques have yet to be applied in tree shrews. Moreover, physiological research tools and materials for the tree shrew remain relatively underdeveloped. This includes tree shrew specific antibodies, although most antibodies against human proteins are suitable for detecting tree shrew proteins. Current tree shrew disease models need to be optimized and studied in depth, and, as such, we to need exhibit patience before adopting the tree shrew in the study of all human diseases. There is, however, no doubt that the tree shrew will play an increasingly important role in the biomedical field.

Table 1 Tree shrew disease models

Disease model	Methods	Characteristics	References
HBV	Infected with 0.1 mL of serum from HBV positive patients by intramuscular injection	More than half of the tree shrews showed anorexia and emaciation 5 days after infection. Both HBsAg- and HBsAb-positive tree shrews reached 9/22 at 15–35 days after infection.	Pang et al., 1981
	Neonatal tree shrews infected with 0.3 mL of HBV inoculum by two subcutaneous injections	13% of neonatal tree shrews showed long-term (more than 48 weeks) chronic infection with HBV. Hepatic histopathological changes were observed in chronically HBV-infected animals.	Wang et al., 2012a
	Infected with human HBV serum, then fed AFB1 diluted with milk, 150 μg/kg, 6 days/week for 105 weeks	HCCs developed in 120.3±16.6 weeks at incidences of 67%	Li et al., 1999b
HCV	Infected intravenously with 0.15 mL of serum from patients with chronic hepatitis C	34.8% of tree shrews developed HCV viremia at different times during 47 weeks of follow-up. Peaks in transaminases, high ALT levels, and anti-HCV antibodies were observed	Xie et al., 1998
HDV/HBV	Infected with HBV-RNA and HDV-RNA serum (0.2 mL) by tail vein injection	HBsAg- and HDAg-positive serum was detected in 6/13 tree shrews 4–5 weeks after inoculation with high ALT levels.	Li et al., 1995
HEV	Infected with 0.2 mL of swine genotype 4 HEV by intravenous injection	HEV RNA was detected in the feces, liver, spleen, kidneys, and bile of tree shrews. Histological examination showed that HEV caused acute liver lesions. Infected tree shrews showed positive IgG and IgM antibodies.	Yu et al., 2016
H1N1	Infected with ~10^5 H1N1 by intranasal administration	3/3 of the infected tree shrew displayed mild systemic and respiratory symptoms and pathological changes in respiratory tracts 14 days after infection.	Yang et al., 2013
HSV	Infected with 10^6 PFU of HSV-1 McKrae virus inoculum on each eye without ocular scarification	About 10% of the tree shrews showed severe nervous system disease symptoms, such as ataxia, astasia, torticollis, star gazing, and other abnormal behaviors from 5 days post infection	Li et al., 2016a

Continued

Disease model		Methods	Characteristics	References
	Bacteria	Infected with 5×10^6 CFU of *Staphylococcus aureus* on the surface of a wound	*S. aureus* caused persistent infection for 7 days and inflammatory response for 4 days after inoculation.	Li et al., 2012
		Infected with 2×10^6 CFU of *Pseudomonas aeruginosa* on the surface of a wound	Dacron graft infection model caused persistent infection for 6 days, with pus observed 3 days after inoculation	
Cancer	Hepatocellular carcinoma (HCC)	Administration of highly purified aflatoxin B1 intermittently in the diet at 2 mg/ kg	9/12 tree shrews developed HCCs between 74 and 172 weeks. Liver tumors in all nine tree shrews were well to poorly differentiated.	Reddy et al., 1976
		Infected with human HBV serum and aflatoxin B1 (200–400 μg/kg body weight per day) for 6 days every week, totally 15–16 mg	For 83–137 weeks, the incidence of HCC was significantly higher in tree shrews infected with HBV and exposed to AFB1 (52.94%) than in those solely infected with HBV (11.11%) or exposed to AFB1 (12.50%). All 13 cases of liver tumor were HCC, including eight cases of trabecular type, three of adenoid type, and two poorly-differentiated.	Yan et al., 1996
	Breast cancer	Spontaneous breast papillary tumor	Tumor cells were positive for PR, highly proliferative, and less apoptotic compared with normal breast epithelial cells.	Xia et al., 2012
		Oral administration of 20 mg of DMBA once every 3 weeks, three times in total in 30 tree shrews, with15 tree shrews implanted with 150 mg of MPA	After 25–33 weeks, tumor incidence in the DMBA plus MPA group reached 50%. All DMBA plus MPA-induced tumors were positive for PR and ERα but negative for HER2. The *PTEN/ PIK3CA*, but not *TP53 and GATA3*, genes were frequently mutated in the breast tumors.	Xia et al., 2014
		Overexpression of the *PyMT* oncogene by lentivirus (10 μL) nipple injection	Most tree shrews developed mammary tumors with a latency of about 3 weeks, and by 7 weeks all injected tree shrews had developed mammary tumors. *PyMT*-induced tree shrew mammary tumors were predominately papillary carcinomas.	Ge et al., 2016
	Lung cancer	DHPN was administered at a dose of 250 mg/kg body weight subcutaneous once a week for 80 weeks	Between 65 and 102 weeks, 78%–89% of tree shrews developed pulmonary adenomas. Clara cells were the main components of these tumors. In two DHPN-treated males, bronchioalveolar carcinomas were observed and 9% of the DHPN-treated animals developed squamous cell carcinomas of the skin and HCC.	Rao & Reddy, 1980
Metabolic diseases	Diabetes	STZ (60, 70, 80 mg/kg) was intraperitoneally injected twice on the first and third day	After 9–16 weeks, the success rates for the 60, 70, and 80 mg/kg STZ injection groups were 66.7%, 66.7%, and 100%, respectively. Tree shrews displayed increased fasting blood and urine glucose, impaired oral glucose tolerance, and disturbed lipids metabolism and renal function.	Wu et al., 2013
	Fatty liver	Treated with alcohol solutions (10% and 20%) for two weeks	After 14 days, the serum ALT, AST, GGT, TC, and TG levels of the alcohol-treated groups significantly increased. Animals exhibited obvious pathological changes, including swelling of the hepatocytes and disarrangement of cell cords.	Xing et al., 2015
		High fat, cholesterol, and cholate diet (HFHC, 20% fat, 1.25% cholesterol and 0.5% sodium cholate by weight)	After 10 weeks, HFHC caused blood dyslipidemia, and induced hepatic lipid accumulation and liver inflammation. HFHC also caused liver fibrosis.	Zhang et al., 2015
	Blood Stasis	Intraperitoneal injection of 25, 50, and 75 mg/kg doses of carrageen glue for 3 days	One day after treatment, tree shrews were in low spirits. Tongue vein was enlarged. Regular probability pain increased and the colors of the tongue, claw, and naso-labial area became darker with increasing dose.	Chen et al., 2016
	Thrombotic cerebral ischemia	The scalp was incised to expose the right skull, which was irradiated with a 560-nm filtered beam for 10 min	Sodium, calcium, and water contents increased to a maximum after 4 hours in ischemic penumbra.	Li et al., 1999a

Continued

Disease model		Methods	Characteristics	References
Mental diseases	Depression	Two male tree shrews were housed in a pair-cage, 1 h direct conflict (fighting) and 23 h indirect influence for 21 days	After 21 days, the subordinate tree shrews showed alterations in body weight, locomotion, avoidance behavior, and urinary cortisol levels.	Wang et al., 2011
	Drug addiction	Intramuscular injection of morphine at increasing doses (5, 10, 15, 20 mg/kg body weight for 7 days). Naloxone (1.25 mg/kg body weight) induced CPA	After 7 days, the tree shrews developed morphine tolerance and chronic morphine dependence with increasing doses.	Sun et al., 2012
		Nicotine solution (10 mg/L nicotine tartrate) in drinking water	Tree shrews preferred nicotine solution, with this drug-taking behavior stable over 14 months.	Opitz & Weischer, 1988
Nerve related diseases	Myopia	Placement in continuous darkness for 10 days	After 10 days, the dark-treatment group eyes shifted toward myopia, and the vitreous chamber became elongated relative to normal eyes	Norton et al., 2006
		Monocular deprivation of pattern vision for short-term (12 days) or long-term (3–20 months) periods	Significant scleral thinning and tissue loss, particularly at the posterior pole of the eye, were associated with ocular enlargement and myopia development after both short- and long-term treatments	McBrien et al., 2001

PFU: plaque forming units; CFU: colony forming unit.

REFERENCES

Ábrahám H, Czéh B, Fuchs E, Seress L. 2005. Mossy cells and different subpopulations of pyramidal neurons are immunoreactive for cocaine- and amphetamine-regulated transcript peptide in the hippocampal formation of non-human primates and tree shrew (*Tupaia belangeri*). *Neuroscience,* **136**(1): 231-240.

Amako Y, Tsukiyama-Kohara K, Katsume A, Hirata Y, Sekiguchi S, Tobita Y, Hayashi Y, Hishima T, Funata N, Yonekawa H, Kohara M. 2010. Pathogenesis of hepatitis C virus infection in *Tupaia belangeri*. *Journal of Virology,* **84**(1): 303-311.

Brack M, Schwartz P, Heinrichs T, Schultz M, Fuchs E. 1996. Tumors of the respiratory tract observed at the German Primate Center, 1978-1994. *Journal of Medical Primatology,* **25**(6): 424-434.

Buchholz DR. 2015. More similar than you think: frog metamorphosis as a model of human perinatal endocrinology. *Developmental Biology,* **408**(2): 188-195.

Capecchi MR. 2005. Gene targeting in mice: functional analysis of the mammalian genome for the twenty-first century. *Nature Reviews Genetics,* **6**(6): 507-512.

Caspi A, Sugden K, Moffitt TE, Taylor A, Craig IW, Harrington H, McClay J, Mill J, Martin J, Braithwaite A, Poulton R. 2003. Influence of life stress on depression: moderation by a polymorphism in the 5-HTT gene. *Science ,* **301**(5631): 386-389.

Chen B, Huang JL,Guo XX, Feng XT, Guo EC, Zhang SR, Chen WY, Hu YL, Zhong ZG. 2016. Study on tree shrews model of blood stasis induced by different dose of carrageen glue. *World Chinese Medicine,* **11**(11): 2219-2222. (in Chinese)

Chen GY, Wang W, Meng SK, Zhang LC, Wang WX, Jiang ZM, Yu M, Cui QH, Li MZ. 2014. CXC chemokine CXCL12 and its receptor CXCR4 in tree shrews (*Tupaia belangeri*): structure, expression and function. *PLoS One,* **9**(5): e98231.

Chen XB, He M, Li GJ, Zhou YC, Zhao GQ, Lei YJ, Yang KY, Tian LW, Huang YC. 2015. Study of the changes on tree shrew bronchial epithelium induced by xuanwei bituminous coal dust. *Chinese Journal of Lung Cancer,* **18**(8): 469-474. (in Chinese)

Elliot OS, Elliot MW, Lisco H. 1966. Breast cancer in a tree shrew (*Tupaia glis*). *Nature,* **211**(5053): 1105.

Fan Y, Huang ZY, Cao CC, Chen CS, Chen YX, Fan DD, He J, Hou HL, Hu L, Hu XT, Jiang XT, Lai R, Lang YS, Liang B, Liao SG, Mu D, Ma YY, Niu YY, Sun XQ, Xia JQ, Xiao J, Xiong ZQ, Xu L, Yang L, Zhang Y, Zhao W, Zhao XD, Zheng YT, Zhou JM, Zhu YB, Zhang GJ, Wang J, Yao YG. 2013. Genome of the Chinese tree shrew. *Nature Communications,* **4**: 1426.

Fan Y, Yu DD, Yao YG. 2014. Tree shrew database (TreeshrewDB): a genomic knowledge base for the Chinese tree shrew. *Scientific Reports,* **4**: 7145.

Feng R, Li SQ, Li F. 2011. Toll-like receptor 4 is involved in ischemic tolerance of postconditioning in hippocampus of tree shrews to thrombotic cerebral ischemia. *Brain Research,* **1384**: 118-127.

Fuchs E, Uno H, Flügge G. 1995. Chronic psychosocial stress induces morphological alterations in hippocampal pyramidal neurons of the tree shrew. *Brain Research,* **673**(2): 275-282.

Fuchs E, Kramer M, Hermes B, Netter P, Hiemke C. 1996. Psychosocial stress in tree shrews: clomipramine counteracts behavioral and endocrine changes. *Pharmacology Biochemistry and Behavior,* **54**(1): 219-228.

Fuchs E, Flügge G. 2002. Social stress in tree shrews: effects on physiology, brain function, and behavior of subordinate individuals. *Pharmacology Biochemistry and Behavior,* **73**(1): 247-258.

Fuchs E. 2005. Social stress in tree shrews as an animal model of depression: an example of a behavioral model of a CNS disorder. *CNS Spectrums,* **10**(3): 182-190.

Ge GZ, Xia HJ, He BL, Zhang HL, Liu WJ, Shao M, Wang CY, Xiao J, Ge F, Li FB, Li Y, Chen CS. 2016. Generation and characterization of a breast carcinoma model by PyMT overexpression in mammary epithelial cells of tree shrew, an animal close to primates in evolution. *International Journal of Cancer,* **138**(3): 642-651.

Glebe D, Bremer CM. 2013. The molecular virology of hepatitis B virus. *Seminars in Liver Disease,* **33**(2): 103-112.

Gravitz L. 2011. Introduction: a smouldering public-health crisis. *Nature,* **474**(7350): S2-S4.

Guo L, Frost MR, Siegwart JT, Jr., Norton TT. 2014. Scleral gene expression during recovery from myopia compared with expression during myopia development in tree shrew. *Molecular Vision,* **20**: 1643-1659.

Han JB, Zhang GH, Duan Y, Ma JP, Zhang XH, Luo RH, Lü LB, Zheng YT. 2011. Sero-epidemiology of six viruses natural infection in *Tupaia belangeri chinensis*. *Zoological Research,* **32**(1): 11-16. (in Chinese)

He BL, Jiao JL, Li B, Wang JT, Wang LM. 2013. Effects of Gastrodin on BDNF Expression in AD Tree Shrew. *Journal of Kunming Medical University,* **34**(9): 29-30, 37.

He L, Frost MR, Siegwart JT, Jr., Norton TT. 2014. Gene expression signatures in tree shrew choroid during lens-induced myopia and recovery. *Experimental Eye Research,* **123**: 56-71.

Hofmann W, Möller P, Schwaier A, Flügel RM, Zöller L, Darai G. 1981. Malignant tumours in Tupaia (tree shrew). *Journal of Medical Primatology,* **10**(2-3): 155-163.

Huang F, Yu WH, He ZL. 2013a. Foamy virus in the tree shrew *Tupaia belangeri* is highly related to simian foamy virus in *Macaca mulatta*. *AIDS Research and Human Retroviruses,* **29**(8): 1177-1178.

Huang XY, Li ML, Xu J, Gao YD, Wang WG, Yin AG, Li XF, Sun XM, Xia XS, Dai JJ. 2013b. Analysis of the molecular characteristics and cloning of full-length coding sequence of *interleukin-2* in tree shrews. *Zoological Research,* **34**(2): 121-126. (in Chinese)

Ishiko S, Yoshida A, Mori F, Abiko T, Kitaya N, Kojima M, Saito K. 1997. Early ocular changes in a tree shrew model of diabetes. *Nippon Ganka Gakkai Zasshi,* **101**(1): 19-23. (in Japanese)

Jiang HJ, Feng F, Dong ED. 2011. Model animals and animal models of human diseases. *Chinese Bulletin of Life Sciences,* **23**(3): 234-238. (in Chinese)

Kazama I. 2016. Burn-induced subepicardial injury in frog heart: a simple model mimicking ST segment changes in ischemic heart disease. *Journal of Veterinary Medical Science,* **78**(2): 313-316.

Khani A, Rainer G. 2012. Recognition memory in tree shrew (*Tupaia belangeri*) after repeated familiarization sessions. *Behavioural Processes,* **90**(3): 364-371.

Li CH, Yan LZ, Ban WZ, Tu Q, Wu Y, Wang L, Bi R, Ji S, Ma YH, Nie WH, Lv LB, Yao YG, Zhao XD, Zheng P. 2017. Long-term propagation of tree shrew spermatogonial stem cells in culture and successful generation of transgenic offspring. *Cell Research,* **27**(2): 241-252.

Li HY, Li JM, Li JX, Wang XX, Dai JJ, Sun XM. 2010. Insulin-resistance tree shrew model induced by high-glucose-fat-diet with dexamethasone. *Laboratory Animal and Comparative Medicine,* **30**(3): 197-200, 204. (in Chinese)

Li JP, Liao Y, Zhang Y, Wang JJ, Wang LC, Feng K, Li QH, Liu LD. 2014. Experimental infection of tree shrews (*Tupaia belangeri*) with Coxsackie virus A16. *Zoological Research,* **35**(6): 485-491.

Li LH, Li ZR, Li X, Wang EL, Lang FC, Xia YJ, Fraser NW, Gao F, Zhou JM. 2016a. Reactivation of HSV-1 following explant of tree shrew brain. *Journal of Neurovirology,* **22**(3): 293-306.

Li LH, Li ZR, Wang EL, Yang R, Xiao Y, Han HB, Lang FC, Li X, Xia YJ, Gao F, Li QH, Fraser NW, Zhou JM. 2016b. Herpes simplex virus 1 infection of tree shrews differs from that of mice in the severity of acute infection and viral transcription in the peripheral nervous system. *Journal of Virology,* **90**(2): 790-804.

Li QF, Ding MQ, Wang H, Mao Q, Wu CQ, Zheng H, Gu CH, Wang YM. 1995. The infection of hepatitis D virus in adult tupaia. *National Medical Journal of China,* **75**(10): 611-613, 639-641. (in Chinese)

Li SA, Lee WH, Zhang Y. 2012. Two bacterial infection models in tree shrew for evaluating the efficacy of antimicrobial agents. *Zoological Research,* **33**(1): 1-6.

Li SQ, Meng Q, Zhang L. 1999a. Experimental therapy of a platelet-activating factor antagonist (ginkgolide B) on photochemically induced thrombotic cerebral ischaemia in tree shrews. *Clinical and Experimental Pharmacology and Physiology,* **26**(10): 824-825.

Li Y, Su JJ, Qin LL, Yang C, Ban KC, Yan RQ. 1999b. Synergistic effect of hepatitis B virus and aflatoxin B1 in hepatocarcinogenesis in tree shrews. *Annals of the Academy of Medicine, Singapore*, 28(1): 67-71.

Li Y, Dai JJ, Sun XM, Xia XS. 2011. Progress in studies on HCV receptor of Tupaia as a potential hepatitis C animal model. *Zoological Research,* **32**(1): 97-103. (in Chinese)

Liang L, Li Y, Yang C, Cao J, Su JJ, Chen MW, Ban KC, Ou C, Duan XX, Yue HF. 2006. Preliminary study of using the artificially fed and young tree shrews as the infection model for human Hepatitis B virus. *Chinese Journal of Zoonoses,* **22**(8): 792-795. (in Chinese)

Lin N, Xiong LL, Zhang RP, Zheng H, Wang L, Qian ZY, Zhang P, Chen ZW, Gao FB, Wang TH. 2016. Erratum to: injection of Aβ1-40 into hippocampus induced cognitive lesion associated with neuronal apoptosis and multiple gene expressions in the tree shrew. *Apoptosis,* **21**(5): 641.

Liu HR, Wu G, Zhou B, Chen BS. 2010. Low cholesteryl ester transfer protein and phospholipid transfer protein activities are the factors making tree shrew and beijing duck resistant to atherosclerosis. *Lipids in Health and Disease,* **9**: 114.

Magariños AM, McEwen BS, Flügge G, Fuchs E. 1996. Chronic psychosocial stress causes apical dendritic atrophy of hippocampal CA3 pyramidal neurons in subordinate tree shrews. *The Journal of Neuroscience,* **16**(10): 3534-3540.

Mali P, Aach J, Stranges PB, Esvelt KM, Moosburner M, Kosuri S, Yang LH, Church GM. 2013. CAS9 transcriptional activators for target specificity screening and paired nickases for cooperative genome engineering. *Nature Biotechnology,* **31**(9): 833-838.

Marsh-Tootle WL, Norton TT. 1989. Refractive and structural measures of lid-suture myopia in tree shrew. *Investigative Ophthalmology & Visual Science,* **30**(10): 2245-2257.

McBrien NA, Norton TT. 1994. Prevention of collagen crosslinking increases form-deprivation myopia in tree shrew. *Experimental Eye Research,* **59**(4): 475-486.

McBrien NA, Cornell LM, Gentle A. 2001. Structural and ultrastructural changes to the sclera in a mammalian model of high myopia. *Investigative Ophthalmology & Visual Science,* **42**(10): 2179-2187.

McBrien NA, Arumugam B, Metlapally S. 2012. The effect of daily transient +4 D positive lens wear on the inhibition of myopia in the tree shrew. *Investigative Ophthalmology & Visual Science,* **53**(3): 1593-1601.

Meng BH, Liang SK, Huang S, Xian S, Shu CD. 2003. The protective effects of rosiglitazone on tree shrew's fatty liver. *Chinese Journal of Digestion,* **23**(12): 718-722. (in Chinese)

Nair J, Topka M, Khani A, Isenschmid M, Rainer G. 2014. Tree shrews (*Tupaia belangeri*) exhibit novelty preference in the novel location memory task with 24-h retention periods. *Frontiers in Psychology,* **5**: 303.

Nestler EJ, Barrot M, Dileone RJ, Eisch AJ, Gold SJ, Monteggia LM. 2002.

Neurobiology of Depression. *Neuron,* **34**(1): 13-25.

Norton TT, Amedo AO, Siegwart JT, Jr. 2006. Darkness causes myopia in visually experienced tree shrews. *Investigative Ophthalmology & Visual Science,* **47**(11): 4700-4707.

Opitz K, Weischer ML. 1988. Volitional oral intake of nicotine in tupaias: drug-induced alterations. *Drug and Alcohol Dependence,* **21**(2): 99-104.

Pan XH, Yang XY, Yao X, Sun XM, Zhu L, Wang JX, Pang RQ, Cai XM, Dai JJ, Ruan GP. 2014. Bone-marrow mesenchymal stem cell transplantation to treat diabetic nephropathy in tree shrews. *Cell Biochemistry & Function,* **32**(5): 453-463.

Pang QF, Wu XB, Xu AY, Wang ZM, Wang GX, Zhu BY, Zhang XS. 1981. Hepatitis b virus (HBV) infection in tree shrews experimental research (abstract). *Journal of Medical Research,* (9): 11-12. (in Chinese)

Park US, Su JJ, Ban KC, Qin LL, Lee EH, Lee YI. 2000. Mutations in the p53 tumor suppressor gene in tree shrew hepatocellular carcinoma associated with hepatitis B virus infection and intake of aflatoxin B1. *Gene,* **251**(1): 73-80.

Pawlik M, Fuchs E, Walker LC, Levy E. 1999. Primate-like amyloid-β sequence but no cerebral amyloidosis in aged tree shrews. *Neurobiology of Aging,* **20**(1): 47-51.

Qian BC, Shi H, Lü YP. 2007. Development of model of nonalcoholic fatty liver disease and steatohepatitis. *Chinese Journal of Comparative Medicine,* **17**(7): 426-430. (in Chinese)

Rabb GB, Getty RE, Williamson WM, Lombard LS. 1966. Spontaneous diabetes mellitus in tree shrews, *Urogale everetti*. *Diabetes,* **15**(5): 327-330.

Ranc V, Petruzziello F, Kretz R, Argandoña EG, Zhang XZ, Rainer G. 2012. Broad characterization of endogenous peptides in the tree shrew visual system. *Journal of Proteomics,* **75**(9): 2526-2535.

Rao MS, Reddy JK. 1980. Carcinogenicity of 2,2'-dihydroxy-di-n-propylnitrosamine in the tree shrew (Tupaia glis): light and electron microscopic features of pulmonary adenomas. *Journal of the National Cancer Institute,* **65**(4): 835-840.

Raphael SW, Zhang YD, Chen YX. 2012. Hepatocellular carcinoma: focus on different aspects of management. *ISRN Oncology,* **2012**: 421673.

Reddy JK, Svoboda DJ, Rao MS. 1976. Induction of liver tumors by aflatoxin B1 in the tree shrew (*Tupaia glis*), a nonhuman primate. *Cancer Research,* **36**(1): 151-160.

Ruan GP, Yao X, Liu JF, He J, Li ZA, Yang JY, Pang RQ, Pan XH. 2016. Establishing a tree shrew model of systemic lupus erythematosus and cell transplantation treatment. *Stem Cell Research & Therapy,* **7**(1): 121.

Ruan P, Yang C, Su JJ, Cao J, Ou C, Luo CP, Tang YP, Wang Q, Yang F, Shi JL, Lu XX, Zhu LQ, Qin H, Sun W, Lao YZ, Li Y. 2013. Histopathological changes in the liver of tree shrew (*Tupaia belangeri chinensis*) persistently infected with hepatitis B virus. *Virology Journal,* **10**(1): 333.

Schmelting B, Corbach-Söhle S, Kohlhause S, Schlumbohm C, Flügge G, Fuchs E. 2014. Agomelatine in the tree shrew model of depression: effects on stress-induced nocturnal hyperthermia and hormonal status. *European Neuropsychopharmacology,* **24**(3): 437-447.

Schwaier A. 1979. Tupaias (tree shrews)—a new animal model for gallstone research. *Research in Experimental Medicine,* **176**(1): 15-24.

Shao M, Ge GZ, Liu WJ, Xiao J, Xia HJ, Fan Y, Zhao F, He BL, Chen CS. 2017. Characterization and phylogenetic analysis of Kruppel-like transcription factor (KLF) gene family in tree shrews (*Tupaia belangeri chinensis*). *Oncotarget,* **7**(10): 16325-16339.

Shaw JE, Sicree RA, Zimmet PZ. 2010. Global estimates of the prevalence of diabetes for 2010 and 2030. *Diabetes Research and Clinical Practice,* **87**(1): 4-14.

Siegwart JT, Jr., Norton TT. 2002. The time course of changes in mRNA levels in tree shrew sclera during induced myopia and recovery. *Investigative Ophthalmology & Visual Science,* **43**(7): 2067-2075.

Siegwart JT, Jr., Norton TT. 2010. Binocular lens treatment in tree shrews: effect of age and comparison of plus lens wear with recovery from minus lens-induced myopia. *Experimental Eye Research,* **91**(5): 660-669.

Srinivasan K, Ramarao P. 2007. Animal models in type 2 diabetes research: an overview. *The Indian Journal of Medical Research,* **125**(3): 451-472.

Su JJ. 1987. Experimental infection of human hepatitis B virus (HBV) in adult tree shrews. *Chinese Journal of Pathology,* **16**(2): 103-106, 22. (in Chinese)

Su JJ, Li Y, Ban KC, Qin LL, Wang HY, Yang C, Ou C, Duan XX, Lee YY, Yan RQ. 2003. Alteration of the p53 gene during tree shrews' hepatocarcinogenesis. *Hepatobiliary & Pancreatic Diseases International,* **2**(4): 612-616.

Su JJ, Ban KC, Li Y, Qin LL, Wang HY, Yang C, Ou C, Duan XX, Lee YL, Yang RQ. 2004. Alteration of *p53* and *p21* during hepatocarcinogenesis in tree shrews. *World Journal Of Gastroenterology,* **10**(24): 3559-3563.

Sun YM, Yang JZ, Sun HY, Ma YY, Wang JH. 2012. Establishment of tree shrew chronic morphine dependent model. *Zoological Research,* **33**(1): 14-18.

Thun MJ, Delancey JO, Center MM, Jemal A, Ward EM. 2010. The global burden of cancer: priorities for prevention. *Carcinogenesis,* **31**(1): 100-110.

Tong YH, Zhou X, Zhao XD. 2014. Tree shrew glioma tumor model. *In*: Zheng YT, Yao YG, Xu L. Basic Biology and Disease Models of Tree Shrews. Kunming: Yunnan Science and Technology Press, 427-437. (in Chinese)

Tong YH, Hao JJ, Tu Q, Yu HL, Yan LZ, Li Y, Lv LB, Wang F, Iavarone A, Zhao XD. 2017. A tree shrew glioblastoma model recapitulates features of human glioblastoma. *Oncotarget,* **8**(11): 17897-17907.

Tong YM, Zhu YZ, Xia XS, Liu Y, Feng Y, Hua X, Chen ZH, Ding H, Gao L, Wang YZ, Feitelson MA, Zhao P, Qi ZT. 2011. Tupaia CD81, SR-BI, claudin-1, and occludin support hepatitis C virus infection. *Journal of Virology,* **85**(6): 2793-2802.

Torre LA, Siegel RL, Jemal A. 2016. Lung Cancer Statistics. *Advances in Experimental Medicine and Biology*, **893**: 1-19.

Van Kampen M, Schmitt U, Hiemke C, Fuchs E. 2000. Diazepam has no beneficial effects on stress-induced behavioural and endocrine changes in male tree shrews. *Pharmacology Biochemistry and Behavior,* **65**(3): 539-546.

Van Kampen M, Kramer M, Hiemke C, Flügge G, Fuchs E. 2002. The chronic psychosocial stress paradigm in male tree shrews: evaluation of a novel animal model for depressive disorders. *Stress,* **5**(1): 37-46.

Veit J, Bhattacharyya A, Kretz R, Rainer G. 2011. Neural response dynamics of spiking and local field potential activity depend on CRT monitor refresh rate in the tree shrew primary visual cortex. *Journal of Neurophysiology,* **106**(5): 2303-2313.

Veit J, Bhattacharyya A, Kretz R, Rainer G. 2014. On the relation between receptive field structure and stimulus selectivity in the tree shrew primary visual cortex. *Cerebral Cortex,* **24**(10): 2761-2771.

Walter E, Keist R, Niederöst B, Pult I, Blum HE. 1996. Hepatitis B virus

infection of tupaia hepatocytes *in vitro* and *in vivo*. *Hepatology,* **24**(1): 1-5.

Wang J, Zhou QX, Tian M, Yang YX, Xu L. 2011. Tree shrew models: a chronic social defeat model of depression and a one-trial captive conditioning model of learning and memory. *Zoological Research,* **32**(1): 24-30.

Wang J, Chai AP, Zhou QX, Lv LB, Wang LP, Yang YX, Xu L. 2013a. Chronic clomipramine treatment reverses core symptom of depression in subordinate tree shrews. *PLoS One,* **8**(12): e80980.

Wang Q, Schwarzenberger P, Yang F, Zhang JJ, Su JJ, Yang C, Cao J, Ou C, Liang L, Shi JL, Yang F, Wang DP, Wang J, Wang XJ, Ruan P, Li Y. 2012a. Experimental chronic hepatitis B infection of neonatal tree shrews (*Tupaia belangeri chinensis*): a model to study molecular causes for susceptibility and disease progression to chronic hepatitis in humans. *Virology Journal,* **9**(1): 170.

Wang SX, Shan D, Dai JK, Niu HC, Ma YY, Lin FC, Lei H. 2013b. Anatomical MRI templates of tree shrew brain for volumetric analysis and voxel-based morphometry. *Journal of Neuroscience Methods,* **220**(1): 9-17.

Wang WG, Huang XY, Xu J, Sun XM, Dai JJ, Li QH. 2012b. Experimental studies on infant Tupaia belangeri chineses with EV71 infection. *Zoological Research,* **33**(1): 7-13. (in Chinese)

Wang YX. 1987. Taxonomic research on Burma-Chinese tree shrew, Tupaia belangeri (Wagner), from Southern China. *Zoological Research,* **8**(3): 213-230. (in Chinese)

Wiens F, Zitzmann A, Lachance MA, Yegles M, Pragst F, Wurst FM, Von Holst D, Guan SL, Spanagel R. 2008. Chronic intake of fermented floral nectar by wild treeshrews. *Proceedings of the National Academy of Sciences of the United States of America,* **105**(30): 10426-10431.

Wu XY, Li YH, Chang Q, Zhang LQ, Liao SS, Liang B. 2013. Streptozotocin induction of type 2 diabetes in tree shrew. *Zoological Research,* **34**(2): 108-115. (in Chinese)

Xia HJ, Wang CY, Zhang HL, He BL, Jiao JL, Chen CS. 2012. Characterization of spontaneous breast tumor in tree shrews (*Tupaia belangeri chinenesis*). *Zoological Research,* **33**(1): 55-59.

Xia HJ, He BL, Wang CY, Zhang HL, Ge GZ, Zhang YX, Lv LB, Jiao JL, Chen CS. 2014. *PTEN/PIK3CA* genes are frequently mutated in spontaneous and medroxyprogesterone acetate-accelerated 7,12-dimethylbenz (a)anthracene-induced mammary tumours of tree shrews. *European Journal of Cancer,* **50**(18): 3230-3242.

Xian S, Huang S, Su JJ, Qin YF, Ou C, Luo ZJ, Wei MY. 2000. A study on experimental diabetes animal models in tree shrews induced by streptozotocin. *Journal of Guangxi Medical University,* **17**(6): 945-948. (in Chinese)

Xie ZC, Riezu-Boj JI, Lasarte JJ, Guillen J, Su JH, Civeira MP, Prieto J. 1998. Transmission of hepatitis C virus infection to tree shrews. *Virology,* **244**(2): 513-520.

Xing HJ, Jia K, He J, Shi CZ, Fang MX, Song LL, Zhang P, Zhao Y, Fu JN, Li SJ. 2015. Establishment of the tree shrew as an alcohol-induced Fatty liver model for the study of alcoholic liver diseases. *PLoS One,* **10**(6): e0128253.

Xu L. 2011. Animal models of human diseases. *Zoological Research,* **32**(1): 1-3. (in Chinese)

Xu L, Zhang Y, Liang B, Lü LB, Chen CS, Chen YB, Zhou JM, Yao YG. 2013. Tree shrews under the spot light: emerging model of human diseases. *Zoological Research*, **34**(2): 59-69.

Xu L, Yu DD, Fan Y, Peng L, Wu Y, Yao YG. 2016. Loss of RIG-I leads to a functional replacement with MDA5 in the Chinese tree shrew. *Proceedings of the National Academy of Sciences of the United States of America,* **113**(39): 10950-10955.

Xu XS, Hou XM, Wang W, Hao PQ, Zhu KL, Yan HK, Huang QS, Yang SH. 2015. DMBA induced breast tumors in tree shrews (Tupaia Belangeri Chinese). *Progress in Modern Biomedicine,* **15**(2): 228-232.

Xu Y, Köck J, Lu YP, Yang DL, Lu MJ, Zhao XP. 2011. Suppression of hepatitis B virus replication in *Tupaia* hepatocytes by tumor necrosis factor alpha of *Tupaia belangeri*. *Comparative Immunology, Microbiology and Infectious Diseases,* **34**(4): 361-368.

Xue LX, Zhang FZ, Sun RJ, Dong ED. 2014. Research status and perspective of disease animal models in China. *Scientia Sinica Vitae,* **44**(9): 851-860.

Yamashita A, Fuchs E, Taira M, Yamamoto T, Hayashi M. 2012. Somatostatin-immunoreactive senile plaque-like structures in the frontal cortex and nucleus accumbens of aged tree shrews and Japanese macaques. *Journal of Medical Primatology,* **41**(3): 147-157.

Yan H, Zhong GC, Xu GW, He WH, Jing ZY, Gao ZC, Huang Y, Qi YH, Peng B, Wang HM, Fu LR, Song M, Chen P, Gao WQ, Ren BJ, Sun YY, Cai T, Feng XF, Sui JH, Li WH. 2012. Sodium taurocholate cotransporting polypeptide is a functional receptor for human hepatitis B and D virus. *eLife,* **1**: e00049.

Yan RQ, Su JJ, Huang DR, Gan YC, Yang C, Huang GH. 1996. Human hepatitis B virus and hepatocellular carcinoma. II. Experimental induction of hepatocellular carcinoma in tree shrews exposed to hepatitis B virus and aflatoxin B1. *Journal of Cancer Research and Clinical Oncology,* **122**(5): 289-295.

Yang C, Ruan P, Ou C, Su JJ, Cao J, Luo CP, Tang YP, Wang Q, Qin H, Sun W, Li Y. 2015. Chronic hepatitis B virus infection and occurrence of hepatocellular carcinoma in tree shrews (*Tupaia belangeri chinensis*). *Virology Journal,* **12**: 26.

Yang F, Cao J, Zhang JJ, Wang Q, Su JJ, Yang C, Ou C, Shi JL, Wang DP, Li Y. 2009. Long-term observation of hepatitis B virus (HBV) replication in new-born tree shrews inoculated with HBV. *Chinese Journal of Hepatology,* **17**(8): 580-584.

Yang ZF, Zhao J, Zhu YT, Wang YT, Liu R, Zhao SS, Li RF, Yang CG, Li JQ, Zhong NS. 2013. The tree shrew provides a useful alternative model for the study of influenza H1N1 virus. *Virology Journal,* **10**(1): 111.

Ye LH, He M, Huang YC, Zhao GQ, Lei YJ, Zhou YC, Chen XB. 2016. Tree shrew as a new animal model for the study of lung cancer. *Oncology Letters,* **11**(3): 2091-2095.

Yu WH, Yang CC, Bi YH, Long FY, Li YL, Wang J, Huang F. 2016. Characterization of hepatitis E virus infection in tree shrew (*Tupaia belangeri chinensis*). *BMC Infectious Diseases,* **16**(1): 80.

Zhan LJ, Ding HR, Lin SZ, Tang J, Deng W, Xu YF, Xu YH, Qin C. 2014. Experimental Mycobacterium tuberculosis infection in the Chinese tree shrew. *FEMS Microbiology Letters* **360**(1):23-32.

Zhang LQ, Zhang ZG, Li YH, Liao SS, Wu XY, Chang Q, Liang B. 2015. Cholesterol induces lipoprotein lipase expression in a tree shrew (*Tupaia belangeri chinensis*) model of non-alcoholic fatty liver disease. *Scientific Reports,* **5**: 15970.

Zhang LQ, Wu XY, Liao SS, Li YH, Zhang ZG, Chang Q, Xiao RY, Liang B. 2016. Tree shrew (Tupaia belangeri chinensis), a novel non-obese animal model of non-alcoholic fatty liver disease. *Biology Open,* **5**(10): 1545-1552.

Zhang XH, Dai ZX, Zhang GH, Han JB, Zheng YT. 2013. Molecular characterization, balancing selection, and genomic organization of the tree shrew (*Tupaia belangeri*) MHC class I gene. *Gene,* **522**(2): 147-155.

Zhao F, Guo XL, Wang YJ, Liu J, Lee WH, Zhang Y. 2014. Drug target mining and analysis of the Chinese tree shrew for pharmacological testing. *PLoS One,* **9**(8): e104191.

Zhao XP, Tang ZY, Klumpp B, Wolff-Vorbeck G, Barth H, Levy S, Von Weizsäcker F, Blum HE, Baumert TF. 2002. Primary hepatocytes of Tupaia belangeri as a potential model for hepatitis C virus infection. *The Journal of Clinical Investigation,* **109**(2): 221-232.

Zhong GC, Yan H, Wang HM, He WH, Jing ZY, Qi YH, Fu LR, Gao ZC, Huang Y, Xu GW, Feng XF, Sui JH, Li WH. 2013. Sodium taurocholate cotransporting polypeptide mediates woolly monkey hepatitis B virus infection of *Tupaia hepatocytes*. *Journal of Virology,* **87**(12): 7176-7184.

A new species of the genus *Amolops* (Anura: Ranidae) from high-altitude Sichuan, southwestern China, with a discussion on the taxonomic status of *Amolops kangtingensis*

Liang Fei[1], Chang-Yuan Ye[1], Yu-Fan Wang[2,3], Ke Jiang[1,*]

[1] *Chengdu Institute of Biology*, *Chinese Academy of Sciences*, *Chengdu Sichuan* 610041, *China*

[2] *State Key Laboratory of Genetic Resources and Evolution*, *Kunming Institute of Zoology*, *Chinese Academy of Sciences*, *Kunming Yunnan* 650223, *China*

[3] *Zhejiang Forest Resource Monitoring Center*, *Hangzhou Zhejiang* 310020, *China*

ABSTRACT

A new species of the genus *Amolops* Cope, 1865 is described from Xinduqiao, Kangding, Sichuan. It was previously identified as *Amolops kangtingensis*, which is synonymized to *Amolops mantzorum* in this study. The new species, *Amolops xinduqiao* sp. nov., is distinguished from all other congeners by the following combination of characters: (1) medium body size, adult males SVL 41.2–47.5 mm (*n*=15, average 43.9 mm), adult females SVL 48.5–56.6 mm (*n*=15, average 52.5 mm); (2) head length equal to width or slightly wider than long; (3) tympanum small, but distinct; (4) vomerine teeth in two tiny rows, separated by a space about one vomerine teeth row; (5) bony projections on lower jaw absent; (6) dorsolateral folds usually absent; (7) tarsal folds or glands on tarsus absent; (8) circummarginal groove on disc of finger I absent; (9) tibiotarsal articulation reaching nostril or beyond; (10) webs of toe IV reaching to distal articulation, other toes fully webbed to disc; and (11) vocal sac absent in males.

Keywords: New species; Sichuan; Taxonomy; *Amolops xinduqiao* sp. nov.; *Amolops kangtingensis*

INTRODUCTION

The genus *Amolops* Cope, 1865, which contains 51 species at present (Frost, 2017), is distributed from Nepal, northern India, western and southern China to Malaysia. These species inhabit rocky streams or water falls, from which they receive their common name as cascade frogs. The monophyly of this genus is supported by previous molecular studies (Cai et al., 2007; Stuart, 2008).

Amolops kangtingensis (Liu, 1950) was confused with *Amolops mantzorum* (David, 1871) for a long time. Liu & Hu (1961) synonymized *A. kangtingensis* with *A. mantzorum* due to the difficulty in identification between these two species under preservative condition. Based on karyotyping studies, Wu et al. (1987) supported the validity of *A. kangtingensis*, which was followed by Dubois (1992) and Zhao & Adler (1993), but rejected by Fei et al. (2005, 2009b, 2012). Lu et al. (2014) discussed the validity of *A. kangtingensis* according to molecular data, and Zhang et al. (2015) recognized *A. kangtingensis* through a combination of morphological, karyotypic, and molecular analyses of different populations of these two species. Based on the species delimitation by Zhang et al. (2015), high altitude (above 3 000 m) populations in the Yalong River Basin are considered different from the mid-high altitude (1 200–2 400 m) populations in the Dadu River Basin. However, the above research supporting the validity of *A. kangtingensis* did not examine the originally designated type locality of *A. kangtingensis*. These earlier studies treated Xinduqiao as the type locality; however, according to the original holotype description and information, the type locality of *A. kangtingensis* was limited to Yalagou of Kangding (in the Dadu River Basin) and *A. kangtingensis* should be synonymized with *A. mantzorum*. Thus, herein we describe the Xinduqiao population as a new species.

Received: 05 March 2017; Accepted: 10 May 2017

Foundation items: This study was supported by the Animal Branch of the Germplasm Bank of Wild Species of the Chinese Academy of Sciences (Large Research Infrastructure Funding)

*Corresponding author, E-mail: jiangke87615@hotmail.com

DOI: 10.24272/j.issn.2095-8137.2017.022

MATERIALS AND METHODS

Sampling

A total of 133 individuals (51 adult males and 82 adult females) of the new species were collected from four localities, including Xinduqiao (47 males and 75 females), Liuba (one male), Dongeluo (two males and one female), and Pengbuxi (one male and six females) of Kangding, Sichuan, China. Following euthanasia, five recently collected specimens (KIZ 014127–31 from Xinduqiao in 2016) were fixed in 10% formalin solution after sampling of tissues (in 95% ethanol), and transferred to 75% ethanol after fieldwork. Other specimens (collected from Xinduqiao in 1973 and 1980, Liuba and Dongeluo in 1980, and Pengbuxi in 1984) were fixed and deposited in 10% formalin solution. Holotype, allotype, and 126 paratypes were deposited in the museum of the Chengdu Institute of Biology (CIB), Chinese Academy of Sciences (CAS), with another five paratypes (KIZ 014127–31) deposited in the museum of the Kunming Institue of Zoolgy (KIZ), CAS.

Morphological analysis

Fifteen males and 15 females from Xinduqiao were measured. All measurements were carried out with slide calipers to the nearest 0.1 mm. Morphological characters used and their measurement methods followed Fei et al. (2009a) and Jiang et al. (2016). The morphological characters and their abbreviations are listed below: SVL, snout-vent length; HL, head length (from posterior corner of mandible to tip of snout); HW, head width (at the angle of the jaw); SL, snout length; INS, internarial space; IOS, interorbital space; UEW, width of upper eyelid; ED, eye diameter (horizontal); TD, tympanum diameter (horizontal); LAHL, length of lower arm and hand; LAD, diameter of lower arm; HAL, hand length; HLL, hindlimb length; TL, tibia length; TW, tibia width; TFL, length of tarsus and foot; FL, foot length.

Morphological data of congeners were obtained from previously published literature (Liu, 1950; Fei et al., 2009b).

RESULTS

According to Fei et al. (2005, 2009b), the morphological data support the Xinduqiao population as a new species of the *Amolops mantzorum* group based on the absence of a dorsolateral fold and the absence of a circummarginal groove on the disc of the first finger. The new species differs from all other species of the *A. mantzorum* group by having a relatively small body size; green or brown-colored dorsum, with relatively small spots, and without spines; and small, but distinct tympanum. Additionally, the molecular data support the differentiation between the high altitude (above 3 000 m) population of western Mt. Zheduo in the Yalong River Basin (including Xinduqiao) and the mid-high altitude (1 200–2 400 m) population of the Dadu River Basin (Lu et al., 2014; Zhang et al., 2015).

Amolops xinduqiao Fei, Ye, Wang, and Jiang, sp. nov. (Figures 1–4)

Staurois kangtingensis: Liu, 1950, Fieldiana: Zool. Mem., 2: 349–353.

Amolops kangtingensis: Wu, Tan, and Zhao, 1987, Acta Herpetol. Sinica, 6(4): 39–41; Lu, Bi, and Fu, 2014, Mol. Phylogenet. Evol., 73: 40–52; Zhang, Yuan, Xia, and Zeng, 2015, Sichuan J. Zool., 34(6): 801–809.

Holotype: CIB 80I0692 (Figure 1 A, B), adult male from Xinduqiao (新都桥, N30.14182°, E101.50044°, altitude 3 400 m), Kangding, Sichuan, PR China, collected by Yongzhao Huang on 14 June 1980.

Allotype: CIB 80I0696 (Figure 1 C, D), adult female, same locality and date as holotype.

Figure 1 Holotype and allotype of *Amolops xinduqiao* sp. nov. (Photos by Liang Fei)

Holotype (CIB 80I0692): adult male, dorsal view (A), ventral view (B); allotype (CIB 80I0696): adult female, dorsolateral view (C), ventral view (D).

Paratypes: Xinduqiao (same locality as holotype): 46♂♂, CIB 73I1151–55, 73I1167–69, 73I1173 (11 September 1973), 80I0689, 80I0704, 80I0725–26, 80I0729–30, 80I0736, 80I0738–45, 80I0747, 80I0750–55, 80I0757, 80I0760–61, 80I0765, 80I0767–73, 80I0775 (14 June 1980), 80A0217 (04 August 1980), KIZ 014127, 014130 (31 August 2016); 74♀♀, CIB73I1156–66, 73I1170–1172, 73I1174 (11 September 1973), 80I0683–88, 80I0690–91, 80I0693–95, 80I0697–0703, 80I0705–0724, 80I0727–28, 80I0731–35, 80I0737, 80I0746, 80I0748–49, 80I0759, 80I0762–64, 80I0766, 80I0774 (04 August 1980), 840735 (23 May 1984), KIZ 014128–29, 014131 (31 August 2016). Liuba (六巴), altitude 3 500 m: 1♂, 80I0516 (04 June 1980). Dongeluo (东俄洛), altitude 3 415 m: 2♂♂, 80I0798–99 (15 June 1980); 1♀, 80I0797 (15 June 1980). Pengbuxi (朋布西), altitude 3 300 m: 1♂, 841289 (31 May 1984); 6♀♀, 841290–93 (31 May 1984), 841424–25 (26 May 1984).

Diagnosis: *Amolops xinduqiao* sp. nov. is distinguished from all other congeners by the following combination of characters: (1) medium body size, adult males SVL 41.2–47.5 mm (*n*=15, average 43.9 mm), adult females SVL 48.5–56.6 mm (*n*=15, average 52.5 mm); (2) head length equal to width or slightly wider than long; (3) tympanum small, but distinct; (4) vomerine teeth in two tiny rows, separated by a space about one vomerine teeth row; (5) bony projections on lower jaw absent; (6) dorsolateral folds usually absent; (7) tarsal folds or glands on tarsus absent; (8) circummarginal groove on disc of finger I absent; (9) tibiotarsal articulation reaching nostril or beyond; (10) webs of toe IV reaching to distal articulation, other toes fully webbed to disc; and (11) vocal sac absent in males.

Holotype description: Medium body size, SVL 46.4 mm, slightly compressed in vertical direction. Head length equal to width; snout projecting forward and depressed, slightly pointed at tip; nostril lateral, at middle of snout and eye; canthus rostralis distinct, slightly constricted behind nostrils; loreal region concave and oblique; eye relatively large (ED/HL=0.40); interorbital space less than width of upper eyelid (IOS/UEW=0.85); tympanum small, but distinct, slightly less than one third of eye diameter (TD/ED=0.32); vomerine teeth weakly developed, in two tiny oblique rows between choanae, separated by a space about one vomerine teeth row; tongue pyriform, deeply notched posteriorly; bony projections on lower jaw absent; and vocal sac and vocal sac opening absent.

Forearm robust. Tips of all four fingers expended into discs, disc on finger I smallest, on finger III largest, approximately equal to diameter of tympanum; circummarginal grooves present on tips of outer three fingers, absent on finger I; relative finger length I<II<IV<III; subarticular tubercle distinct; supernumerary tubercles at base of three outer fingers; three metacarpal tubercles, elliptical and flat; and fringe absent.

Hindlimb slender, tibiotarsal articulation reaching nostril, heels overlapping when hind limbs flexed and held perpendicular to body. All five toe tips expanded into discs, relatively smaller than finger discs; relative toe length I<II<III<V<IV; fully webbed on all toes, except toe IV, which is webbed to distal articulation with fringe to base of disc; elongate, oval inner metatarsal tubercle, no outer metatarsal tubercle.

Dorsal side smooth, with sparse tubercles on lateral side of head and body, and around vent; supratympanic fold absent; dorsolateral fold absent; ventral surfaces smooth except lightly flat tubercles on basal ventral surface of thigh.

Coloration of holotype in preservative: Dorsal and lateral sides of head and body gray-brown, with indistinct gray spots; limbs gray-brown, with indistinct gray transverse bands. Ventral sides uniformly light brown, indistinct gray spots on throat and chest.

Second sexual characters: Male without vocal sac or vocal sac opening; inner side of first finger with developed velvety nuptial pad, without spine; forearm of male stronger than forearm of female, and snout-vent length of male smaller than snout-vent length of female.

Variation: The type series measurements are summarized in Table 1–2.

Coloration of paratype in life (KIZ 014127, adult male) (Figure 2; Figure 4A, B): Dorsal head and body brown, with irregular small green spots; lateral head black, edge of upper lip black, white stripe from tip of snout to anterior joint of shoulder; upper part of lateral body green, with indistinct black spots, lower part of lateral body white, with black spots and large blotches; dorsal side of limbs light brown, with black transverse bands. Ventral head and body cream-white, irregular dark gray

Figure 2 Adult male *Amolops xinduqiao* sp. nov. (paratype, KIZ014127) (Photos by Yufan Wang)
A: dorsolateral view; B: dorsal view; C: ventral view.

Table 1 Morphological measurements (mm) of adult males of *Amolops xinduqiao* sp. nov.

Number	Status	SVL	HL	HW	SL	INS	IOS	UEW	ED	TD	LAHL	LAD	HAL	HLL	TL	TW	TFL	FL
CIB80I0692	Holotype	46.4	16.4	16.4	6.5	5.3	4.0	4.7	6.6	2.1	22.8	7.5	14.2	81.6	25.6	7.4	36.5	24.4
CIB80I0704	Paratype	47.5	15.6	16.9	6.5	5.0	4.5	4.3	6.2	2.7	24.8	6.7	14.8	90.0	28.0	7.2	39.4	27.2
CIB80I0725	Paratype	42.5	14.9	14.9	6.9	5.2	4.1	3.4	6.4	2.0	21.4	5.8	12.7	76.8	24.8	6.3	34.0	23.2
CIB80I0729	Paratype	45.3	15.6	15.9	6.4	5.0	4.3	3.8	6.5	2.5	23.2	6.4	14.4	83.2	26.8	7.6	38.2	26.6
CIB80I0730	Paratype	44.9	15.0	16.8	6.4	4.9	4.5	3.7	6.2	2.4	23.7	6.1	14.1	82.1	26.5	6.8	36.6	25.9
CIB80I0737	Paratype	41.6	14.5	14.8	5.5	5.2	3.8	3.6	6.6	2.3	21.2	6.0	12.9	70.8	23.9	5.8	32.9	22.9
CIB80I0738	Paratype	41.8	14.6	15.1	5.6	4.7	4.3	3.6	5.8	2.1	21.7	5.4	13.5	79.1	24.5	5.8	34.3	22.6
CIB80I0739	Paratype	42.1	14.5	14.8	6.4	4.9	3.8	3.3	5.8	2.4	22.2	5.7	13.6	76.9	24.6	6.8	35.3	24.7
CIB80I0740	Paratype	41.2	15.3	15.0	6.4	5.0	4.1	3.6	6.4	2.0	22.1	6.0	12.9	72.1	23.6	6.6	33.9	24.0
CIB80I0741	Paratype	41.9	14.8	14.4	6.3	4.8	3.5	3.9	6.7	2.2	21.1	5.9	12.7	72.4	24.0	5.9	33.9	22.7
CIB80I0742	Paratype	42.6	14.0	14.6	6.0	4.8	3.7	3.4	6.2	2.5	21.5	5.4	12.9	77.1	24.8	6.7	35.3	24.3
CIB80I0743	Paratype	45.0	15.6	15.9	6.6	5.3	4.4	4.0	6.3	2.1	22.3	6.6	13.1	75.2	25.4	6.4	35.6	25.6
CIB80I0744	Paratype	45.4	14.2	15.2	5.7	4.4	4.4	3.5	6.2	2.3	23.0	6.1	13.6	81.7	25.7	6.8	36.8	25.8
CIB80I0747	Paratype	45.8	15.8	16.1	5.9	5.2	3.6	3.5	6.9	2.2	22.5	6.6	13.7	77.8	25.7	7.3	36.5	25.4
CIB80I0775	Paratype	44.2	14.6	14.3	6.1	4.9	4.0	3.4	6.1	2.5	21.9	6.0	12.9	74.5	24.3	7.2	33.7	23.8
Range		41.2–47.5	14.0–16.4	14.3–16.9	5.5–6.9	4.4–5.3	3.5–4.5	3.3–4.7	5.8–6.9	2.0–2.7	21.1–24.8	5.4–7.5	12.7–14.8	70.8–90.0	23.6–28.0	5.8–7.6	32.9–39.4	22.6–27.2
Average		43.9	15.0	15.4	6.2	5.0	4.1	3.7	6.3	2.3	22.4	6.2	13.5	78.1	25.3	6.7	35.6	24.6
Ratio to SVL			34.2%	35.1%	14.1%	11.3%	9.2%	8.5%	14.4%	5.2%	51.1%	14.1%	30.7%	177.9%	57.5%	15.3%	81.0%	56.1%

Table 2 Morphological measurements (mm) of adult females of *Amolops xinduqiao* sp. nov.

Number	Status	SVL	HL	HW	SL	INS	IOS	UEW	ED	TD	LAHL	LAD	HAL	HLL	TL	TW	TFL	FL
CIB80I0696	Allotype	53.7	17.4	17.8	7.8	5.7	4.8	4.5	6.7	2.1	27.8	5.6	17.0	100.2	30.9	8.2	43.9	30.8
CIB80I0683	Paratype	52.8	17.2	17.5	7.3	5.8	4.5	4.3	6.7	2.1	25.9	5.3	15.6	89.5	28.8	7.4	39.4	28.4
CIB80I0685	Paratype	50.5	17.0	18.1	6.9	5.6	4.6	4.3	6.2	2.2	26.3	5.2	15.6	88.3	28.8	8.2	40.1	28.9
CIB80I0687	Paratype	54.1	18.4	19.6	7.7	6.0	5.2	4.6	7.3	2.6	28.2	5.7	16.4	96.7	31.0	8.0	43.9	30.5
CIB80I0688	Paratype	49.5	17.3	17.1	7.3	5.5	4.7	3.8	6.2	1.8	26.0	4.8	15.8	85.5	29.0	6.2	40.4	29.0
CIB80I0694	Paratype	51.9	17.3	16.7	7.1	5.7	4.7	4.3	7.2	2.3	26.4	4.7	15.6	89.5	28.3	6.0	41.6	28.5
CIB80I0695	Paratype	56.6	18.1	18.9	8.2	5.9	4.9	4.3	6.4	2.7	29.1	5.4	16.6	102.6	32.0	8.4	44.2	30.0
CIB80I0705	Paratype	52.7	17.2	18.1	7.9	5.3	4.5	3.9	7.1	2.2	26.0	4.9	15.5	91.2	28.6	7.6	41.4	29.1
CIB80I0707	Paratype	50.9	16.6	16.6	7.3	5.3	4.6	4.2	6.9	1.8	26.2	4.9	16.1	93.6	28.5	6.9	40.9	28.9
CIB80I0709	Paratype	54.3	17.2	17.6	7.9	5.3	5.0	4.1	6.6	2.2	25.7	5.7	15.1	95.0	29.7	7.1	41.4	28.8
CIB80I0712	Paratype	50.6	17.1	17.2	7.4	5.3	4.6	4.3	6.1	2.3	25.9	4.9	15.8	88.2	29.4	7.1	40.2	27.0
CIB80I0718	Paratype	54.6	18.1	17.8	8.0	5.4	4.7	4.5	6.8	2.4	27.1	4.8	16.1	97.6	30.7	7.4	42.9	30.2
CIB80I0721	Paratype	48.5	17.0	17.0	7.1	5.4	4.2	4.8	6.4	2.0	24.8	4.8	14.9	88.3	29.4	7.1	40.4	28.9
CIB80I0723	Paratype	53.6	17.8	17.7	7.3	5.8	4.6	3.8	6.3	2.8	26.9	5.4	15.6	95.3	28.1	7.6	41.1	28.3
CIB80I0753	Paratype	53.5	17.1	17.3	7.3	5.5	4.4	4.5	6.9	1.9	25.8	5.2	15.6	86.4	28.2	6.9	39.3	28.2
Range		48.5–56.6	16.6–18.4	16.6–19.6	6.9–8.2	5.3–6.0	4.2–5.2	3.8–4.8	6.1–7.3	1.8–2.8	24.8–29.1	4.7–5.7	14.9–17.0	85.5–102.6	28.1–32.0	6.0–8.4	39.3–44.2	27.0–30.8
Average		52.5	17.4	17.7	7.5	5.6	4.7	4.3	6.7	2.2	26.6	5.2	15.8	92.7	29.5	7.3	41.4	29.0
Ratio to SVL			33.1%	33.7%	14.3%	10.6%	8.9%	8.2%	12.7%	4.3%	50.6%	9.8%	30.1%	176.5%	56.2%	13.9%	78.9%	55.2%

spots on throat, chest, and sides of belly; ventral side of limbs flesh-colored, without spots; toe webs gray with yellow; iris light brown, with small black spots.

Coloration of paratype in life (KIZ 014129, adult female) (Figure 3; Figure 4C, D): Dorsal head and body green, with reticulate black-brown spots; lateral head green, with black spots, edge of upper lip black, white stripe from tip of snout to anterior of shoulder; upper part of lateral body green, lower part of lateral body white, both with large black blotches; dorsal side of limbs green-yellow, with distinct black transverse bands and spots. Ventral head and body cream-white, irregular gray spots on throat and chest; ventral side of limbs flesh-colored, without spots; toe webs gray with yellow; iris yellow-gray, with small black spots.

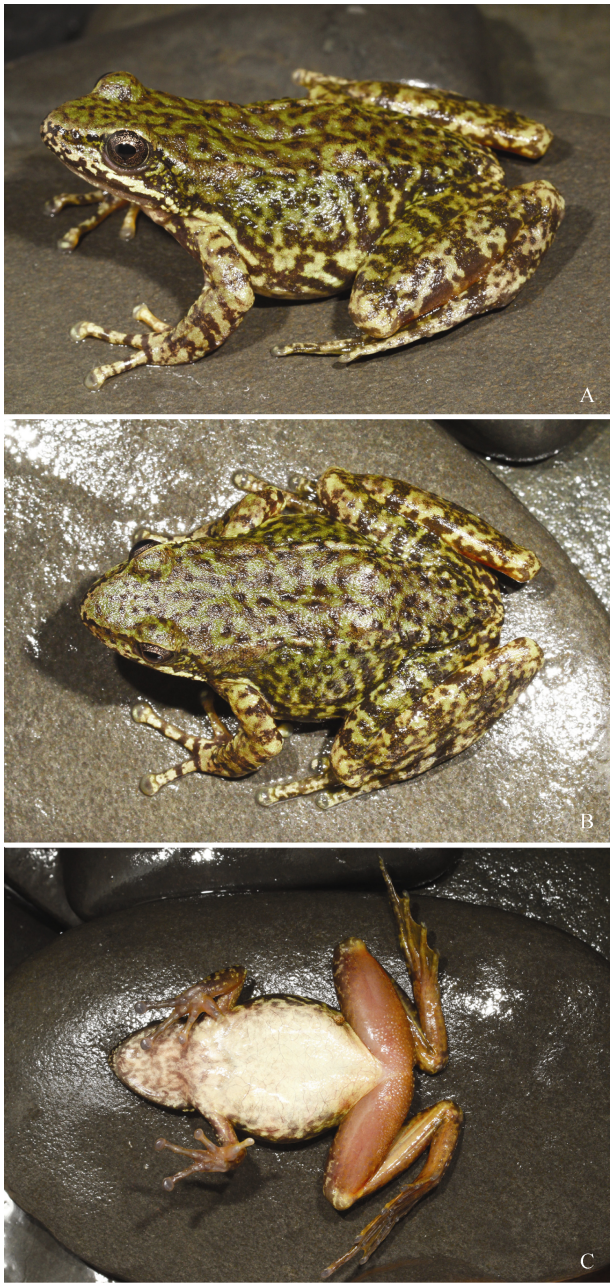

Figure 3 Adult female *Amolops xinduqiao* sp. nov. (paratype, KIZ014129) (Photos by Yufan Wang)
A: dorsolateral view; B: dorsal view; C: ventral view.

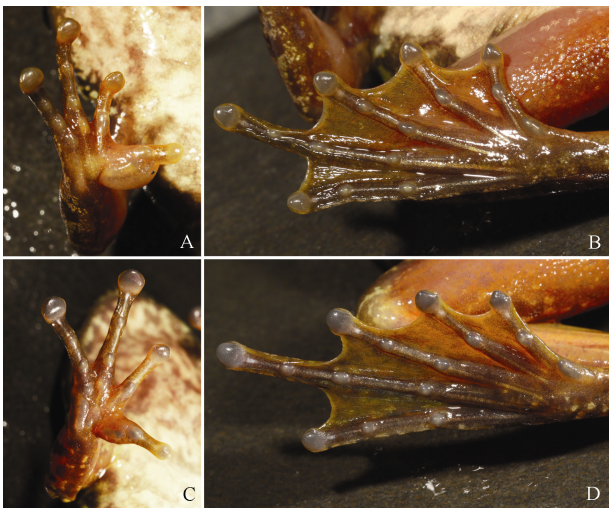

Figure 4 Ventral view of hand and foot of *Amolops xinduqiao* sp. nov.
Paratype (KIZ014127) hand (A) and foot (B) of adult male; Paratype (KIZ014129) hand (C) and foot (D) of adult female.

Habitat: This frog lives at an altitude of 3 300 to 3 500 m, close to slow-moving mountain rivers or large streams in habitats with a few tall trees and with dense shrubs and weeds. Adult frogs often perch on rocks for foraging at night, but hide under rocks and grass during the day. Male and female frogs were collected during amplexus in a river near Xinduqiao on 11 September 1973, with dissection of the female specimens showing eggs with a diameter of 2.5 mm in the fallopian tube about to be spawned. Dissection of a female specimen collected on 04 June 1980, showed the biggest eggs in the ovaries to be 1.5 mm in diameter, and not yet mature. It is reasoned that the breeding season of this frog might be around September. However, breeding habitats and egg masses have yet to be confirmed.

Comparison: According to Fei et al. (2005, 2009b, 2012), five species, i.e., *A. granulosus* (Liu & Hu, 1961), *A. lifanensis* (Liu, 1945), *A. loloensis* (Liu, 1950), *A. mantzorum* (David, 1871), and *A. viridimaculatus* (Jiang, 1983), exist in the *A. mantzorum* species group, which is characterized by the absence of a dorsolateral fold and circummarginal groove at the first finger.

Amolops xinduqiao sp. nov. differs from *A. granulosus* by having a smooth dorsal surface, without spines, and no vocal sac (*v.s.* spines on dorsal surface and a pair of internal subgular vocal sacs) (Fei et al., 2009b).

Amolops xinduqiao sp. nov. differs from *A. lifanensis*, *A. loloensis*, *A. mantzorum*, and *A. viridimaculatus* by having a smaller body size, males SVL 41.2–47.5 mm (*n*=15), females SVL 48.5–56.6 mm (*n*=15) (*v.s.* males SVL 52.0–56.0 mm (*n*=5), females SVL 61.0–79.0 mm (*n*=10) in *A. lifanensis*; males SVL 54.5–62.0 mm (*n*=19), females SVL 69.5–77.5 mm (*n*=20) in *A.*

loloensis; males SVL 49.0–57.0 mm (*n*=10), females SVL 59.0–72.0 mm (*n*=10) in *A. mantzorum*; males SVL 72.7–82.3 mm (*n*=19), females SVL 83.0–94.3 mm (*n*=10) in *A. viridimaculatus*) (Fei et al., 2009b).

Amolops xinduqiao sp. nov. further differs from *A. lifanensis* by having a distinct tympanum (*v.s*. tympanum indistinct); differs from *A. loloensis* and *A. viridimaculatus* by having no large brown or green spots on dorsum (*v.s*. large brown spots on dorsum in *A. loloensis*, large green spots on dorsum in *A. viridimaculatus*); differs from *A. mantzorum* by different dorsal coloration and pattern, dorsum brown, with irregular green spots, or dorsum green, with reticulate black-brown spots (*v.s.* dorsum brown, with a few large green blotches (Figure 5)) (Fei et al., 2009b).

Figure 5 Topotype of *Amolops mantzorum*, Baoxing, Sichuan (Photos by Liang Fei)
A: dorsolateral view; B: ventral view.

Etymology: The specific name "*xinduqiao*" is named after the type locality Xinduqiao of Kangding, Sichuan. According to the Latin name, we suggest the English common name as "Xinduqiao torrent frog or Xinduqiao cascade frog", and the Chinese common name as "新都桥湍蛙".

DISCUSSION

Amolops kangtingensis was described by Liu (1950). Based on the original designation, the holotype (Figure 6) is a female from "Kangting (=Kangding), Sikang (now part of Sichuan), 8 000 feet (~2 400 m)", with catalogue number 49412 in the Chicago Natural History Museum (now Field Museum of Natural History), and corresponding to field number 582 (from the collection database of the Field Museum). The holotype (No. 582) measurements were provided in the measurement table on page 351 (Liu, 1950), with body length 74.0 mm. Liu (1950) designated 29 paratypes, with the localities and altitudes provided, including: (1) 16 males, five females, and two young individuals collected with the holotype from Yalakou (=Yalagou) inside Kangting City (with three males and four females measured); four specimens from Tatu River (=Dadu River, altitude 4 500 feet (~1 370 m)) of Luting (=Luding), with the 27 frogs representing *A. kangtingensis* (=*A. mantzorum*); and (2) two paratypes from Chuwo (=Zhuwo, altitude 11 000 feet (~3 350 m)) of Luhohsien (=Luhuo) and Hsintuchiao (=Xinduqiao, altitude 11 200 feet (~3 410 m)) representing *A. xinduqiao* sp. nov.

Figure 6 Holotype of *Amolops kangtingensis* (No. 49412, female) (Provided by Alan Resetar, the Field Museum, USA)
A: dorsal view; B: ventral view.

According to the molecular data provided by Lu et al. (2014) and Zhang et al. (2015), the high altitude (above 3 000 m) populations of western Mt. Zheduo in the Yalong River Basin (including localities Jiagenba, Pengbuxi, Xinduqiao of Kangding, as well as Luhuo and Yajiang) form a monophyletic group, which should be identified as *A. xinduqiao* sp. nov. The populations of western Mt. Zheduo differ from the mid-high altitude (1200–2400 m) populations of the Dadu River Basin (including localities Kangding City (county town), Yalagou of Kangding, and Luding), which should be identified as *A. mantzorum*.

Based on the original designation, the holotype of *A. kangtingensis* was collected from Yalagou of Kangding City at an altitude of ~2 400 m, and should be identified as *A.*

mantzorum according to Lu et al. (2014) and Zhang et al. (2015). The large body size (female SVL 74.0 mm) of the holotype of *A. kangtingensis* also differs from *A. xinduqiao* sp. nov. (females SVL up to 56.6 mm). Additionally, the measurements of the paratypes of *A. kangtingensis* (males SVL 53.0–57.0 mm, females SVL 70.0–74.0 mm) provided by Liu (1950) are similar to those of the topotypes of *A. mantzorum* (males SVL 49.0–57.0 mm, females SVL 59.0–72.0 mm (Fei et al., 2009b)), but different from *A. xinduqiao* sp. nov. Thus, as above, the type locality of *A. kangtingensis* is limited to Yalagou of Kangding, and *A. kangtingensis* should be synonymized with *A. mantzorum*.

ACKNOWLEDGEMENTS

We are grateful to Dr. Jing Che (KIZ) for her kind support in this study. We thank Mr. Qi Liu for fieldwork in Xinduqiao, Prof. Yuezhao Wang, Prof. Yueying Chen, and Mr. Ke Lu (CIB) for their help and permission to examine the related museum specimens, and the Field Museum (USA) for supplying photos of holotype of *Amolops kangtingensis*. We also thank the reviewers for their critical reading of this manuscript.

REFERENCES

Cai HX, Che J, Pang JF, Zhao EM, Zhang YP. 2007. Paraphyly of Chinese *Amolops* (Anura, Ranidae) and phylogenetic position of the rare Chinese frog, *Amolops tormotus*. *Zootaxa*, 1531: 49–55.

Dubois A. 1992. Notes sur la classification des Ranidae (Amphibiens Anoures). *Bulletin Mensuel de la Société Linnéenne de Lyon*, 61 (10): 305–352.

Fei L, Ye CY, Huang YZ. 2005. An Illustrated Key to Chinese Amphibians. Chengdu: Sichuan Publishing House of Science and Technology, 1-340. (in Chinese)

Fei L, Hu SQ, Ye CY, Huang YZ. 2009a. Fauna Sinica, Amphibia, Vol. 2: Anura. Beijing: Science Press, 1-959. (in Chinese)

Fei L, Hu SQ, Ye CY, Huang YZ. 2009b. Fauna Sinica, Amphibia, Vol. 3 Anura Ranidae. Beijing: Science Press, 959-1847. (in Chinese)

Fei L, Ye CY, Jiang JP. 2012. Colored Atlas of Chinese Amphibians and Their Distributions. Chengdu: Sichuan Publishing House of Science and Technology, 1-619. (in Chinese)

Frost DR. 2017. Amphibian Species of the World: an Online Reference. Version 6.0. [DB/OL]. [2017-03-10]. http://research.amnh.org/herpetology/amphibia/index.html.

Jiang K, Wang K, Yan F, Xie J, Zou DH, Liu WL, Jiang JP, Li C, Che J. 2016. A new species of the genus *Amolops* (Amphibia: Ranidae) from southeastern Tibet, China. *Zoological Research*, **37**(1): 31-40.

Liu CC. 1950. Amphibians of Western China. Fieldiana, Zoology Memoirs, 2: 1-400.

Liu CJ, Hu SQ. 1961. Tailless Amphibians of China. Beijing: Science Press, 1-364. (in Chinese)

Lu B, Bi K, Fu JZ. 2014. A phylogeographic evaluation of the *Amolops mantzorum* species group: Cryptic species and plateau uplift. *Molecular Phylogenetics and Evolution,* **73**: 40-52.

Stuart BL. 2008. The phylogenetic problem of *Huia* (Amphibia: Ranidae). *Molecular Phylogenetics and Evolution,* **46**(1): 49-60.

Wu GF, Tan AM, Zhao EM. 1987. Cytoological evidence for the validity of *Amolops kangtingensis*. *Acta Herpetologica Sinica,* **6**(1): 39-41. (in Chinese)

Zhang CH, Yuan SQ, Xia Y, Zeng XM. 2015. Species delimitation of *Amolops kangtingensis*. *Sichuan Journal of Zoology,* **34**(6): 801-809. (in Chinese)

Zhao EM, Adler K. 1993. Herpetology of China. Oxford: Society for the Study of Amphibians & Reptiles, 1-522.

Pulmonary immune cells and inflammatory cytokine dysregulation are associated with mortality of IL-1R1$^{-/-}$ mice infected with influenza virus (H1N1)

Lei Guo[1,#], Yan-Cui Wang[1,#], Jun-Jie Mei[1,2], Ruo-Tong Ning[1], Jing-Jing Wang[1], Jia-Qi Li[1], Xi Wang[1], Hui-Wen Zheng[1], Hai-Tao Fan[1], Long-Ding Liu[1,*]

[1] *Department of Viral Immunology*, *Institute of Medical Biology*, *Chinese Academy of Medical Science and Peking Union Medical College*, *Kunming Yunnan* 650118, *China*

[2] *Division of Neonatology*, *Department of Pediatrics*, *Children's Hospital of Philadelphia*, *Perelman School of Medicine*, *University of Pennsylvania*, *Philadelphia* 19104, *USA*

ABSTRACT

Respirovirus infection can cause viral pneumonia and acute lung injury (ALI). The interleukin-1 (IL-1) family consists of proinflammatory cytokines that play essential roles in regulating immune and inflammatory responses *in vivo*. IL-1 signaling is associated with protection against respiratory influenza virus infection by mediation of the pulmonary anti-viral immune response and inflammation. We analyzed the infiltration lung immune leukocytes and cytokines that contribute to inflammatory lung pathology and mortality of fatal H1N1 virus-infected IL-1 receptor 1 (IL-1R1) deficient mice. Results showed that early innate immune cells and cytokine/chemokine dysregulation were observed with significantly decreased neutrophil infiltration and IL-6, TNF-α, G-CSF, KC, and MIP-2 cytokine levels in the bronchoalveolar lavage fluid of infected IL-1R1$^{-/-}$ mice in comparison with that of wild type infected mice. The adaptive immune response against the H1N1 virus in IL-1R1$^{-/-}$ mice was impaired with downregulated anti-viral Th1 cell, CD8+ cell, and antibody functions, which contributes to attenuated viral clearance. Histological analysis revealed reduced lung inflammation during early infection but severe lung pathology in late infection in IL-1R1$^{-/-}$ mice compared with that in WT infected mice. Moreover, the infected IL-1R1$^{-/-}$ mice showed markedly reduced neutrophil generation in bone marrow and neutrophil recruitment to the inflamed lung. Together, these results suggest that IL-1 signaling is associated with pulmonary anti-influenza immune response and inflammatory lung injury, particularly via the influence on neutrophil mobilization and inflammatory cytokine/chemokine production.

Keywords: Influenza; Lung inflammation; IL-1 receptor 1; Neutrophil

INTRODUCTION

Respirovirus infection causes respiratory illness that affects millions of people every year (Coates et al., 2015). The virus enters a host through an upper respiratory infection, and directly infects and proliferates in the airway epithelial cells, alveolar epithelial cells, and immune cells. Viral infection triggers cellular immune pathways to express abundant inflammatory cytokines and chemokines, including TNF-α, IL-1α/β, IL-2, IL-4, IL-6, IFN-α/β, CXCL-1/2, CXCL-9/10, MIP-1/2, and MCP-1, in the respiratory tract and alveolar spaces (Kohlmeier & Woodland, 2009; Sanders et al., 2011). These cytokines, in turn, recruit innate immune cells such as macrophages, granulocytes, dendritic cells (DCs), and natural killer (NK) cells into the infected lung to exert anti-viral innate immune responses. Following infection, antigen-presenting cells (APCs) migrate back to the lung-draining lymph node and activate adaptive immune T cells and B cells. Thus, the activated cellular and humoral immune responses ultimately clear viral replication and infection (Braciale et al., 2012; Tripathi

Received: 28 February 2017; Accepted: 19 April 2017

Foundation items: This work was supported by the National Natural Science Foundation of China (31300143, 31570900), the Applied Basic Research Foundation of Yunnan Province, China (2015FB139), and the Chinese Academy of Medical Science (CAMS) Innovation Fund for Medical Sciences (2016-I2M-1-014)

[#]Authors contributed equally to this work

[*]Corresponding author, E-mail: liuld@imbcams.com.cn

DOI: 10.24272/j.issn.2095-8137.2017.035

et al., 2015). Although an effective anti-viral immune response is necessary for viral clearance, a prolonged or exaggerated response can damage the respiratory tract, endangering respiration physiology. In clinically critical influenza A virus (IAV) infection, mortality is often correlated with severe pneumonia and inflammatory lung injury characterized by massive inflammatory cell infiltration and a cytokine storm in the lung (Damjanovic et al., 2012).

Interleukin-1 (IL-1) signaling is accomplished by two major proinflammatory cytokines, namely, IL-1α and IL-1β, both of which bind to the type I IL-1 receptor (IL-1R1) of structural and immune cells in different tissues, leading to transcription and expression of multiple immune/inflammation-associated genes, including cytokines, chemokines, and adhesion molecules (Weber et al., 2010). The main function of IL-1 signaling is the regulation of innate immune reactions and inflammatory responses to infections or sterile insults from damaged cells (Dinarello, 2009). Using an IL-1R1 knockout (IL-1R1$^{-/-}$) mouse model, Schmitz et al. revealed that IL-1 plays an essential role in protecting mice from IAV infection and limiting viral proliferation. IL-1 deficiency leads to reduced lung immunopathology at the early infection stage and impairment of the anti-viral immune response (Schmitz et al., 2005). To gain insight into the lung immune and inflammation responses regulated by IL-1 signaling from the initial to late infection periods of fatal IAV infection, we continuously monitored lung leukocyte infiltration and cytokine expression in IL-1R1$^{-/-}$ mice infected with a lethal dose of influenza H1N1. Our results suggest that the lack of IL-1 signaling induces an impaired innate and adaptive immune response, together with an increased inflammation response and immunopathology following fatal IAV infection in the infected mouse lung, and contributes to impaired viral clearance and high mortality.

MATERIALS AND METHODS

Animals and virus

The IL-1R1$^{-/-}$ and wild type (WT) control C57BL/6 mice were purchased from Jackson Laboratories (USA). The mice were raised and maintained in individually ventilated cages at the Central Animal Care Services of the Institute of Medical Biology, Chinese Academy of Medical Sciences (IMB, CAMS), under specific-pathogen-free conditions. Male mice aged 8–12 weeks were used in all experiments. The mouse-adapted A/Puerto Rico/8/1934 H1N1 (A/PR/8) influenza virus was stored in our laboratory. The virus was grown in chorioallantoic fluid of 9-day-old embryonated chicken eggs. The titer of the virus was determined by 50% cell culture infective dose ($CCID_{50}$) in Madin-Darby canine kidney (MDCK) cells as per Reed and Muench (Szretter et al., 2007).

Mouse infection model

The WT and IL-1R1$^{-/-}$ mice (*n*=35 of each group) were anesthetized by intraperitoneal injection of pentobarbital (50 mg/kg) and then inoculated intranasally with 2 000 $CCID_{50}$ of influenza virus in 30 μL of PBS. Weight loss was monitored and survival curves were generated. All animal experiments were conducted in a biosafety laboratory (BSL-2) with approval from the Animal Ethics Committee of IMB, CAMS, under permit number [2014]43 and in accordance with the National Guidelines on Animal Work in China.

Viral loads

Mice (*n*=3 of each group) were sacrificed every two days post-infection (dpi), with lung tissue samples then harvested and weighed. Samples were mechanically homogenized using a TGrinder instrument (Tiangen Biotechnologies, China), and RNA was isolated using TRNzol A+ reagent (Tiangen Biotechnologies, China). The RNA concentration of each sample was determined by UV 260/280 using a Nanodrop 2000 (Thermo-Fisher Scientific, USA). Total RNA (100 ng) was reverse transcribed and amplified using the One Step PrimeScript™ RT-PCR Kit (Takara Biotechnologies, China) on an Applied Biosystems 7500 Real-Time PCR System (Life Technologies, USA). To determine the viral loads, the primers and probe for the viral matrix protein gene (M gene) were used: 5'-AAGACCAATCCTGTCACCTCTGA-3' (forward), 5'-CAAAGCGTCTACGCTGC AGTCC-3' (reverse), 5'-(FAM)-TTTGTGTTCACGCTCACCGT-(TAMRA)-3' (probe). The M genes of the A/PR/8 viruses were cloned into the pMD18-T vector, which was used to create a standard curve by 10-fold serial dilution. Viral copy numbers were normalized to the original tissue sample masses and calculated based on the standard curve described above. The RNA samples from each individual were quantified in triplicate.

BALF cells and total proteins

The mice were anesthetized, sacrificed, and bled (*n*=4 of each group). After the trachea was exposed, the lungs were lavaged four times with 0.8 mL of cold, sterile PBS, and the bronchoalveolar lavage fluid (BALF) was centrifuged at 1 500 g for 10 min at 4 °C. Supernatants were collected and stored at -80 °C for protein, chemokine, and cytokine detection. Total leukocytes in the BALF were counted and resuspended at 10^5/mL with PBS. The solutions (200 μL) were then cytospun onto slides, and cells were stained with a Wright's-Giemsa stain kit (Nanjing Jiancheng Bioengineering, China) for differential leukocyte counts in five random fields under a microscope.

Lung pathology and wet/dry weight

Mice were euthanized and the lungs were slowly inflated by instilling 1 mL of 4% formaldehyde intratracheally. The trachea was tightened, and the lungs were fixed in formalin for 48 h at 4 °C and paraffin embedded. Lung tissue sections (5 μm) were then stained with hematoxylin and eosin (H&E) according to routine procedures. Images were obtained by light microscopy. Lung histological scores were measured by a blinded pathologist with a 0 to 4-point scale according to combined assessments of alveolar structure, inflammatory cell infiltration, aggregation in alveolar spaces and septa, bronchiolitis, and lung edema. A score of 0 represented no damage; I represented mild damage; 2 represented moderate damage; 3 represented severe damage; and 4 represented very severe histological changes, with an increment of 0.5 if the

inflammation fell between two integers. In each tissue sample three random areas were scored and the mean value was calculated. The histology score was the median value of four mice.

The lungs of mice (*n*=3 of each group) were harvested at 9 dpi and weighed immediately (wet weight). The lung tissue was then dried in an oven at 60 °C for 72 h and reweighed (dry weight). The wet-to-dry ratio was calculated for each animal to assess tissue edema.

Hemagglutination inhibition (HI) assay

Sera were prepared from the blood of infected mice (*n*=4 of each group) at 8 dpi. Before the test, any non-specific inhibitors of hemagglutination were removed by diluting sera with receptor destroying enzyme (RDE, Denka Seiken Co., Ltd, Japan) at a 1: 5 ratio, and incubating at 37 °C overnight. The enzyme was inactivated by 2 h-incubation at 56 °C followed by the addition of 0.1% sodium citrate. The HI assay was performed using the A/PR/8 strain with 1% chicken erythrocytes in V-bottom 96-well microtiter plates.

Flow cytometry

Bone marrow and mediastinal lymph nodes were aseptically removed at the time of necropsy (*n*=4 of each group). Single-cell suspensions were obtained by flushing the bone marrow or gently pressing the lymph node against a 70-μm strainer into PBS. Cells were washed in fluorescence-activated cell sorting (FACS) buffer after lysing with ammonium chloride potassium (ACK) buffer. Cell surface staining was done using anti-mouse Gr-1-FITC, CD3-PerCP, CD4-PE, CD8-FITC, and CD19-APC (BD Biosciences, USA). For influenza-specific CD8+ cells, mediastinal lymph node cells were stimulated overnight with formalin-inactivated Influenza A PR/8/34 H1N1 (MOI=4). Brefeldin A (BFA, 1 μmol/L) was added after overnight stimulation and cells were incubated for an additional 5 h. After that, cells were surface stained with anti-mouse CD8-FITC, then permeabilized with Cytofix-Cytoperm solution (BD Biosciences, USA) and stained with intracellular anti-mouse IFN-γ-APC. Flow cytometry data were collected on the FACS Canto (BD Biosciences, USA) and analyzed using FlowJo version 7.6.1.

Cytokine assays

The Bio-Plex Suspension Array System (Bio-Rad, USA) was used to evaluate the BALF cytokines. The mouse cytokine Th1/Th2 assay was introduced to test IL-2, IL-4, IL-5, IL10, IL-12p70, and IFN-γ according to the user manual. The concentrations of cytokines, G-CSF, TNF-α, IL-1β, IL-6, KC, and MIP-2 in the mouse BALF and sera were determined with ELISA kits (Neobioscience, China) in accordance with the manufacturer's instructions.

Statistical analyses

We performed all statistical analyses with GraphPad Prism software (version 4). The data obtained from all experiments are presented as the means±*SD*, with $P<0.05$ considered statistically significant using Student's *t*-test.

RESULTS

Survival and viral loads in H1N1-infected mouse lungs

The deaths of WT mice were primarily observed at 7–9 dpi, with no deaths occurring after this time (survival rate 58%) (Figure 1A), whereas the IL-1R1$^{-/-}$ mice began to die at 5 dpi. All IL-1R1$^{-/-}$ mice died by 9 dpi, with no survivors (Figure 1A). Viral replication in the infected mouse lungs was quantified using viral load tests, which reached high levels in both WT and IL-1R1$^{-/-}$ mice at 3 dpi (approximately 10^6 copies/100 ng RNA) (Figure 1B). The viral loads of WT mice began to decline at 5 dpi, and the virus was cleared to approximately 2×10^2 copies/100 ng RNA at 11 dpi. In IL-1R1$^{-/-}$ mice, the viral loads began to decrease at 7 dpi, but remained at high levels of 10^5 and 10^4 copies/100 ng RNA at 7 and 9 dpi, respectively, which were significantly different than the levels observed in WT mice (Figure 1B). These results revealed that in comparison to WT mice, IL-1R1$^{-/-}$ mice suffered high mortality under fatal H1N1 virus challenge, and failed to effectively clear the H1N1 influenza virus during the progression of infection.

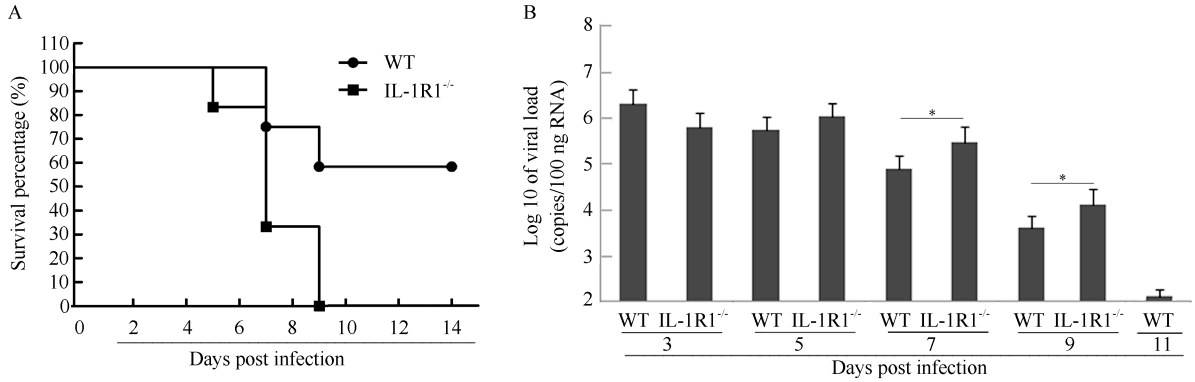

Figure 1 IL-1R1$^{-/-}$ results in enhanced mortality and impaired viral clearance after infection with H1N1 influenza virus

WT and IL-1R1$^{-/-}$ mice were infected intranasally with a fatal dose of the H1N1 A/PR/8 virus (2 000 $CCID_{50}$). A: A Kaplan-Meier survival curve of infected mice (*n*=12) is shown; B: Lungs were harvested from the infected mice at the indicated dpi, and homogenates were prepared for viral loads. Viral loads were determined based on the number of influenza M gene RNA copies detected by RT-PCR. Error bars represent the standard deviation of triplicate samples, *: $P<0.05$ based on Student's *t*-test.

Histopathology of infected lungs and BALF inflammatory cytokine levels

The H&E staining of the lung tissue revealed the presence of lung inflammation in both WT and IL-1R1$^{-/-}$ mice at 3 dpi. Symptoms included inflammatory cell infiltration into the lung parenchyma and interstitium, thickening of bronchial epithelium, and alveolar expansion (Figure 2A). Unlike WT mice, IL-1R1$^{-/-}$

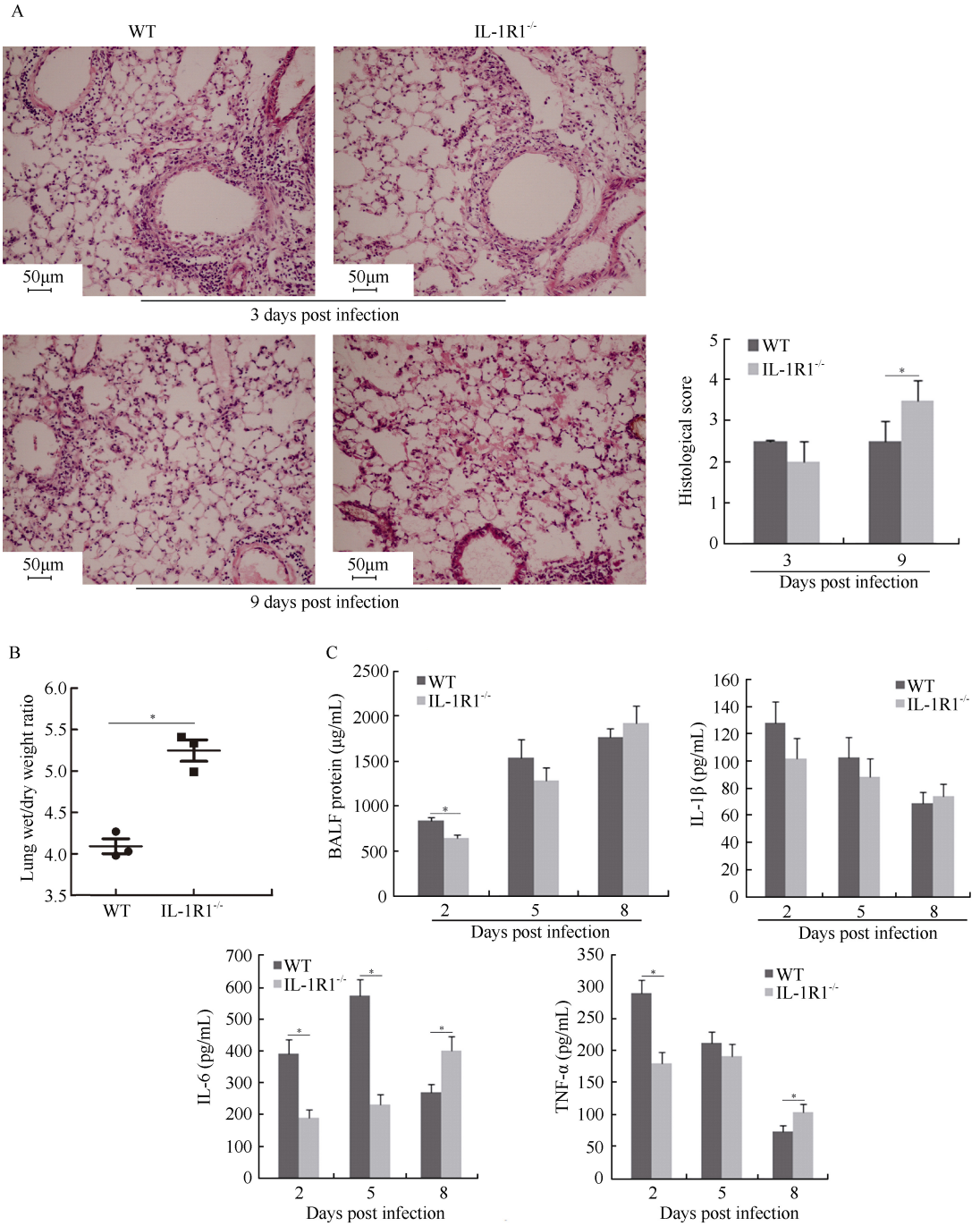

Figure 2 Increased lung inflammation and damage in IL-1R1$^{-/-}$ mice after H1N1 influenza virus infection

A: Histopathology of H&E stained lung sections from WT and IL-1R1$^{-/-}$ mice at 3 and 9 dpi. Lung injury histological scores as described in Materials and Methods. Data shown represent histology scores of median values from four mice. Scale bar, 50 μm; B: Infected mouse lung wet-to-dry ratios were used to assess lung edema at 9 dpi; C: Total protein concentrations and expression levels of IL-1β, TNF-α, and IL-6 cytokines in the BALF of infected mouse lungs were determined at 2, 5, and 8 dpi. Error bars represent the standard deviation of three samples. *: P<0.05 based on Student's t-test.

mice had less inflammatory cell aggregation in the bronchial walls and alveolar spaces (Figure 2A). At the late stage of infection (9 dpi), lung inflammation had gradually regressed in the surviving WT mice, with the alveolar structure tending to be complete and a small number of inflammatory cells aggregating around a portion of the lung parenchyma (Figure 2A). However, both disruption of the alveolar structure and formation of a hyaline membrane were seen in the lungs of dying IL-1R1$^{-/-}$ mice during late infection, with congestion and swelling of the lung interstitium (Figure 2A). Histological scores demonstrated that IL-1R1$^{-/-}$ mice exhibited less severe lung pathology than that of WT mice during the early infection stage, but significantly more severe lung pathology during the late infection stage (Figure 2A). The lung wet-to-dry ratios of IL-1R1$^{-/-}$ mice were significantly higher than those of WT mice at 9 dpi, suggesting that the IL-1R1$^{-/-}$ mice suffered more severe lung edema during late infection (Figure 2B). Analysis of the total protein concentrations and inflammatory cytokine levels in the BALF from infected mice showed that the protein concentration and IL-1β, IL-6, and TNF-α levels were significantly higher in WT mice than in IL-1R1$^{-/-}$ mice at 2 dpi (Figure 2C). At 8 dpi, the levels of IL-6 and TNF-α were significantly higher in IL-1R1$^{-/-}$ mice than in WT mice (Figure 2C). Thus, compared with the decreasing inflammation and pathology in the lungs of WT mice, the inflammatory lung pathology was continuously aggravated in IL-1R1$^{-/-}$ mice.

BALF leukocytes and viral-induced immune response analysis

Lung BALF leukocytes from infected WT and IL-1R1$^{-/-}$ mice were continuously monitored. Analysis of total leukocyte numbers in the BALF of both WT and IL-1R1$^{-/-}$ mice showed that the number of leukocytes increased sharply during initial infection (2–5 dpi) and peaked at 5 dpi before decreasing gradually (Figure 3). In IL-1R1$^{-/-}$ mice, however, the numbers of leukocytes were significantly lower than those of WT mice at every post-infection time point. Cell smearing and counting for different leukocytes in the lung BALF were performed. Results showed that during infection, the numbers of neutrophils were significantly lower in IL-1R1$^{-/-}$ mice than in WT mice, whereas the numbers of macrophages and monocytes tended to be the same (Figure 3). The BALF lymphocytes increased following infection, and the numbers of lymphocytes in IL-1R1$^{-/-}$ mice were significantly lower than that in WT mice at the late stage of infection (5–8 dpi) (Figure 3). Further, viral-induced T, B lymphocyte immune responses were analyzed. The numbers of BALF CD4+, CD8+, and CD19+ lymphocytes were lower in IL-1R1$^{-/-}$ mice than in WT mice, with statistically significant differences in CD4+ and CD8+ T lymphocytes (Figure 4A). Lymphocytes from the lung-draining mediastinal lymph nodes of infected mice were isolated and challenged with the H1N1 virus, with subsequent flow cytometry revealing that the percentages of CD8 and IFN-γ double-positive cells in IL-1R1$^{-/-}$

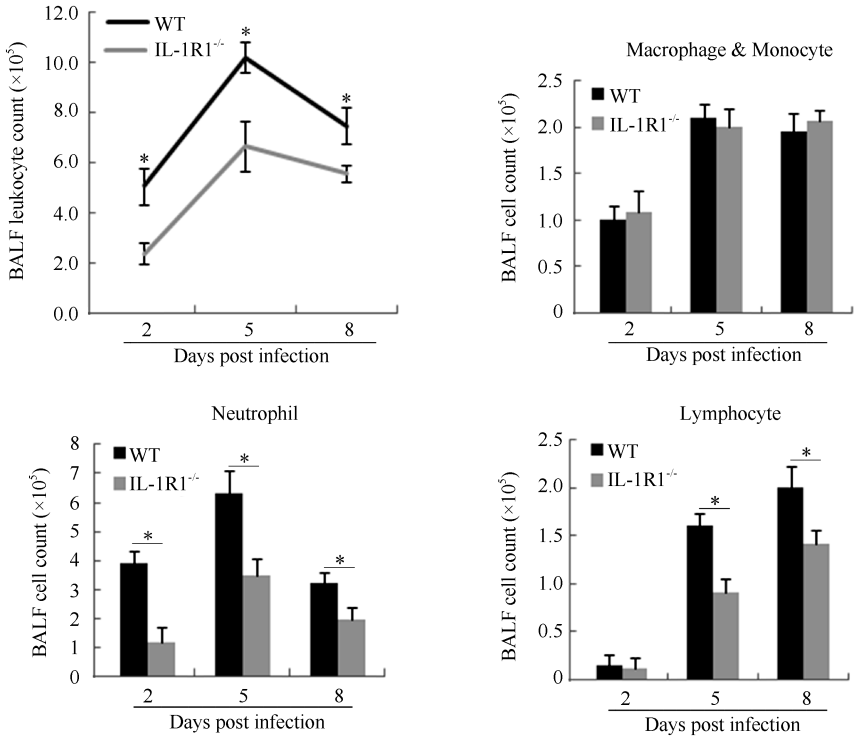

Figure 3 Alteration in accumulation of leukocytes in the lung BALF of IL-1R1$^{-/-}$ mice after H1N1 influenza virus infection

Lung BALF from infected WT and IL-1R1$^{-/-}$ mice was collected at the indicated post-infection time points. Total BALF leukocyte numbers were counted after dissolving red cells. Total numbers of macrophages/monocytes, neutrophils, and lymphocytes were determined by differential counts according to morphological criteria after cytospinning. Error bars represent the standard deviation of three samples. *: P<0.05 based on Student's t-test.

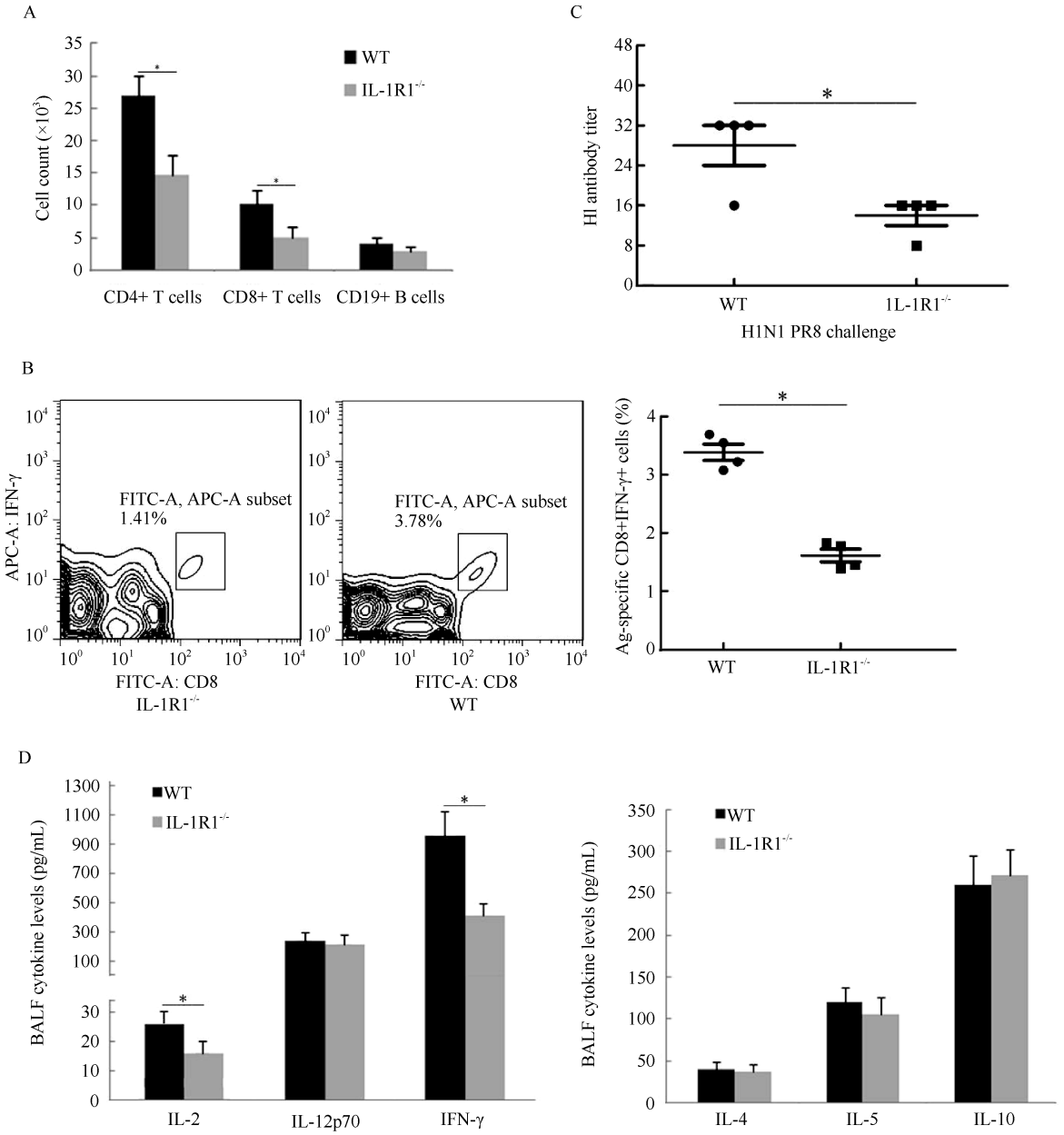

Figure 4 Impaired adaptive immune response in the lung of H1N1 infected IL-1R1$^{-/-}$ mice

The BALF, serum, and lymphocytes from lung-draining mediastinal lymph nodes of infected mice were collected at 8 dpi. A: Numbers of CD4 T cells, CD8 T cells, and CD19 B cells in the BALF were determined by flow cytometry; B: Percentages of CD8+ and IFN-γ+ cells from the mediastinal lymph node lymphocytes were determined by flow cytometry; C: HI titers of serum against H1N1 A/PR/8 were evaluated; D: Cytokine levels of IL-2, IL-12p70, IFN-γ, IL-4, IL-5, and IL-10 in the BALF were determined by Bio-Plex Mouse Cytokine Th1/Th2 assay. Error bars represent the standard deviation of four samples. *: $P<0.05$ based on Student's *t*-test.

mice were significantly lower than that in WT mice (Figure 4B). In addition, HI assay revealed a significant decrease in specific antibodies against H1N1 in the sera of infected IL-1R1$^{-/-}$ mice compared with that of infected WT mice (Figure 4C). We used the Bio-Plex Mouse Cytokine Th1/Th2 assay to analyze Th1 and Th2 cytokines in the lung BALF of infected mice. Although the levels of Th2 cytokines were almost the same in both groups of mice, the expression levels of Th1 cytokines IL-2 and IFN-γ were significantly lower in IL-1R1 knockout mice than in WT mice (Figure 4D). Collectively, these data suggest that IL-1R1 deficiency in mice results in an impairment of the anti-viral immune response in infected lungs, with decreased neutrophil accumulation and downregulated T and B lymphocyte immune responses.

Analysis of neutrophils in blood and bone marrow and G-CSF, KC, and MIP-2 levels in lung BALF and serum

Neutrophils are generated in the bone marrow and released into peripheral blood circulation to monitor the immune status of the body. When a peripheral organ such as the lung releases inflammatory signals, activated neutrophils are recruited from the vasculature to the inflammatory tissue to exert their functions (Kolaczkowska & Kubes, 2013). To determine whether the decrease in neutrophils in lung BALF from infected IL-1R1$^{-/-}$ mice was caused by impeded neutrophil recruitment and/or neutrophil generation, numbers of neutrophils in the peripheral blood and bone marrow were analyzed. Results showed that IL-1R1$^{-/-}$ mice had significantly fewer neutrophils than WT mice at 3 and 5 dpi in serum (Figure 5A). In the bone marrow, the Gr-1+ cell population of IL-1R1$^{-/-}$ mice was significantly lower than that of WT mice at 5 dpi (Figure 5B). The cytokine G-CSF plays an important role in the generation and maturation of bone marrow neutrophils (Bendall & Bradstock, 2014). The levels of G-CSF in the serum and lung BALF of IL-1R1$^{-/-}$ mice were lower than that of WT mice during infection (Figure 5C). The above results indicate that IL-1R1 is essential for the generation of neutrophils in the bone marrow. In addition, mouse chemokines KC and MIP-2 play major roles in neutrophil recruitment to inflammatory tissues (Olson & Ley, 2002). Analysis of the lung BALF and serum KC and MIP-2 levels showed that both chemokines were significantly lower in IL-1R1$^{-/-}$ mice than in WT mice, especially at 2 and 5 dpi (Figure 5D). These results reveal that knocking out IL-1R1 inhibited neutrophil generation and recruitment to H1N1-infected mouse lungs.

DISCUSSION

Understanding the contributions of IAV-infected lung pathology over the course of an acute infection remains a puzzle because distinct IAV infection and proliferation in the respiratory system can cause direct viral injury and indirect immunolesions with activated innate and adaptive anti-viral immune responses. IL-1,

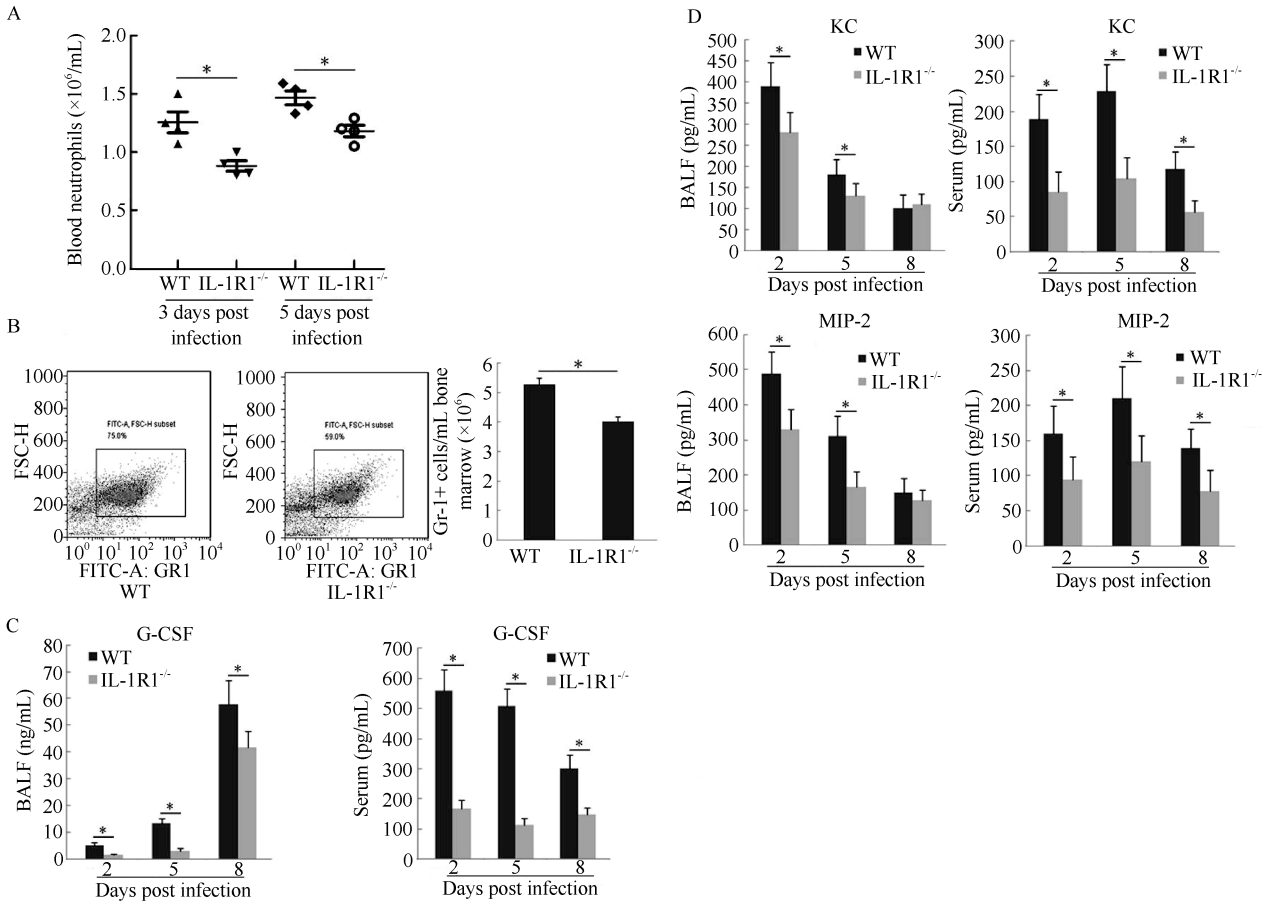

Figure 5 IL-1R1$^{-/-}$ interferes with neutrophil generation and mobilization to the H1N1-infected mouse lung

Blood, serum, BALF, and bone marrow samples of infected mice were collected at the indicated post-infection time points. A: Blood was collected in EDTA-coated tubes by retro-orbital bleeding, and neutrophil numbers were determined using a Hemavet 950 Automated Veterinary Analyzer; B: Bone marrow cells were collected and counted at 5 dpi, and the percentages and numbers of Gr-1+ cells were analyzed by flow cytometry; C: Levels of G-CSF in the BALF and serum were measured using an ELISA assay; D: Levels of KC and MIP-2 in the BALF and serum were measured using an ELISA assay. Error bars represent the standard deviation of four samples. *: P<0.05 based on Student's t-test.

which consists of two major proinflammatory cytokines (IL-1α and IL-1β), is highly expressed in respiratory cells upon pathogen invasion (Strieter et al., 2003). IL-1α and IL-1β bind to IL-1R1, leading to the activation of IL-1 signal-regulated innate immune and inflammatory physiological functions. The role of IL-1R1 signaling in the morbidity and mortality of IAV infection was previously investigated (Schmitz et al., 2005), and our results confirm the importance of IL-1R1 signaling in protecting mice against fatal IAV infection and moderating the inhibition of viral replication. In the previous work, the inflammatory lung pathology of WT mice was more severe than that of IL-1R1$^{-/-}$ mice at the early infection stage (3 dpi). Our work also indicated that IL-1R1$^{-/-}$ mice had less severe lung inflammation pathology than that of WT mice at the same early infection stage. However, at the late stage of infection (9 dpi), while lung inflammation of WT mice had gradually regressed, lung pathology in IL-1R1$^{-/-}$ mice was aggravated and resulted in lung damage and edema, characterized by alveolar structure disruption and hyaline membrane formation in the lung parenchyma as well as congestion and swelling of the lung interstitium. Quantitative analysis of lung histological changes, determination of BALF protein concentration, and measurement of proinflammatory cytokines IL-1β, IL-6, and TNF-α indicated that the loss of IL-1R1 signaling reduced lung inflammation at the beginning of IAV infection, but contributed to lung inflammatory injury following infection. This is similar to the roles of critical proinflammatory cytokines TNF-α and IL-6, with the absence of either protein resulting in severe lung inflammation and immunopathology in mice, as well as altered inflammatory cell infiltration at late stage respiratory influenza infection (Damjanovic et al., 2011; Dienz et al., 2012). Considering the limited inhibition of viral replication that occurs through IL-1R1 signaling, it seems that inflammatory injury plays a more important role in influenza-induced acute lung injury than direct viral proliferation effects upon respiratory H1N1 infection.

Decreased innate cellular influx into the airways of IL-1R1$^{-/-}$ mice was observed in the early infection period, which was primarily due to the significantly reduced neutrophil infiltration into the infected lungs, based on the BALF cell count. Among the first immune cells to arrive at a site of infection, neutrophils exert innate immune anti-IAV effects by eliminating infected cells and clearing the virus, dead cells, and debris (Mantovani et al., 2011). In addition to their phagocytic and cytotoxic activities, neutrophils facilitate the adaptive immune response against invasive pathogens by serving as APCs, influencing the maturation of DCs, promoting T cell responses, and supporting B cell activity (Leliefeld et al., 2015). Our results revealed that the loss of IL-1R1 signaling downregulated the anti-IAV adaptive immune response in the infected lung with decreased BALF T and B lymphocyte numbers, IAV-specific CD8 cytotoxic T cells, and serum antibodies. We also found that IL-1R1 signaling played an important role in the Th1 and Th2 immune response. However, the role of IL-1 signaling in the development of Th1 and Th2 responses is controversial. Some studies have suggested that IL-1 is responsible for the Th2 response (Greenbaum et al., 1988; Lichtman et al., 1988; Satoskar et al., 1998), whereas others indicate that it is involved in regulating the Th1 response (Durrant et al., 2013; O'Garra & Murphy, 1994). These variations might be due to the different pathogens and insults used, and differences between *in vitro* and *in vivo* experiments. Our data suggest that IL-1R1 signaling is required for Th1 responses, but is not essential for the generation of Th2 responses in the local IAV-infected mouse lung. Together, loss of IL-1R1 impaired the IAV-specific adaptive immune response by directly blocking the proinflammatory IL-1 signal, and possibly by the indirect effect of downregulating neutrophils that function in activating adaptive immunity.

Our findings of decreased neutrophils in the BALF, peripheral blood, and bone marrow of IAV-infected IL-1R1$^{-/-}$ mice suggests that IL-1 signaling influences neutrophil homeostasis. Indeed, the downstream consequences of IL-1 pathway activation include the upregulation of a cascade of inflammatory mediators. This includes the increased expression of cytokines and chemokines such as IL-6, TNF-α, G-CSF, CXCL1, and CXCL2 (Besnard et al., 2012; Dinarello, 2009). G-CSF stimulates the production and maturation of neutrophils by promoting the proliferation and differentiation of myeloid progenitors. In addition, G-CSF promotes neutrophil release from the bone marrow into circulation (Bendall & Bradstock, 2014; Furze & Rankin, 2008). In the present study, we found lower concentrations of the G-CSF protein in both the BALF and serum of IL-1R1$^{-/-}$ mice. Thus, IL-1 signaling possibly affects neutrophil generation in the bone marrow of IAV-infected mice via the G-CSF pathway. Both CXCL1 and CXCL2 (murine KC and MIP-2) have previously been suggested as the two most important chemokines for neutrophil mobilization from bone marrow and recruitment into the lung in rodents (Olson & Ley, 2002; Strydom & Rankin, 2013). Our results also demonstrated that the expressions of CXCL1 and CXCL2 were reduced at the local (infected lung) and system (serum) level in IL-1R1$^{-/-}$ mice. Therefore, based on our results, IL-1 signaling might influence neutrophil homeostasis through neutrophil generation and mobilization, thus contributing to anti-viral neutrophil physiology.

Our results showed that IL-1 signaling is critical to pulmonary anti-influenza immune responses and lung immunopathology, likely due to its effects on regulating innate immune cell infiltration and inflammatory cytokine/chemokine production, especially that of neutrophils. Neutrophils are essential innate immune and inflammatory cells during respiratory influenza infection, and IL-1 signaling might mediate neutrophil generation and recruitment to the infected mouse lung through the G-CSF and CXCL1/2 pathways.

REFERENCES

Bendall LJ, Bradstock KF. 2014. G-CSF: from granulopoietic stimulant to bone marrow stem cell mobilizing agent. *Cytokine & Growth Factor Reviews,* **25**(4): 355-367.

Besnard AG, Togbe D, Couillin I, Tan ZM, Zheng SG, Erard F, Le Bert M, Quesniaux V, Ryffel B. 2012. Inflammasome-IL-1-Th17 response in allergic lung inflammation. *Journal of Molecular Cell Biology,* **4**(1): 3-10.

Braciale TJ, Sun J, Kim TS. 2012. Regulating the adaptive immune response to respiratory virus infection. *Nature Reviews Immunology,* **12**(4): 295-305.

Coates BM, Staricha KL, Wiese KM, Ridge KM. 2015. Influenza a virus infection, innate immunity, and childhood. *JAMA Pediatrics,* **169**(10): 956-963.

Damjanovic D, Small CL, Jeyananthan M, McCormick S, Xing Z. 2012. Immunopathology in influenza virus infection: uncoupling the friend from foe. *Clinical Immunology,* **144**(1): 57-69.

Damjanovic D, Divangahi M, Kugathasan K, Small CL, Zganiacz A, Brown EG, Hogaboam CM, Gauldie J, Xing Z. 2011. Negative regulation of lung inflammation and immunopathology by TNF-α during acute influenza infection. American Journal of Pathology, **179**(6): 2963-2976.

Dienz O, Rud JG, Eaton SM, Lanthier PA, Burg E, Drew A, Bunn J, Suratt BT, Haynes L, Rincon M. 2012. Essential role of IL-6 in protection against H1N1 influenza virus by promoting neutrophil survival in the lung. *Mucosal Immunology*, **5**(3): 258-266.

Dinarello CA. 2009. Immunological and inflammatory functions of the interleukin-1 family. *Annual Review of Immunology,* **27**(1): 519-550.

Durrant DM, Robinette ML, Klein RS. 2013. IL-1R1 is required for dendritic cell-mediated T cell reactivation within the CNS during West Nile virus encephalitis. *The Journal of Experimental Medicine,* **210**(3): 503-516.

Furze RC, Rankin SM. 2008. Neutrophil mobilization and clearance in the bone marrow. *Immunology,* **125**(3): 281-288.

Greenbaum LA, Horowitz JB, Woods A, Pasqualini T, Reich EP, Bottomly K. 1988. Autocrine growth of CD4+T cells. Differential effects of IL-1 on helper and inflammatory T cells. *The Journal of Immunology,* **140**(5): 1555-1560.

Kohlmeier JE, Woodland DL. 2009. Immunity to respiratory viruses. *Annual Review of Immunology,* **27**(1): 61-82.

Kolaczkowska E, Kubes P. 2013. Neutrophil recruitment and function in health and inflammation. *Nature Reviews Immunology,* **13**(3): 159-175.

Leliefeld PHC, Koenderman L, Pillay J. 2015. How neutrophils shape adaptive immune responses. *Frontiers in Immunology,* **6**: 471.

Lichtman AH, Chin J, Schmidt JA, Abbas AK. 1988. Role of interleukin 1 in the activation of T lymphocytes. *Proceedings of the National Academy of Sciences of the United States of America,* **85**(24): 9699-9703.

Mantovani A, Cassatella MA, Costantini C, Jaillon S. 2011. Neutrophils in the activation and regulation of innate and adaptive immunity. *Nature Reviews Immunology,* **11**(8): 519-531.

O'Garra A, Murphy K. 1994. Role of cytokines in determining T-lymphocyte function. *Current Opinion in Immunology,* **6**(3): 458-466.

Olson TS, Ley K. 2002. Chemokines and chemokine receptors in leukocyte trafficking. *American Journal of Physiology—Regulatory, Integrative and Comparative Physiology,* **283**(1): R7-R28.

Sanders CJ, Doherty PC, Thomas PG. 2011. Respiratory epithelial cells in innate immunity to influenza virus infection. *Cell and Tissue Research,* **343**(1): 13-21.

Satoskar AR, Okano M, Connaughton S, Raisanen-Sokolwski A, David JR, Labow M. 1998. Enhanced Th2-like responses in IL-1 type 1 receptor-deficient mice. *European Journal of Immunology,* **28**(7): 2066-2074.

Schmitz N, Kurrer M, Bachmann MF, Kopf M. 2005. Interleukin-1 is responsible for acute lung immunopathology but increases survival of respiratory influenza virus infection. *Journal of Virology,* **79**(10): 6441-6448.

Strieter RM, Belperio JA, Keane MP. 2003. Host innate defenses in the lung: the role of cytokines. *Current Opinion in Infectious Diseases,* **16**(3): 193-198.

Strydom N, Rankin SM. 2013. Regulation of circulating neutrophil numbers under homeostasis and in disease. *Journal of Innate Immunity,* **5**(4): 304-314.

Szretter KJ, Gangappa S, Lu XH, Smith C, Shieh WJ, Zaki SR, Sambhara S, Tumpey TM, Katz JM. 2007. Role of host cytokine responses in the pathogenesis of avian H5N1 influenza viruses in mice. *Journal of Virology,* **81**(6): 2736-2744.

Tripathi S, White MR, Hartshorn KL. 2015. The amazing innate immune response to influenza A virus infection. *Innate Immunity,* **21**(1): 73-98.

Weber A, Wasiliew P, Kracht M. 2010. Interleukin-1 (IL-1) pathway. *Science Signaling,* **3**(105): cm1.

GCH1 plays a role in the high-altitude adaptation of Tibetans

Yong-Bo Guo[1,2,#], Yao-Xi He[2,4,#], Chao-Ying Cui[3,#], Ouzhuluobu[3], Baimakangzhuo[3], Duojizhuoma[3], Dejiquzong[3], Bianba[3], Yi Peng[2], Cai-juan Bai[3], Gonggalanzi[3], Yong-Yue Pan[3], Qula[3], Kangmin[3], Cirenyangji[3], Baimayangji[3], Wei Guo[3], Yangla[3], Hui Zhang[2], Xiao-Ming Zhang[2], Wang-Shan Zheng[1,2], Shu-Hua Xu[5,8,9], Hua Chen[6], Sheng-Guo Zhao[1], Yuan Cai[1], Shi-Ming Liu[7], Tian-Yi Wu[7], Xue-Bin Qi[2,*], Bing Su[2,*]

[1] *College of Animal Science and Technology*, *Gansu Agricultural University*, *Lanzhou Gansu* 730070, *China*

[2] *State Key Laboratory of Genetic Resources and Evolution*, *Kunming Institute of Zoology*, *Chinese Academy of Sciences*, *Kunming Yunnan* 650223, *China*

[3] *High Altitude Medical Research Center*, *School of Medicine*, *Tibetan University*, *Lhasa Tibet* 850000, *China*

[4] *Kunming College of Life Science*, *University of Chinese Academy of Sciences*, *Kunming Yunnan 650204*, *China*

[5] *Chinese Academy of Sciences Key Laboratory of Computational Biology*, *Max Planck Independent Research Group on Population Genomics, CAS-MPG Partner Institute for Computational Biology (PICB)*, *Shanghai Institutes for Biological Sciences*, *Chinese Academy of Sciences, Shanghai* 200031, *China*

[6] *Center for Computational Genomics*, *Beijing Institute of Genomics*, *Chinese Academy of Sciences*, *Beijing* 100101, *China*

[7] *National Key Laboratory of High Altitude Medicine*, *High Altitude Medical Research Institute*, *Xining Qinghai* 810012, *China*

[8] *School of Life Science and Technology*, *Shanghai Tech University*, *Shanghai* 200031, *China*

[9] *Collaborative Innovation Center of Genetics and Development*, *Shanghai* 200438, *China*

ABSTRACT

Tibetans are well adapted to high-altitude hypoxia. Previous genome-wide scans have reported many candidate genes for this adaptation, but only a few have been studied. Here we report on a hypoxia gene (*GCH1*, GTP-cyclohydrolase I), involved in maintaining nitric oxide synthetase (NOS) function and normal blood pressure, that harbors many potentially adaptive variants in Tibetans. We resequenced an 80.8 kb fragment covering the entire gene region of *GCH1* in 50 unrelated Tibetans. Combined with previously published data, we demonstrated many *GCH1* variants showing deep divergence between highlander Tibetans and lowlander Han Chinese. Neutrality tests confirmed a signal of positive Darwinian selection on *GCH1* in Tibetans. Moreover, association analysis indicated that the Tibetan version of *GCH1* was significantly associated with multiple physiological traits in Tibetans, including blood nitric oxide concentration, blood oxygen saturation, and hemoglobin concentration. Taken together, we propose that *GCH1* plays a role in the genetic adaptation of Tibetans to high altitude hypoxia.

Keywords: *GCH1*; Positive selection; Tibetan; Hypoxia adaptation; Nitric oxide; Hemoglobin; Oxygen saturation

INTRODUCTION

Tibetans are a well-known example of successful adaptation to extreme environments at high-altitude. Compared to lowlanders moving to high altitude, Tibetans show greater lung capacity, function, diffusion, and ventilation, as well as lower hemoglobin (Hb) levels, better blood oxygen saturation, low hypoxic pulmonary vasoconstriction, high nitric oxide (NO) concentrations, and lower incidence of reduced birth weight (Beall, 2006; Beall et al., 1997; Erzurum et al., 2007; Wu & Kayser, 2006). These traits have been acquired during a long period of natural

Received: 24 March 2017; Accepted: 27 April 2017

Foundation items: This study was supported by grants from the Strategic Priority Research Program of the Chinese Academy of Sciences (XDB13010000), the National Natural Science Foundation of China (91631306 to BS, 31671329 to XQ, 31460287 to Ou., 31501013 to HZ and 31360032 to CC), the National 973 program (2012CB518202 to TW), the State Key Laboratory of Genetic Resources and Evolution (GREKF15-05, GREKF16-04), and the Zhufeng Scholar Program of Tibetan University

[#]Authors contributed equally to this work

[*]Corresponding authors, E-mail: sub@mail.kiz.ac.cn; qixuebin@mail.kiz.ac.cn

DOI: 10.24272/j.issn.2095-8137.2017.037

selection at high altitude after the ancestors of modern Tibetans permanently settled on the Qinghai-Tibetan Plateau during the early Upper Paleolithic period (Qi et al., 2013).

Various research groups have compared the genetic differences between Tibetan and Han Chinese using genome-wide scans, with two key genes identified (hypoxia-inducible factor 2α, *HIF2α*, also called *EPAS1*, and *EGLN1*) in the hypoxic pathway showing deep between-population divergence (Beall et al., 2010; Bigham et al., 2010; Peng et al., 2011; Simonson et al., 2010; Xu et al., 2011; Yi et al., 2010). For these two genes, Tibetan-specific haplotypes have been found, which are highly enriched in Tibetans (~80%), but rare or absent in other world populations (Lorenzo et al., 2014; Peng et al., 2011, 2017; Xiang et al., 2013). The function of selection on these two genes have been shown to cause blunted physiological responses under high altitude hypoxic conditions (Lorenzo et al., 2014; Peng et al., 2017; Xiang et al., 2013). For example, the Tibetan versions of *EPAS1* and *EGLN1* protect Tibetans from the over production of red blood cells (polycythemia), a common deleterious physiological response when lowlanders migrate to high altitude areas (Beall et al., 2010; Erzurum et al., 2007; Lorenzo et al., 2014; Peng et al., 2011, 2017; Petousi et al., 2014; Xiang et al., 2013; Xu et al., 2011; Zhang et al., 2010).

Many genes are likely involved in complex traits like high altitude adaptation. In addition to *EPAS1* and *EGLN1*, previous genome-wide studies have identified other candidate genes that might also contribute to genetic adaptation in Tibetans (Beall et al., 2010; Bigham et al., 2010; Peng et al., 2011; Simonson et al., 2010; Xu et al., 2011; Yi et al., 2010). The GTP-cyclohydrolase I (*GCH1*) gene is a reported candidate that shows relatively deep allelic divergence between Tibetans and Han Chinese, a sign of positive Darwinian selection (Peng et al., 2011). *GCH1* is located on human chromosome 14 (14q22.1-q22.2), spanning 60.8 kb with six exons. Furthermore, *GCH1* is a rate-limiting enzyme in the *de novo* synthesis of tetrahydrobiopterin (BH4). It has been reported that under hypoxia, *GCH1* can promote cancer growth, and its expression and that of endothelial nitric oxide synthetase (*eNOS*) is upregulated (Pickert et al., 2013). *GCH1* is considered as a major factor in maintaining nitric oxide synthetase (NOS) function and normal blood pressure, and its inhibition can increase blood pressure due to NOS uncoupling, which is found in many cardiovascular diseases such as hypertension and atherosclerosis (Antoniades et al., 2006). Hence, the known functional role of *GCH1* also makes it a candidate for high-altitude adaptation in Tibetans.

We resequenced an 80.8 kb fragment covering the entire gene region of *GCH1* in 50 unrelated Tibetans. Combined with published data, we found signals of positive selection on *GCH1* in Tibetans, with multiple sequence variants showing deep genetic divergence between highlander Tibetans and lowlander Han Chinese. Genetic association analysis detected significant correlation of the *GCH1* variants with multiple physiological traits of Tibetans, including blood nitric oxide (NO) concentration, blood oxygen saturation level, and hemoglobin concentration. Hence, *GCH1* might play an essential role in high-altitude adaptation in Tibetans.

MATERIALS AND METHODS

DNA sample collection and resequencing of GCH1 gene fragment

The 50 unrelated Tibetan samples were obtained from previous research (Peng et al., 2011). We resequenced an 80.8 kb fragment covering the gene region of *GCH1* and its flanking sequences (10 kb up- and down-stream of *GCH1*). For association analysis, we collected blood samples and extracted DNA from 226 unrelated adult Tibetans, whose physiological data were also collected with written informed consent. The protocol of this study was evaluated and approved by the Internal Review Board of Kunming Institute of China, Chinese Academy of Sciences.

Detection of selection on GCH1 in Tibetans

The initially identified sequence variants were filtered by removing single nucleotide polymorphisms (SNPs) showing a significant deviation from the Hardy-Weinberg Equilibrium (HWE<0.000 1), and those with an excessive missing genotype rate (MGR>0.05). Four methods were used for selection testing, including two allele-frequency-based and two haplotype-based tests. Locus specific F_{ST} was calculated between 83 Tibetans and three reference populations (103 Han Chinese, CHB; 99 Europeans, CEU; and 108 Africans, YRI) following Weir & Cockerham (1984). The Tajima's *D*-test was also performed following the published procedure (Tajima, 1989).

The two haplotype-based tests included the iHS and XP-EHH tests (Sabeti et al., 2002). The iHS score was calculated for each site using selscan (Szpiech & Hernandez, 2014) based on the phased haplotypes, and only those allelic loci whose ancestral alleles were known with certainty were included in the analysis (Voight et al., 2006). The XP-EHH (Sabeti et al., 2007) analysis was used to detect the extended haplotypes due to positive selection. Han Chinese were used as the reference population in the XP-EHH test. We computed XP-EHH scores using selscan (Szpiech & Hernandez, 2014) based on phased haplotypes of Tibetans and Han Chinese. The XP-EHH score of each SNP was standardized by the mean XP-EHH and the standard deviation (*SD*) over the genome.

Functional prediction of GCH1 candidate SNPs

Functional enrichment analyses of the candidate variants were performed using the Combined Annotation Dependent Depletion (CADD) database (http://krishna.gs.washington.edu/download/CADD/v1.3/1000G_phase3_inclAnno.tsv.gz), which incorporates data from ENCODE (http://genome.ucsc.edu/ENCODE/) and NIH Roadmap Epigenomics using ChromHMM (https://sites.google.com/site/anshulkundaje/projects/epigenome roadmap#TOC-Core-Integrative-chromatin-state-maps-127-Epigenomes-) (Ernst & Kellis, 2012).

Evolutionary constraint is an indication of functional importance. We used Genome Evolutionary Rate Profiling (GERP) to evaluate how conserved a test SNP was compared with SNP-containing sequences from different species (http://mendel.stanford.edu/SidowLab/downloads/gerp/). The GERP++ method was used to calculate site-specific RS scores (Davydov

et al., 2010). A positive GERP++ score indicates evolutionary constraint, and the greater the score, the greater the level of evolutionary constraint inferred to be acting on that site.

The H3K4Me1 value indicates the maximum ENCODE H3K4 methylation level (maximum value observed across 16 ENCODE cell lines at a given position), suggestive of an enhancer or other regulatory activities. The H3K4Me3 value indicates the maximum ENCODE H3K4 trimethylation level, and is an indication of a promoter. The DNase *P* value indicates evidence for open chromatin. The transcription factor binding site (TFBS) is indicated by the number of different overlapping ChIP transcription factor binding sites. In addition, the splice site results indicate if the tested variant is within an ACCEPTOR or a DONOR (Supplementary Table S1).

Measurements of physiological traits

Physiological data and blood samples were collected from 226 unrelated Tibetans permanently residing in Bange county (*n*=135, 37.41±3.8 years old) at an elevation of 4 700 m and Lhasa city (*n*=91, 35.33±6.8 years old) at an elevation of 3 600 m. Written informed consent from all participants was obtained. For physiological parameters, we collected hemoglobin (Hb) concentration, arterial oxygen saturation (SaO_2) level, and blood nitric oxide concentration, representing key adaptive physiological traits in Tibetans (Wu & Kayser, 2006).

The Hb level in blood was measured using a HemoCue Hb 201+ analyzer (Angelholm, Sweden). The SaO_2 level was measured using fingertip blood with a hand-held pulse oximeter (Nellcor NPB-40, CA, USA). Blood NO was measured using a nitric oxide analyzer (Sievers Model-280, GE Analytical Instruments; Boulder, CO, USA).

SNP genotyping and association analysis

We selected nine tag SNPs, covering the entire gene region of *GCH1* (Table 1). Genotyping was conducted by SNaPshot on an ABI 3130 sequencer (Applied Bio-Systems, Forster City, CA, USA). Genetic association analysis was executed using PLINK 1.07 (Purcell et al., 2007). We used an additive model in the association analysis as all candidate SNPs were non-coding and likely influenced the level of gene expression. Permutations (100 000 times for each test) were performed for statistical assessment and correction for multiple tests.

Table 1 Association of nine *GCH1* variants with three physiological traits in Tibetans

Traits	SNP_ID	Male (*n*=91)		Female (*n*=135)		All (*n*=226)		
		Beta	EMP'	Beta	EMP'	Beta	EMP''	R^2 (%)
Hb	rs7148266	–4.33	0.48	–0.53	0.78	–1.51	0.78	0.05
	rs17128004	–3.02	0.65	–0.49	0.86	–1.10	0.86	0.01
	rs4411417	–4.33	0.48	–1.27	0.86	–1.85	0.69	0.23
	rs2183082	1.17	0.86	–2.10	0.57	–0.65	0.86	0.08
	rs10220344	1.17	0.86	–2.10	0.57	–0.65	0.86	0.08
	rs146540091	–62.95	0.05	–17.31	0.25	–35.15	0.02	1.65
	rs117863726	–62.95	0.05	–17.61	0.47	–36.27	0.02	2.39
	rs10136972	12.97	0.03	0.21	1.00	4.28	0.28	1.29
	rs112700866	22.04	0.05	–0.78	1.00	10.25	0.16	0.67
NO	rs7148266	–15.97	0.04	–10.82	0.04	–12.96	2.32E-03	3.05
	rs17128004	–17.23	0.03	–10.77	0.04	–13.42	2.32E-03	3.08
	rs4411417	–15.97	0.04	–11.67	0.04	–13.63	2.75E-03	3.76
	rs2183082	–6.35	0.54	–6.05	0.17	–6.32	0.08	1.28
	rs10220344	–6.35	0.54	–6.05	0.17	–6.32	0.08	1.28
	rs146540091	–162.70	3.53E–03	13.14	0.78	–41.65	0.07	3.36
	rs117863726	–162.70	3.53E–03	13.07	0.65	–41.05	0.07	1.40
	rs10136972	–5.71	0.65	–14.60	0.01	–11.35	0.02	1.88
	rs112700866	–10.98	0.35	4.97	0.73	–2.78	0.86	0.03
SaO_2	rs7148266	–0.84	0.38	0.55	0.78	0.05	0.86	0.01
	rs17128004	–1.08	0.33	–0.05	1.00	–0.44	0.48	0.07
	rs4411417	–0.84	0.38	0.57	0.65	0.03	1.00	2.50E-03
	rs2183082	–0.50	0.57	–0.38	0.78	–0.44	0.52	0.03
	rs10220344	–0.50	0.57	–0.38	0.78	–0.44	0.52	0.03
	rs146540091	12.53	0.05	–1.61	0.78	3.07	0.54	3.22
	rs117863726	12.53	0.05	6.66	0.14	8.53	0.02	2.47
	rs10136972	–1.86	0.27	–1.84	0.11	–1.84	0.05	0.75
	rs112700866	–1.68	0.67	–3.46	0.17	–2.76	0.16	0.75

Hb, hemoglobin concentration; NO, blood nitric oxide concentration; SaO_2, blood oxygen saturation level. EMP', *P* value after multiple test corrections; EMP'', *P* value after multiple test corrections with sex as the covariant.

RESULTS

Resequencing of GCH1 in Tibetans and tests of selection

Previous DNA array-based genome-wide studies have only covered a limited number of *GCH1* sequence variants (Peng et al., 2011). To obtain complete sequence data of *GCH1*, we first resequenced an 80.8 kb fragment covering the entire gene region of *GCH1* (60.8 kb) as well as the flanking sequences (10 kb from upstream and 10 kb from downstream regions). In total, we sequenced 50 unrelated Tibetan individuals, as reported previously (Peng et al., 2011). In addition, we obtained the *GCH1* sequences of 33 Tibetans from recently published whole genome sequencing data (Lu et al., 2016), for a final sample size of 83.

We identified a total of 384 *GCH1* sequence variants (SNPs) in the 83 unrelated Tibetans, among which 245 were shared between Tibetans and the three lowland reference populations from the 1000 Genomes Project (http://www.1000genomes.org) (103 Han Chinese, CHB; 99 Europeans, CEU and 108 Africans, YRI). The remaining 139 SNPs were rare in Tibetans (<1.0%), and therefore not included in our analysis. The 245 SNPs were all located in the non-coding regions of *GCH1*.

To detect whether *GCH1* was under selection in Tibetans, we conducted four different tests of selection, including two allele-frequency-based tests (F_{ST} and Tajima's *D*) and two haplotype-based tests (iHS and XP-EHH). We identified 49 *GCH1* SNPs with large between-population (Tibetan vs. Han) divergence (F_{ST}>0.2), much larger than the genome average (F_{ST}=0.03). These high-F_{ST} variants also showed high iHS and XP-EHH values (iHS>0.2 and/or XP-EHH>0.2) (Figure 1). They were aggregated in a relatively short region (7.5 kb) covering intron-1 and intron-2 of *GCH1*. These results suggest a clear signal of positive Darwinian selection on *GCH1* in Tibetans (Supplementary Table S1)

Functional prediction and genetic association analysis

To determine the potential function of the SNPs with selection signals, we performed functional predictions using evolutionary constraint (GERP), transcription factor binding sites (TFBS), splicing motif, H3K4Me1/H3K4Me3 sites, and DNase-I hypersensitive sites. Results showed that there might be multiple functional sites, reflected by the consistent signals of different functional predictions (Supplementary Table S1).

To test whether these candidate *GCH1* variants contribute to the adaptive physiological traits of Tibetans, we measured blood NO concentrations, SaO_2 levels, and Hb concentrations in 226 unrelated adult Tibetans (refer to methods for details). For genotyping, we selected nine tag SNPs to represent the entire gene region of *GCH1*. Notably, four SNPs (rs7148266, rs17128004, rs4411417, and rs10136972) showed significant association with blood NO levels, with the adaptive alleles exhibiting decreased NO. Each SNP accounted for 1.88%–3.76% of NO variance (Figure 2). Similar results were observed when males and females were analyzed separately (Table 1). Additionally, two SNPs (rs146540091 and rs137863726) showed association with hemoglobin concentration, with the adaptive alleles having lower Hb levels, consistent with previous results for *EPAS1* and *EGLN1* (Peng et al., 2011, 2017; Xiang et al., 2013). Another SNP (rs137863726) was associated with blood oxygen saturation, with the adaptive allele exhibiting higher SaO_2 levels.

For the four SNPs (rs7148266, rs17128004, rs4411417, and rs10136972) showing significant association with blood NO levels, functional prediction analysis indicated that they were located in the *GCH1* intron regions with peak signals for H3K4Me1, H3K4Me3, DNase-I, and TFBS. For example, the H3K4Me1 peak values for rs10136972 and rs4411417 were 8.2 and 5.9, respectively, indicating their potential role in gene expression regulation of *GCH1*.

DISCUSSION

Hypoxia serves as a key stress in high altitude environments. For lowlanders, prolonged exposure to high altitude hypoxia can cause chronic mountain sickness, reflected by the over production of red blood cells (polycythemia) as well as other deleterious physiological changes (Hackett & Roach, 2001; Macinnis et al., 2010). Tibetans are genetically adapted to high altitude hypoxia, and exhibit blunted physiological responses, e.g., relatively low hemoglobin levels (Lorenzo et al., 2014; Peng et al., 2011, 2017; Xiang et al., 2013). Key hypoxic pathway genes *EPAS1* and *EGLN1* were reported to be responsible for these blunted physiological responses (Lorenzo et al., 2014; Peng et al., 2017; Xiang et al., 2013). However, while the Tibetan version of these two genes provide protection against polycythemia, they do not explain all physiological changes in Tibetans, suggesting there might be other genes involved given the complexity of high altitude adaptation.

Based on resequencing and population analysis, we confirmed a signal of selection on *GCH1* in Tibetans. We identified more than 40 variants showing deep allelic divergence between highlander Tibetans and lowlander Han Chinese, with some having potential functional effects based on prediction using ENCODE. *GCH1* is a rate-limiting enzyme, acting as a crucial factor for maintaining normal NO synthetase function and blood pressure. Inhibition of *GCH1* activity is related to several cardiovascular diseases, with *GCH1* found to prevent hypoxia-induced pulmonary hypertension (Khoo et al., 2005). Hence, the function of selection on *GCH1* in Tibetans is expected to help maintain proper cardiovascular function at high altitude.

Hypoxic pulmonary vasoconstriction and pulmonary vascular structural remodeling are dominant pathophysiological characteristics of hypoxic pulmonary hypertension (Galiè et al., 2016; McLaughlin & McGoon, 2006; Schermuly et al., 2011). When lowlanders move to high altitudes, pulmonary hypertension usually occurs within a few weeks (Wilkins et al., 2015; Wu & Kayser, 2006); however, Tibetans rarely develop this condition. We showed that *GCH1* SNPs were associated with NO levels in the blood. *GCH1* is involved in the synthesis of tetrahydrobiopterin (BH4), a vital regulator of eNOS, the endothelial-form enzyme producing NO, an important molecule for vasodilation, which is considered the main reason for the superior blood flow and pulmonary pressure in Tibetans (Pickert

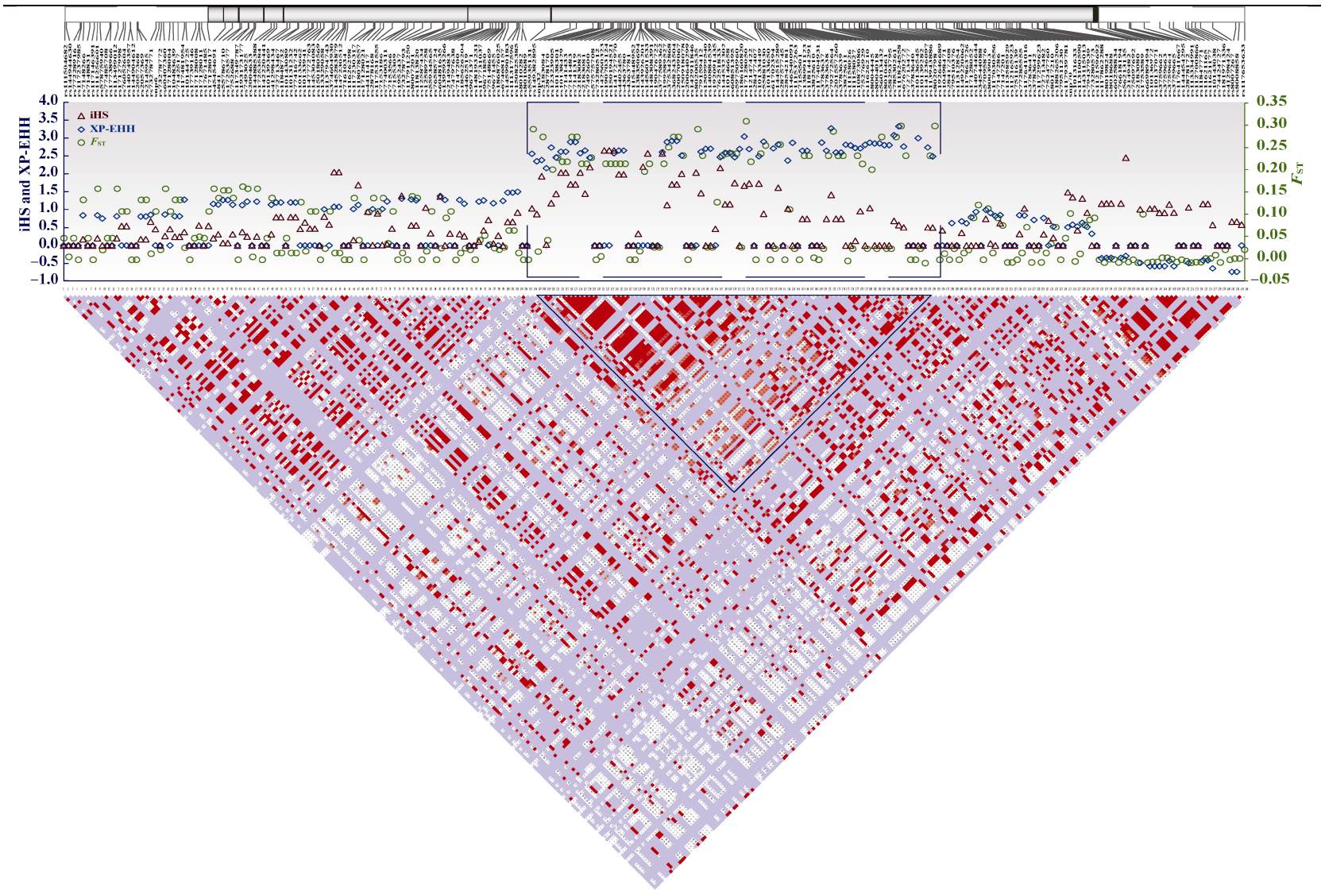

Figure 1 Genetic divergence of 245 *GCH1* variants between Tibetans and Han Chinese (F_{ST}, iHS, and XP-EHH)

Top panel displays *GCH1* gene structure with locations of the variants, and bottom panel is the map of linkage disequilibrium (LD).

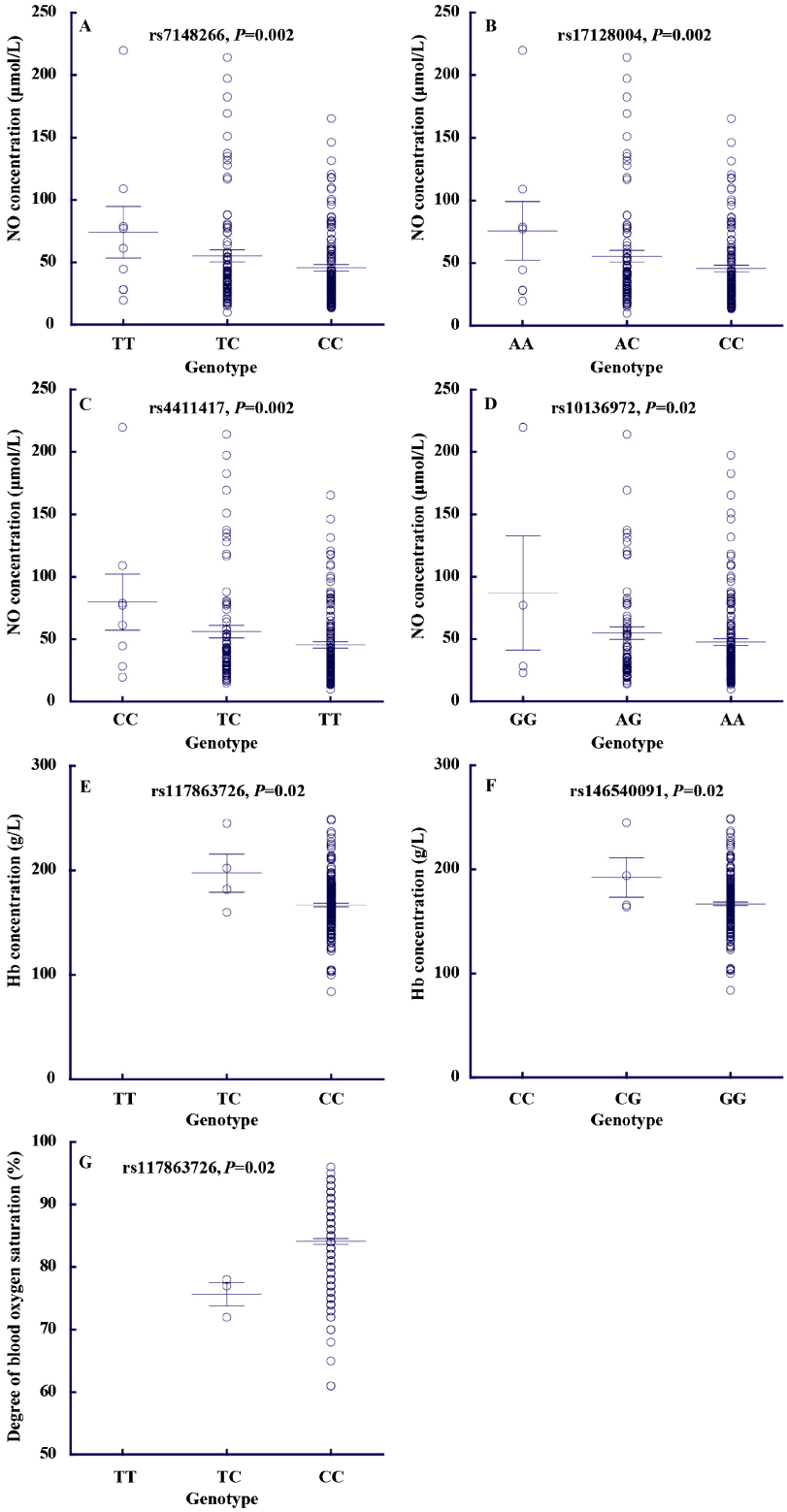

Figure 2 Genetic association of seven *GCH1* variants with three physiological traits (blood NO concentration, blood oxygen saturation level, and hemoglobin concentration)

et al., 2013). In hph-1 mice, deficiency of BH4 causes hypoxia-induced pulmonary hypertension even under normoxic conditions (Khoo et al., 2005). The overexpression of *GCH1* in mice could prevent hypoxia-induced pulmonary hypertension due to the augmentation of BH4 (Khoo et al., 2005). Hence, it is possible that *GCH1* regulates pulmonary vasoconstriction responses in Tibetans by influencing NO production in the blood. We observed four *GCH1* variants showing significant association with blood NO levels. As these variants are located in the *GCH1* intron regions with peak enhancer and/or promoter activity signals, they are likely involved in the regulation of *GCH1* expression and eventually affect blood NO production, which needs further investigation. We also observed associations of *GCH1* SNPs with oxygen saturation and hemoglobin; however, the underlying molecular mechanisms are yet to be studied.

In summary, we demonstrated that *GCH1* has been under positive selection in Tibetans. We identified many variants with deep allelic divergence between Tibetans and lowlanders. The association and known function results suggest the potential involvement of *GCH1* in the regulation of multiple physiological traits in Tibetans.

ACKNOWLEDGEMENTS

We are grateful to all the volunteers participated in this study.

REFERENCES

Antoniades C, Shirodaria C, Warrick N, Cai SJ, de Bono J, Lee J, Leeson P, Neubauer S, Ratnatunga C, Pillai R, Refsum H, Channon KM. 2006. 5-methyltetrahydrofolate rapidly improves endothelial function and decreases superoxide production in human vessels: effects on vascular tetrahydrobiopterin availability and endothelial nitric oxide synthase coupling. *Circulation,* **114**(11): 1193-1201.

Beall CM, Strohl KP, Blangero J, Williams-Blangero S, Almasy LA, Decker MJ, Worthman CM, Goldstein MC, Vargas E, Villena M, Soria R, Alarcon AM, Gonzales C. 1997. Ventilation and hypoxic ventilatory response of Tibetan and Aymara high altitude natives. *American Journal of Physical Anthropology,* **104**(4): 427-447.

Beall CM. 2006. Andean, Tibetan, and Ethiopian patterns of adaptation to high-altitude hypoxia. *Integrative and Comparative Biology,* **46**(1): 18-24.

Beall CM, Cavalleri GL, Deng LB, Elston RC, Gao Y, Knight J, Li CH, Li JC, Liang Y, McCormack M, Montgomery HE, Pan H, Robbins PA, Shianna KV, Tam SC, Tsering N, Veeramah KR, Wang W, Wangdui P, Weale ME, Xu YM, Xu Z, Yang L, Zaman MJ, Zeng CQ, Zhang L, Zhang XL, Zhaxi P, Zheng YT. 2010. Natural selection on *EPAS1* (*HIF2α*) associated with low hemoglobin concentration in Tibetan highlanders. *Proceedings of the National Academy of Sciences of the United States of America,* **107**(25): 11459-11464.

Bigham A, Bauchet M, Pinto D, Mao XY, Akey JM, Mei R, Scherer SW, Julian CG, Wilson MJ, Herráez DL, Brutsaert T, Parra EJ, Moore LG, Shriver MD. 2010. Identifying signatures of natural selection in Tibetan and Andean populations using dense genome scan data. *PLoS Genetics,* **6**(9): e1001116.

Davydov EV, Goode DL, Sirota M, Cooper GM, Sidow A, Batzoglou S. 2010. Identifying a high fraction of the human genome to be under selective constraint using GERP++. *PLoS Computational Biology,* **6**(12): e1001025.

Ernst J, Kellis M. 2012. ChromHMM: automating chromatin-state discovery and characterization. *Nature Methods,* **9**(3): 215-216.

Erzurum SC, Ghosh S, Janocha AJ, Xu W, Bauer S, Bryan NS, Tejero J, Hemann C, Hille R, Stuehr DJ, Feelisch M, Beall CM. 2007. Higher blood flow and circulating NO products offset high-altitude hypoxia among Tibetans. *Proceedings of the National Academy of Sciences of the United States of America,* **104**(45): 17593-17598.

Galiè N, Humbert M, Vachiery JL, Gibbs S, Lang I, Torbicki A, Simonneau G, Peacock A, Noordegraaf AV, Beghetti M, Ghofrani A, Sanchez MAG, Hansmann G, Klepetko W, Lancellotti P, Matucci M, McDonagh T, Pierard LA, Trindade PT, Zompatori M, Hoeper M, Aboyans V, Vaz Carneiro A, Achenbach S, Agewall S, Allanore Y, Asteggiano R, Badano LP, Barberà JA, Bouvaist H, Bueno H, Byrne RA, Carerj S, Castro G, Erol C, Falk V, Funck-Brentano C, Gorenflo M, Granton J, Iung B, Kiely DG, Kirchhof P, Kjellstrom B, Landmesser U, Lekakis J, Lionis C, Lip GY, Orfanos SE, Park MH, Piepoli MF, Ponikowski P, Revel MP, Rigau D, Rosenkranz S, Völler H, Zamorano JL. 2016. 2015 ESC/ERS Guidelines for the diagnosis and treatment of pulmonary hypertension: the joint task force for the diagnosis and treatment of pulmonary hypertension of the european society of cardiology (ESC) and the european respiratory society (ERS): endorsed by: association for european paediatric and congenital cardiology (AEPC), international society for heart and lung transplantation (ISHLT). *European Heart Journal,* **37**(1): 67-119.

Hackett PH, Roach RC. 2001. High-altitude illness. *The New England Journal of Medicine,* **345**(2): 107-114.

Khoo JP, Zhao L, Alp NJ, Bendall JK, Nicoli T, Rockett K, Wilkins MR, Channon KM. 2005. Pivotal role for endothelial tetrahydrobiopterin in pulmonary hypertension. *Circulation,* **111**(16): 2126-2133.

Lorenzo FR, Huff C, Myllymäki M, Olenchock B, Swierczek S, Tashi T, Gordeuk V, Wuren T, Ri-Li G, McClain DA, Khan TM, Koul PA, Guchhait P, Salama ME, Xing JC, Semenza GL, Liberzon E, Wilson A, Simonson TS, Jorde LB, Kaelin WG, Jr., Koivunen P, Prchal JT. 2014. A genetic mechanism for Tibetan high-altitude adaptation. *Nature Genetics,* **46**(9): 951-956.

Lu DS, Lou HY, Yuan K, Wang XJ, Wang YC, Zhang C, Lu Y, Yang X, Deng L, Zhou Y, Feng QD, Hu Y, Ding QL, Yang YJ, Li SL, Jin L, Guan YQ, Su B, Kang LL, Xu SH. 2016. Ancestral origins and genetic history of tibetan highlanders. *The American Journal of Human Genetics,* **99**(3): 580-594.

Macinnis MJ, Koehle MS, Rupert JL. 2010. Evidence for a genetic basis for altitude illness: 2010 update. *High Altitude Medicine & Biology,* **11**(4): 349-368.

McLaughlin VV, McGoon MD. 2006. Pulmonary arterial hypertension. *Circulation,* **114**(13): 1417-1431.

Peng Y, Yang ZH, Zhang H, Cui CY, Qi XB, Luo XJ, Tao X, Wu TY, Ouzhuluobu, Basang, Ciwangsangbu, Danzengduojie, Chen H, Shi H, Su B. 2011. Genetic variations in tibetan populations and high-altitude adaptation at the himalayas. *Molecular Biology and Evolution,* **28**(2): 1075-1081.

Peng Y, Cui CY, He YX, Ouzhuluobu, Zhang H, Yang DY, Zhang Q, Bianbazhuoma, Yang LX, He YB, Xiang K, Zhang XM, Bhandari S, Shi P, Yangla, Dejiquzong, Baimakangzhuo, Duojizhuoma, Pan YY, Cirenyangji, Baimayangji, Gonggalanzi, Bai CJ, Bianba, Basang, Ciwangsangbu, Xu SH, Chen H, Liu SM, Wu TY, Qi XB, Su B. 2017. Down-regulation of *EPAS1* transcription and genetic adaptation of tibetans to high-altitude hypoxia. *Molecular Biology and Evolution,* **34**(4): 818-830.

Petousi N, Croft QPP, Cavalleri GL, Cheng HY, Formenti F, Ishida K, Lunn D, McCormack M, Shianna KV, Talbot NP, Ratcliffe PJ, Robbins PA. 2014.

Tibetans living at sea level have a hyporesponsive hypoxia-inducible factor system and blunted physiological responses to hypoxia. *Journal of Applied Physiology,* **116**(7): 893-904.

Pickert G, Lim HY, Weigert A, Häussler A, Myrczek T, Waldner M, Labocha S, Ferreirós N, Geisslinger G, Lötsch J, Becker C, Brüne B, Tegeder I. 2013. Inhibition of GTP cyclohydrolase attenuates tumor growth by reducing angiogenesis and M2-like polarization of tumor associated macrophages. *International Journal of Cancer,* **132**(3): 591-604.

Purcell S, Neale B, Todd-Brown K, Thomas L, Ferreira MAR, Bender D, Maller J, Sklar P, de Bakker PIW, Daly MJ, Sham PC. 2007. PLINK: a tool set for whole-genome association and population-based linkage analyses. *The American Journal of Human Genetics,* **81**(3): 559-575.

Qi XB, Cui CY, Peng Y, Zhang XM, Yang ZH, Zhong H, Zhang H, Xiang K, Cao XY, Wang Y, Ouzhuluobu, Basang, Ciwangsangbu, Bianba, Gonggalanzi, Wu TY, Chen H, Shi H, Su B. 2013. Genetic evidence of paleolithic colonization and neolithic expansion of modern humans on the tibetan plateau. *Molecular Biology and Evolution,* **30**(8): 1761-1778.

Sabeti PC, Reich DE, Higgins JM, Levine HZP, Richter DJ, Schaffner SF, Gabriel SB, Platko JV, Patterson NJ, McDonald GJ, Ackerman HC, Campbell SJ, Altshuler D, Cooper R, Kwiatkowski D, Ward R, Lander ES. 2002. Detecting recent positive selection in the human genome from haplotype structure. *Nature,* **419**(6909): 832-837.

Sabeti PC, Varilly P, Fry B, Lohmueller J, Hostetter E, Cotsapas C, Xie XH, Byrne EH, McCarroll SA, Gaudet R, Schaffner SF, Lander ES, The International HapMap Consortium. 2007. Genome-wide detection and characterization of positive selection in human populations. *Nature,* **449**(7164): 913-918.

Schermuly RT, Ghofrani HA, Wilkins MR, Grimminger F. 2011. Mechanisms of disease: pulmonary arterial hypertension. *Nature Reviews Cardiology,* **8**(8): 443-455.

Simonson TS, Yang YZ, Huff CD, Yun HX, Qin G, Witherspoon DJ, Bai ZZ, Lorenzo FR, Xing JC, Jorde LB, Prchal JT, Ge RL. 2010. Genetic evidence for high-altitude adaptation in Tibet. *Science,* **329**(5987): 72-75.

Szpiech ZA, Hernandez RD. 2014. Selscan: an efficient multithreaded program to perform EHH-based scans for positive selection. *Molecular Biology and Evolution,* **31**(10): 2824-2827.

Tajima F. 1989. Statistical method for testing the neutral mutation hypothesis by DNA polymorphism. *Genetics,* **123**(3): 585-595.

Voight BF, Kudaravalli S, Wen XQ, Pritchard JK. 2006. A map of recent positive selection in the human genome. *PLoS Biology,* **4**(3): e72.

Weir BS, Cockerham CC. 1984. Estimating F-statistics for the analysis of population structure. *Evolution,* **38**(6): 1358-1370.

Wilkins MR, Ghofrani HA, Weissmann N, Aldashev A, Zhao L. 2015. Pathophysiology and treatment of high-altitude pulmonary vascular disease. *Circulation,* **131**(6): 582-590.

Wu TY, Kayser B. 2006. High altitude adaptation in Tibetans. *High Altitude Medicine & Biology,* **7**(3): 193-208.

Xiang K, Ouzhuluobu, Peng Y, Yang ZH, Zhang XM, Cui CY, Zhang H, Li M, Zhang YF, Bianba, Gonggalanzi, Basang, Ciwangsangbu, Wu TY, Chen H, Shi H, Qi XB, Su B. 2013. Identification of a Tibetan-specific mutation in the hypoxic gene *EGLN1* and its contribution to high-altitude adaptation. *Molecular Biology and Evolution,* **30**(8): 1889-1898.

Xu SH, Li SL, Yang YJ, Tan JZ, Lou HY, Jin WF, Yang L, Pan XD, Wang JC, Shen YP, Wu BL, Wang HY, Jin L. 2011. A genome-wide search for signals of high-altitude adaptation in Tibetans. *Molecular Biology and Evolution,* **28**(2): 1003-1011.

Yi X, Liang Y, Huerta-Sanchez E, Jin X, Cuo ZXP, Pool JE, Xu X, Jiang H, Vinckenbosch N, Korneliussen TS, Zheng HC, Liu T, He WM, Li K, Luo RB, Nie XF, Wu HL, Zhao MR, Cao HZ, Zou J, Shan Y, Li SZ, Yang Q, Asan, Ni PX, Tian G, Xu JM, Liu X, Jiang T, Wu RH, Zhou GY, Tang MF, Qin JJ, Wang T, Feng SJ, Li GH, Huasang, Luosang JB, Wang W, Chen F, Wang YD, Zheng XG, Li Z, Bianba Z, Yang G, Wang XP, Tang SH, Gao GY, Chen Y, Luo Z, Gusang L, Cao Z, Zhang QH, Ouyang WH, Ren XL, Liang HQ, Zheng HS, Huang YB, Li JX, Bolund L, Kristiansen K, Li YR, Zhang Y, Zhang XQ, Li RQ, Li SG, Yang HM, Nielsen R, Wang J, Wang J. 2010. Sequencing of 50 human exomes reveals adaptation to high altitude. *Science,* **329**(5987): 75-78.

Zhang L, Chen WZ, Liu YJ, Hu X, Zhou K, Chen L, Peng S, Zhu H, Zou HL, Bai J, Wang ZB. 2010. Feasibility of magnetic resonance imaging-guided high intensity focused ultrasound therapy for ablating uterine fibroids in patients with bowel lies anterior to uterus. *European Journal of Radiology,* **73**(2): 396-403.

EP300 contributes to high-altitude adaptation in Tibetans by regulating nitric oxide production

Wang-Shan Zheng[1,2,#], Yao-Xi He[2,4,#], Chao-Ying Cui[3,#], Ouzhuluobu[3], Dejiquzong[3], Yi Peng[2], Cai-Juan Bai[3], Duojizhuoma[3], Gonggalanzi[3], Bianba[3], Baimakangzhuo[3], Yong-Yue Pan[3], Qula[3], Kangmin[3], Cirenyangji[3], Baimayangji[3], Wei Guo[3], Yangla[3], Hui Zhang[2], Xiao-Ming Zhang[2], Yong-Bo Guo[1,2], Shu-Hua Xu[5,8,9], Hua Chen[6], Sheng-Guo Zhao[1], Yuan Cai[1], Shi-Ming Liu[7], Tian-Yi Wu[7], Xue-Bin Qi[2,*], Bing Su[2,*]

[1] *College of Animal Science and Technology*, *Gansu Agricultural University*, *Lanzhou Gansu* 730070, *China*

[2] *State Key Laboratory of Genetic Resources and Evolution*, *Kunming Institute of Zoology*, *Chinese Academy of Sciences*, *Kunming Yunnan* 650223, *China*

[3] *High Altitude Medical Research Center*, *School of Medicine*, *Tibetan University*, *Lhasa Tibet* 850000, *China*

[4] *Kunming College of Life Science, University of Chinese Academy of Sciences*, *Kunming Yunnan* 650204, *China*

[5] *Chinese Academy of Sciences Key Laboratory of Computational Biology*, *Max Planck Independent Research Group on Population Genomics*, *CAS-MPG Partner Institute for Computational Biology*, *Shanghai Institutes for Biological Sciences*, *Chinese Academy of Sciences, Shanghai* 200031, *China*

[6] *Center for Computational Genomics*, *Beijing Institute of Genomics*, *Chinese Academy of Sciences*, *Beijing* 100101, *China*

[7] *National Key Laboratory of High Altitude Medicine*, *High Altitude Medical Research Institute*, *Xining Qinghai* 810012, *China*

[8] *School of Life Science and Technology*, *Shanghai Tech University*, *Shanghai* 200031, *China*

[9] *Collaborative Innovation Center of Genetics and Development*, *Shanghai* 200438, *China*

ABSTRACT

The genetic adaptation of Tibetans to high altitude hypoxia likely involves a group of genes in the hypoxic pathway, as suggested by earlier studies. To test the adaptive role of the previously reported candidate gene *EP300* (histone acetyltransferase p300), we conducted resequencing of a 108.9 kb gene region of *EP300* in 80 unrelated Tibetans. The allele-frequency and haplotype-based neutrality tests detected signals of positive Darwinian selection on *EP300* in Tibetans, with a group of variants showing allelic divergence between Tibetans and lowland reference populations, including Han Chinese, Europeans, and Africans. Functional prediction suggested the involvement of multiple *EP300* variants in gene expression regulation. More importantly, genetic association tests in 226 Tibetans indicated significant correlation of the adaptive *EP300* variants with blood nitric oxide (NO) concentration. Collectively, we propose that *EP300* harbors adaptive variants in Tibetans, which might contribute to high-altitude adaptation through regulating NO production.

Keywords: Tibetans; High altitude; Hypoxia; *EP300*; Genetic adaptation; Nitric oxide

INTRODUCTION

Tibetans are well adapted to high-altitude environments, in which the key environmental stress is hypobaric hypoxia. Physiologically, Tibetans show blunted responses to high altitude hypoxia, with low pulmonary vasoconstrictor response and low hemoglobin concentration compared with lowlanders moving to high altitude (Wu & Kayser, 2006). Previous genetic studies have reported a group of genes that show deep genetic divergence between Tibetans and Han Chinese. These genes are involved in the hypoxic pathway and therefore likely play important roles in the

Received: 24 March 2017; Accepted: 27 April 2017

Foundation items: This study was supported by grants from the Strategic Priority Research Program of the Chinese Academy of Sciences (XDB13010000), the National Natural Science Foundation of China (91631306 to BS, 31671329 to XQ, 31460287 to Ou, 31501013 to HZ, and 31360032 to CC), the National 973 program (2012CB518202 to TW), the State Key Laboratory of Genetic Resources and Evolution (GREKF15-05, GREKF16-04), and the Zhufeng Scholar Program of Tibetan University

[#]Authors contributed equally to this work

[*]Corresponding authors, E-mail: sub@mail.kiz.ac.cn; qixuebin@mail.kiz.ac.cn

DOI: 10.24272/j.issn.2095-8137.2017.036

genetic adaptation to high altitude hypoxia found in Tibetans (Beall et al., 2010; Bigham et al., 2010; Peng et al., 2011; Simonson et al., 2010; Wang et al., 2011; Xu et al., 2011; Yi et al., 2010).

Hypoxia inducible factor 2α *(HIF2α*, also called *EPAS1*) and its negative regulator *EGLN1* are considered key genes responsible for Tibetan adaptation (Lorenzo et al., 2014; Peng et al., 2017; Xiang et al., 2013). Compared with these two genes, other reported candidate genes show relatively less between-population divergence, implying that they are probably modifiers for high-altitude adaptation. One reported example is heme oxygenase-2 (*HMOX2*), with Tibetan-enriched adaptive mutations of *HMOX2* shown to cause more efficient breakdown of heme during hemoglobin metabolism (Yang et al., 2016). However, the functional roles of other modifier genes are unknown. In addition, although we have a fundamental understanding of the genetic basis for Tibetan adaptation to high altitude, the studied genes thus far only explain a small part of the adaptive traits in Tibetans, highlighting the need for further genetic studies.

In reported genome-wide comparisons between Tibetans and Han Chinese, histone acetyltransferase p300 (*EP300*) is among the candidate genes showing signals of selection (Peng et al., 2011). *EP300* is located on human chromosome 22 (22q13.2), spanning about 88.9 kb with 31 exons (Eckner et al., 1994). It functions as a histone acetyltransferase regulating the transcription of genes by chromatin remodeling, and plays an essential role in regulating cell growth and division and promoting cell maturation and differentiation (Goodman & Smolik, 2000; Ogryzko et al., 1996). *EP300* is also a hypoxia switch, regulating hypoxia inducible factor 1α (*HIF1α*) transactivation through specific recognition and hydroxylation of asparagine (Anokhina & Buravkova, 2010; Liao & Johnson, 2007; Peng et al., 2011; Teufel et al., 2007). More importantly, *EP300* plays a role in the stimulation of hypoxia-induced genes, such as vascular endothelial growth factor (*VEGF*) (Gray et al., 2005; Teufel et al., 2007; Zhang et al., 2013). Furthermore, disruption of *EP300* function can cause Rubinstein-Taybi syndrome, a condition characterized by short stature, moderate to severe intellectual disability, distinctive facial features, and broad thumbs and first toes, an indication of its functional importance (Negri et al., 2016; Solomon et al., 2015; Teufel et al., 2007).

To understand the potential role of *EP300* in Tibetan adaptation to high altitude hypoxia, we resequenced the entire genomic region of *EP300*. Neutrality tests suggested a signal of positive Darwinian selection on *EP300* in Tibetans. Genetic association analysis indicated the involvement of *EP300* in regulating nitric oxide production.

MATERIALS AND METHODS

Tibetan samples and *EP300* resequencing

We resequenced a 108.9 kb genomic fragment of 47 unrelated Tibetan individuals, with sample details reported in previous study (Peng et al., 2011). We also obtained sequence data of the same gene region of 33 Tibetans from previously published genome sequencing (Lu et al., 2016). In total, we had sequencing data from 80 unrelated Tibetans.

Selection tests of candidate variants

From the resequencing data (108.9 kb) of 80 Tibetans, we obtained 250 sequence variants. For quality control, we removed variants showing a significant deviation from the Hardy-Weinberg Equilibrium (HWE<0.000 1) and variants with an excessive missing genotype rate (MGR>0.05). A total of 185 variants remained after the filtering process. Following the methodology of Weir & Cockerham (1984), locus specific F_{ST} was calculated between Tibetans and the three lowland reference populations from the 1000 Genomes Project, which included 103 Han Chinese (CHB), 99 Europeans (CEU), and 108 Africans (YRI). Tajima's *D*-test was also performed to detect selection (Tajima, 1989).

For haplotype-based selection tests, the iHS score was calculated for each variant in Tibetans using selscan (Szpiech & Hernandez, 2014) based on the phased haplotypes, and only loci whose ancestral alleles were known with certainty were included (Voight et al., 2006). Additionally, XP-EHH analysis was used to detect the extended haplotypes resulting from positive selection (Sabeti et al., 2007). We computed XP-EHH scores using selscan (Szpiech & Hernandez, 2014) based on phased haplotypes of Tibetans and Han Chinese (reference population). The XP-EHH score of each variant was standardized by the mean XP-EHH and the standard deviation over the entire genome.

Functional prediction and expression quantitative trait loci (eQTL) analysis of *EP300* candidate SNPs

Functional enrichment analyses of the candidate variants were performed using the Combined Annotation Dependent Depletion (CADD) database (http://krishna.gs.washington.edu/download/CADD/v1.3/1000G_phase3_inclAnno.tsv.gz), which incorporates data from ENCODE and NIH Roadmap Epigenomics using ChromHMM (https://sites.google.com/site/anshulkundaje/projects/epigenome roadmap#TOC-Core-Integrative-chromatin-state-maps-127-Epigenomes-) (Ernst & Kellis, 2012).

We measured the evolutionary constraints of each variant using Genome Evolutionary Rate Profiling (GERP) (http://mendel.stanford.edu/SidowLab/downloads/gerp/). The GERP++ method was used to calculate site-specific RS scores and discover evolutionarily constrained elements (Davydov et al., 2010). Positive scores suggest evolutionary constraint, with higher scores indicating higher levels of evolutionary constraint.

The H3K4Me1 value indicates the maximum ENCODE H3K4 methylation level (maximum value observed across 16 ENCODE cell lines at a given position), where modification of histone proteins is suggestive of an enhancer and, to a lesser extent, other regulatory activities. The H3K4Me3 value indicates the maximum ENCODE H3K4 trimethylation level (maximum value observed across 16 ENCODE cell lines at a given position), where modification of histone proteins is suggestive of a promoter. The DNase-I hypersensitivity sites indicate chromatin regions hypersensitive to cutting by the DNase enzyme. In general, gene regulatory regions tend to be DNase-sensitive, and promoters are particularly DNase-sensitive. DNase-P indicates the *P*-value (PHRED-scale) of DNase

evidence for open chromatin. The transcription factor binding site (TFBS) is indicated by the number of different overlapping ChIP transcription factor binding sites. It also defines the boundaries between active and heterochromatic DNA. Transcriptional repressor CTCF is a versatile transcription regulator involved in regulating the 3D structure of chromatin. In addition, splice site analysis indicates whether the tested variants are located in the ACCEPTOR or DONOR sequences.

The eQTL analysis for candidate *EP300* single nucleotide polymorphisms (SNPs) was conducted using publicly available datasets (Blood eQTL Browser: http://genenetwork.nl/bloodeqtlbrowser/).

Measurements of physiological traits

Physiological data and blood samples were collected from 226 unrelated Tibetans permanently residing in Bange County (*n*=127, 37.41±3.8 years old) at an elevation of 4 700 m and Lhasa city (*n*=99, 35.33±6.8 years old) at an elevation of 3 600 m. Written informed consent was obtained from all participants. For physiological parameters, we determined the hemoglobin (Hb) concentration, arterial oxygen saturation (SaO_2) level, and blood nitric oxide (NO) concentration, which are key adaptive physiological traits in Tibetans (Wu & Kayser, 2006).

The Hb concentration was measured using a HemoCue Hb 201+ analyzer (Angelholm, Sweden) and SaO_2 was measured from the forefinger tip with a hand-held pulse oximeter (Nellcor NPB-40, CA, USA) at rest. Venous blood was collected for Hb measurement and DNA extraction. To reveal the NO level in serum, predominant species NO^{2-} and NO^{3-} were measured using a nitric oxide analyzer (Sievers Model-280, GE Analytical Instruments, Boulder, CO, USA).

Genotyping and association analysis

We genotyped six candidate variants and conducted association analysis in 226 Tibetans. The variants were rs58268766, rs2076578, rs2076580, rs5758251, rs5758256, and rs2143694. Genotyping was conducted by the SNaPshot method on an ABI 3130 sequencer (Applied Bio-systems, Forster City, CA, USA). Genetic association analysis was conducted using PLINK 1.07 (Purcell et al., 2007). An additive genetic model was used because all tested variants were located in the non-coding region of *EP300* and likely influenced gene expression. For multiple test correction, we performed 100 000 permutations.

RESULTS

Resequencing of *EP300* in Tibetans and neutrality tests

We resequenced a 108.9 kb *EP300* genomic region, covering the 88.9 kb gene region as well as two 10 kb flanking regions upstream and downstream of *EP300*. In total, we obtained *EP300* sequencing data of 80 unrelated Tibetans.

We identified a total of 185 *EP300* sequence variants among the 80 unrelated Tibetans. After comparing with three lowlander populations, including Han Chinese, Europeans, and Africans, there were 149 shared variants. The remaining 36 variants were all rare mutations in Tibetans (<1.0%). To detect selection signals of these variants, we performed neutrality tests, including both allele-frequency-based (F_{ST} and Tajima's *D*) and haplotype-based tests (iHS and XP-EHH). Consistent with previous research (Peng et al., 2011), we observed many variants showing above-genome-average divergence (F_{ST}>0.03) between Tibetans and Han Chinese. The highest F_{ST} was 0.14 for rs2076580. The derived allele at rs2076580 was predominant in Tibetans (76%), much higher than the frequencies in the lowland reference populations (48% in Han Chinese, 34% in Europeans, and only 3% in Africans). Consistently, in the haplotype-based XP-EHH test, we found 34 *EP300* variants showing high scores (XP-EHH>0.2) (Supplementary Table S1). These high-XP-EHH variants were likely under positive Darwinian selection, and were located in a LD block spanning about 6 kb from intron-6 to the 3' flanking region (Figure 1). The allele-frequency-based Tajima's *D*-test was not significant, likely due to its insensitivity to recent selection. Overall, compared with the reported strong selection on *EPAS1* and *EGLN1* (Peng et al., 2011; Xiang et al., 2013; Xu et al., 2011), the selection on *EP300* in Tibetans was relatively weak, consistent with a modifier role in genetic adaptation to high altitude.

Functional prediction and eQTL analysis of candidate *EP300* variants

With the detected signal of selection on *EP300* in Tibetans, the next question was what were the functional consequences of the variants under selection? We chose 34 candidate variants that showed high XP-EHH scores (>2.0), and except for two synonymous variants, most were non-coding. We performed functional prediction based on sequence conservation (GERP), transcription factor binding sites (TFBS), splicing motif, H3K4Me1/H3K4Me3 sites, and DNAase-I hypersensitive sites. There were 14 variants showing conserved sequences across species (GREP++ >5.0), an implication of functional constraint. In addition, multiple variants were located in the H3K4Me1/H3K4Me3 sites, suggesting their potential involvement in enhancer or promoter activities (Supplementary Table S1).

We also performed eQTL analysis using published data (Blood eQTL Browser: http://genenetwork.nl/bloodeqtlbrowser/), and found that three candidate variants showed highly significant association with the expression of *EP300* in blood ($P=1.64\times10^{-54}$ for rs2076578, $P=3.63\times10^{-54}$ for rs575825, and $P=3.26\times10^{-54}$ for rs2143694), suggesting that these variants are probably involved in the expression regulation of *EP300*. However, further experiments are needed to test their suggestive functions.

Genetic association analysis of candidate *EP300* variants with multiple physiological traits in Tibetans

To test whether the candidate *EP300* variants contributed to the adaptive traits in Tibetans, we collected data on three physiological parameters, including Hb, SaO_2, and NO. A total of 226 unrelated adult Tibetans were included (91 males and 135 females from Lhasa and Bange, Tibetan Autonomous Region of China). Six candidate variants were selected based on their F_{ST} values and XP-EHH scores (F_{ST}>0.1 and XP-EHH>2.0). As shown in Table 1, five of the six variants showed significant association with blood NO level when an additive genetic model was assumed (P<0.05, after multiple test corrections with permutations). The same result was observed when males and females were analyzed separately (Table 1),

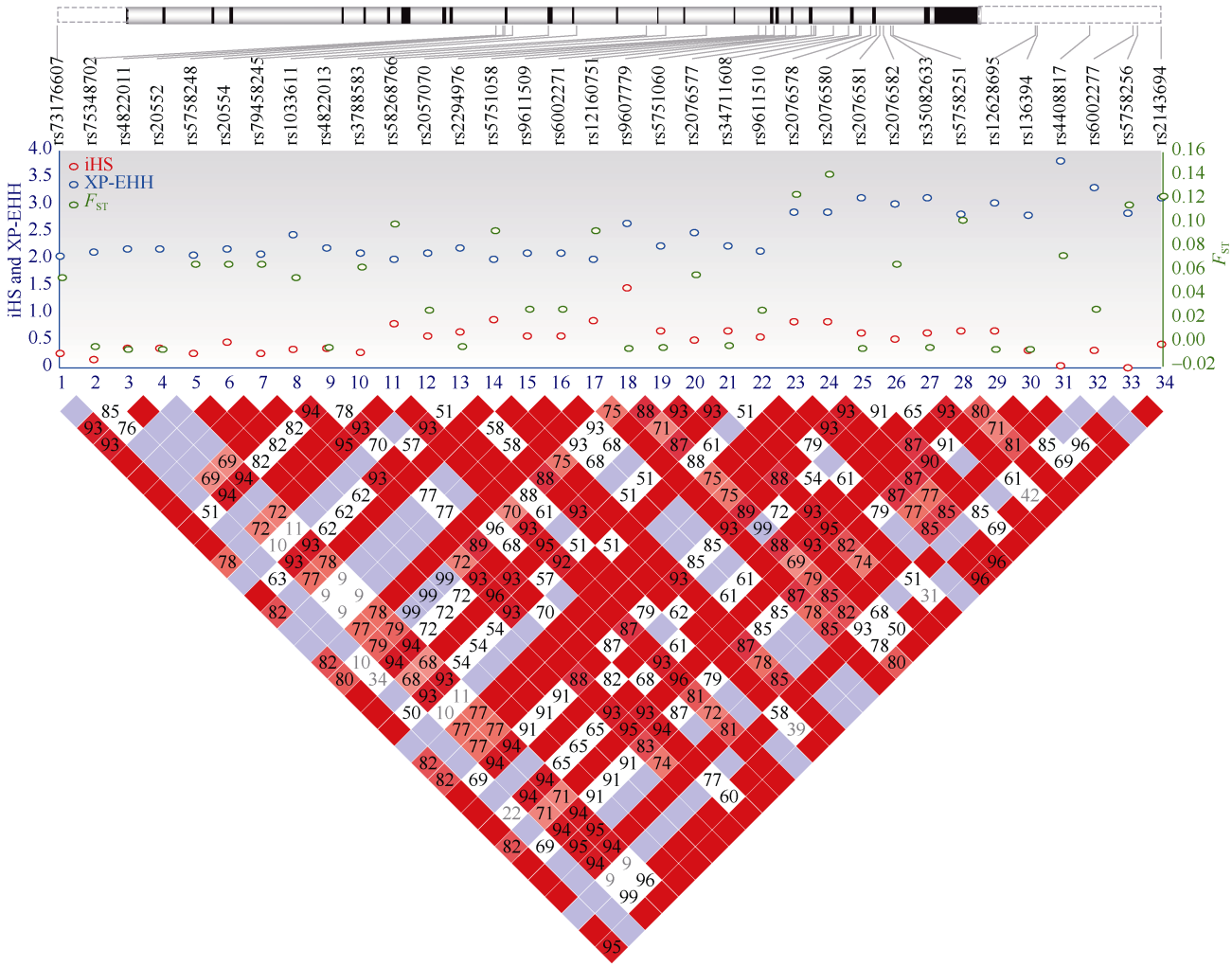

Figure 1 Information on 34 *EP300* candidate variants

Top panel indicates gene structure. Middle panel shows the selection test results (F_{ST}, iHS, and XP-EHH). Bottom panel displays the linkage disequilibrium (LD) map of 34 variants.

with no gender difference detected for average blood NO level. The presumably adaptive alleles were correlated with a decreased NO level and explained about 3% of NO variance. For example, the three genotypes at rs2076580 had NO levels of 61.53 μmol/L (GG genotype), 54.96 μmol/L (GA genotype), and 43.43 μmol/L (AA genotype), respectively, and each adaptive allele caused, on average, 15.8% decrease in NO in the blood (Figure 2). Hence, the *EP300* variants are likely involved in the regulation of blood NO production. In contrast, no association was detected for Hb or SaO_2.

DISCUSSION

EP300 is a candidate gene showing relatively deep allelic divergence between Tibetans and lowlanders (Peng et al., 2011). As previous data were obtained from DNA arrays with limited *EP300* variant coverage, whether *EP300* plays a role in Tibetan adaptation to high altitude has remained inconclusive. In this study, we resequenced the entire *EP300* gene region. In combination with published data, we showed that *EP300* in Tibetans has undergone positive Darwinian selection. *EP300* acts as a transcriptional coactivator of *HIF1α*, one of the most important hypoxic genes (Freedman et al., 2002; Gray et al., 2005; Lando et al., 2002). Functional prediction analysis suggested multiple *EP300* SNPs with potential functional effects. Hence, the function of selection on *EP300* is probably related to its role in the hypoxic pathway.

Importantly, we observed a significant association of many high XP-EHH variants with NO concentration. It has been proposed previously that high NO levels are an adaptive feature of Tibetans for high altitude living. Prior studies have shown that the NO levels of 88 Tibetans living at 4 300 m elevation were 10 times higher than those of 50 European-Americans living at 203 m

Table 1 Association of six *EP300* variants with three physiological traits in Tibetans

Trait	SNP ID	Male (*n*=91)		Female (*n*=135)		All (*n*=226)		
		Beta	EMP'	Beta	EMP'	Beta	EMP''	R^2 (%)
Hb	rs58268766	–1.83	0.63	3.16	0.25	0.63	0.86	7.24E-03
	rs2076578	–0.74	0.78	3.97	0.16	1.52	0.69	0.03
	rs2076580	–0.74	0.78	3.78	0.16	1.41	0.69	0.01
	rs5758251	–0.74	0.78	4.26	0.14	1.65	0.63	0.03
	rs5758256	8.59	0.24	–6.73	0.24	–1.11	1.00	3.26E-04
	rs2143694	–0.74	0.78	3.78	0.16	1.41	0.69	0.01
NO	rs58268766	–9.80	0.09	–9.06	0.06	–9.14	1.23E-02	2.98
	rs2076578	–10.00	0.08	–9.68	4.81E-02	–9.58	1.20E-02	3.13
	rs2076580	–10.00	0.08	–9.89	4.19E-02	–9.68	1.23E-02	3.21
	rs5758251	–10.00	0.08	–9.93	4.03E-02	–9.68	7.62E-03	3.20
	rs5758256	13.04	0.31	8.84	0.31	10.47	0.12	0.88
	rs2143694	–10.00	0.08	–9.89	4.19E-02	–9.68	1.23E-02	3.21
$Sa0_2$	rs58268766	1.12	0.31	0.35	0.86	0.65	0.33	0.93
	rs2076578	0.94	0.38	0.21	1.00	0.51	0.40	0.67
	rs2076580	0.94	0.38	0.27	0.86	0.54	0.38	0.70
	rs5758251	0.94	0.38	0.30	0.86	0.56	0.38	0.72
	rs5758256	1.26	0.28	1.39	0.33	1.75	0.14	1.37
	rs2143694	0.94	0.38	0.27	0.86	0.54	0.38	0.70

Hb, hemoglobin concentration; NO, blood nitric oxide concentration; SaO_2, blood oxygen saturation level. EMP', *P* value after multiple test corrections; EMP'', *P* value after multiple test corrections with sex as the covariant.

elevation (Beall, 2007; Levett et al., 2011). High NO levels would allow for better vasodilation and therefore better blood flow (Beall, 2007), which is an adaptive physiological trait observed in Tibetans. Enzymes eNOS and iNOS synthesize NO products in the body. They are encoded by *NOS3* and *NOS2*, respectively, and both contain hypoxia-response-element (HRE) motifs in the gene promoter regions (Coulet et al., 2003; Melillo et al., 1995). In other words, *NOS3* and *NOS2* can be directly regulated by *HIF1*α and *HIF2*α. Therefore, the observed association of *EP300* with blood NO level can be explained by the co-transactivating role of *EP300* in expression regulation of *HIF1*α and eventually its downstream genes, including *NOS3* and *NOS2*. Notably, eNOS mainly functions in blood vessels (Matouk & Marsden, 2008). As *EP300* works in histone modification (Goodman & Smolik, 2000; Ogryzko et al., 1996), whether the functional role of *EP300* in high-altitude adaptation involves downstream gene regulation through chromatin remodeling is yet to be tested.

Under hypoxic conditions, in addition to the pathway of stabilizing HIF with reduced PHD2 hydroxylation, the nitroso sulfation of the HIF element is also important (Foster et al., 2003), and NO is the key component of nitroso sulfation. It has been reported that hypoxia upregulates iNOS, and thereby increases NO products in tissues and cells, especially in the case of chronic hypoxia. NO helps create a blunted response to hypoxia by inhibiting the oxygen consumption of mitochondria and consequently provide more oxygen for PHDs to reduce the levels of HIF proteins caused by hypoxia (Won et al., 2007). Collectively, NO is not only involved in the process of blood flow control, but is also a regulator of blood oxygen utilization (Ho et al., 2012). As shown in our results, the adaptive alleles were associated with a decreased level of blood NO, which might serve as a protection measure for Tibetans from overproduction of NO, and might be similar to the relatively low hemoglobin concentrations observed in Tibetans (Beall et al., 2010).

In summary, we proved that *EP300* has been under positive Darwinian selection, with a significant association with blood NO levels in Tibetans. These data suggest that *EP300* likely contributes to Tibetan adaptation to high-altitude. However, further studies are needed to reveal the underlying molecular mechanism.

ACKNOWLEDGEMENTS

We are grateful to all the volunteers participated in this study.

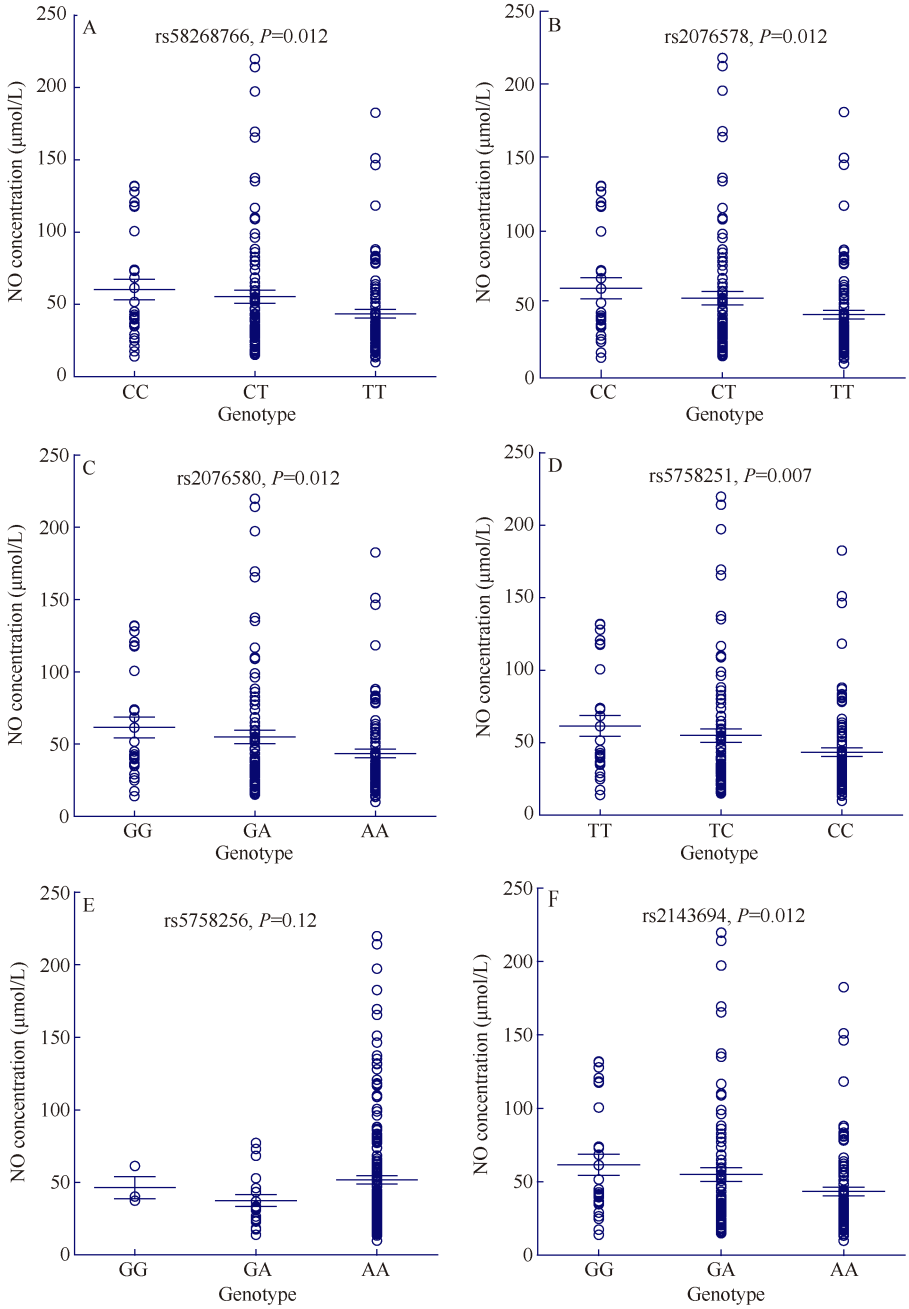

Figure 2 NO levels of different genotypes of six *EP300* variants in 226 Tibetans

Except for rs5758256, the variants showed almost the same pattern due to their tight linkage (r^2>0.94). An additive genetic model was used for statistical assessment.

REFERENCES

Anokhina EB, Buravkova LB. 2010. Mechanisms of regulation of transcription factor HIF under hypoxia. *Biochemistry (Moscow),* **75**(2): 151-158.

Beall CM. 2007. Two routes to functional adaptation: tibetan and Andean high-altitude natives. *Proceedings of the National Academy of Sciences of the United States of America,* **104**(S1): 8655-8660.

Beall CM, Cavalleri GL, Deng LB, Elston RC, Gao Y, Knight J, Li CH, Li JC, Liang Y, McCormack M, Montgomery HE, Pan H, Robbins PA, Shianna KV, Tam SC, Tsering N, Veeramah KR, Wang W, Wangdui P, Weale ME, Xu YM, Xu Z, Yang L, Zaman MJ, Zeng CQ, Zhang L, Zhang XL, Zhaxi PC, Zheng YT. 2010. Natural selection on *EPAS1* (*HIF2α)* associated with low hemoglobin concentration in Tibetan highlanders. *Proceedings of the National Academy of Sciences of the United States of America,* **107**(25):

11459-11464.

Bigham A, Bauchet M, Pinto D, Mao XY, Akey JM, Mei R, Scherer SW, Julian CG, Wilson MJ, Herráez DL, Brutsaert T, Parra EJ, Moore LG, Shriver MD. 2010. Identifying signatures of natural selection in Tibetan and Andean populations using dense genome scan data. *PLoS Genetics,* **6**(9): e1001116.

Coulet F, Nadaud S, Agrapart M, Soubrier F. 2003. Identification of hypoxia-response element in the human endothelial nitric-oxide synthase gene promoter. *Journal of Biological Chemistry,* **278**(47): 46230-46240.

Davydov EV, Goode DL, Sirota M, Cooper GM, Sidow A, Batzoglou S. 2010. Identifying a high fraction of the human genome to be under selective constraint using GERP++. *PLoS Computational Biology,* **6**(12): e1001025.

Eckner R, Ewen ME, Newsome D, Gerdes M, Decaprio JA, Lawrence JB, Livingston DM. 1994. Molecular cloning and functional analysis of the adenovirus E1A-associated 300-kD protein (p300) reveals a protein with properties of a transcriptional adaptor. *Genes & Development,* **8**(8): 869-884.

Ernst J, Kellis M. 2012. ChromHMM: automating chromatin-state discovery and characterization. *Nature Methods,* **9**(3): 215-216.

Foster MW, Mcmahon TJ, Stamler JS. 2003. S-nitrosylation in health and disease. *Trends in Molecular Medicine,* **9**(4): 160-168.

Freedman SJ, Sun ZYJ, Poy F, Kung AL, Livingston DM, Wagner G, Eck MJ. 2002. Structural basis for recruitment of CBP/p300 by hypoxia-inducible factor-1α. *Proceedings of the National Academy of Sciences of the United States of America,* **99**(8): 5367-5372.

Goodman RH, Smolik S. 2000. CBP/p300 in cell growth, transformation, and development. *Genes & Development,* **14**(13): 1553-1577.

Gray MJ, Zhang J, Ellis LM, Semenza GL, Evans DB, Watowich SS, Gallick GE. 2005. HIF-1*α,* STAT3, CBP/p300 and Ref-1/APE are components of a transcriptional complex that regulates Src-dependent hypoxia-induced expression of VEGF in pancreatic and prostate carcinomas. *Oncogene,* **24**(19): 3110-3120.

Ho JJ, Man HSJ, Marsden PA. 2012. Nitric oxide signaling in hypoxia. *Journal of Molecular Medicine,* **90**(3): 217-231.

Lando D, Peet DJ, Whelan DA, Gorman JJ, Whitelaw ML. 2002. Asparagine hydroxylation of the HIF transactivation domain: a hypoxic switch. *Science,* **295**(5556): 858-861.

Levett DZ, Fernandez BO, Riley HL, Martin DS, Mitchell K, Leckstrom CA, Ince C, Whipp BJ, Mythen MG, Montgomery HE, Grocott MP, Feelisch M, Caudwell Extreme Everest Research Group. 2011. The role of nitrogen oxides in human adaptation to hypoxia. *Scientific Reports,* **1**: 109.

Liao D, Johnson RS. 2007. Hypoxia: a key regulator of angiogenesis in cancer. *Cancer and Metastasis Reviews,* **26**(2): 281-290.

Lorenzo FR, Huff C, Myllymäki M, Olenchock B, Swierczek S, Tashi T, Gordeuk V, Wuren T, Ri-Li G, McClain DA, Khan TM, Koul PA, Guchhait P, Salama ME, Xing JC, Semenza GL, Liberzon E, Wilson A, Simonson TS, Jorde LB, Kaelin WG, Jr., Koivunen P, Prchal JT. 2014. A genetic mechanism for Tibetan high-altitude adaptation. *Nature Genetics,* **46**(9): 951-956.

Lu DS, Lou HY, Yuan K, Wang XJ, Wang YC, Zhang C, Lu Y, Yang X, Deng L, Zhou Y, Feng QD, Hu Y, Ding QL, Yang YJ, Li SL, Jin L, Guan YQ, Su B, Kang LL, Xu SH. 2016. Ancestral origins and genetic history of tibetan highlanders. *The American Journal of Human Genetics,* **99**(3): 580-594.

Matouk CC, Marsden PA. 2008. Epigenetic regulation of vascular endothelial gene expression. *Circulation Research,* **102**(8): 873-887.

Melillo G, Musso T, Sica A, Taylor LS, Cox GW, Varesio L. 1995. A hypoxia-responsive element mediates a novel pathway of activation of the inducible nitric oxide synthase promoter. *Journal of Experimental Medicine,* **182**(6): 1683-1693.

Negri G, Magini P, Milani D, Colapietro P, Rusconi D, Scarano E, Bonati MT, Priolo M, Crippa M, Mazzanti L, Wischmeijer A, Tamburrino F, Pippucci T, Finelli P, Larizza L, Gervasini C. 2016. From whole gene deletion to point mutations of *EP300*-positive Rubinstein-Taybi patients: new insights into the mutational spectrum and peculiar clinical hallmarks. *Human Mutation,* **37**(2): 175-183.

Ogryzko VV, Schiltz RL, Russanova V, Howard BH, Nakatani Y. 1996. The transcriptional coactivators p300 and CBP are histone acetyltransferases. *Cell,* **87**(5): 953-959.

Peng Y, Cui CY, He YX, Ouzhuluobu, Zhang H, Yang DY, Zhang Q, Bianbazhuoma, Yang LX, He YB, Xiang K, Zhang XM, Bhandari S, Shi P, Yangla, Dejiquzong, Baimakangzhuo, Duojizhuoma, Pan YY, Cirenyangji, Baimayangji, Gonggalanzi, Bai CJ, Bianba, Basang, Ciwangsangbu, Xu SH, Chen H, Liu SM, Wu TY, Qi XB, Su B. 2017. Down-regulation of EPAS1 transcription and genetic adaptation of tibetans to high-altitude hypoxia. Molecular biology and evolution. *Molecular Biology and Evolution,* **34**(4): 818-830.

Peng Y, Yang Z, Zhang H, Cui C, Qi X, Luo X, Tao X, Wu T, Ouzhuluobu, Basang, Ciwangsangbu, Danzengduojie, Chen H, Shi H, Su B. 2011. Genetic variations in Tibetan populations and high-altitude adaptation at the Himalayas. *Molecular Biology and Evolution,* **28**(2): 1075-1081.

Purcell S, Neale B, Todd-Brown K, Thomas L, Ferreira MAR, Bender D, Maller J, Sklar P, de Bakker PI, Daly MJ, Sham PC. 2007. PLINK: a tool set for whole-genome association and population-based linkage analyses. *American Journal of Human Genetics,* **81**(3): 559-575.

Sabeti PC, Varilly P, Fry B, Lohmueller J, Hostetter E, Cotsapas C, Xie XH, Byrne EH, McCarroll SA, Gaudet R, Schaffner SF, Lander ES, The International HapMap Consortium. 2007. Genome-wide detection and characterization of positive selection in human populations. *Nature,* **449**(7164): 913-918.

Simonson TS, Yang YZ, Huff CD, Yun HX, Qin G, Witherspoon DJ, Bai ZZ, Lorenzo FR, Xing JC, Jorde LB, Prchal JT, Ge RL. 2010. Genetic evidence for high-altitude adaptation in Tibet. *Science,* **329**(5987): 72-75.

Solomon BD, Bodian DL, Khromykh A, Mora GG, Lanpher BC, Iyer RK, Baveja R, Vockley JG, Niederhuber JE. 2015. Expanding the phenotypic spectrum in EP300-related Rubinstein-Taybi syndrome. *American Journal of Medical Genetics. Part A,* **167**(5): 1111-1116.

Szpiech ZA, Hernandez RD. 2014. Selscan: an efficient multithreaded program to perform EHH-based scans for positive selection. *Molecular Biology and Evolution,* **31**(10): 2824-2827.

Tajima F. 1989. Statistical method for testing the neutral mutation hypothesis by DNA polymorphism. *Genetics,* **123**(3): 585-595.

Teufel DP, Freund SM, Bycroft M, Fersht AR. 2007. Four domains of p300 each bind tightly to a sequence spanning both transactivation subdomains of p53. *Proceedings of the National Academy of Sciences of the United States of America,* **104**(17): 7009-7014.

Voight BF, Kudaravalli S, Wen XQ, Pritchard JK. 2006. A map of recent positive selection in the human genome. *PLoS Biology,* **4**(3): e72.

Wang BB, Zhang YB, Zhang F, Lin HB, Wang XM, Wan N, Ye ZQ, Weng HY,

Zhang LL, Li X, Yan JW, Wang PP, Wu TT, Cheng LF, Wang J, Wang DM, Ma X, Yu J. 2011. On the origin of Tibetans and their genetic basis in adapting high-altitude environments. *PLoS One,* **6**(2): e17002.

Weir BS, Cockerham CC. 1984. Estimating F-statistics for the analysis of population structure. *Evolution,* **38**(6): 1358-1370.

Won D, Zhu SN, Chen M, Teichert AM, Fish JE, Matouk CC, Bonert M, Ojha M, Marsden PA, Cybulsky MI. 2007. Relative reduction of endothelial nitric-oxide synthase expression and transcription in atherosclerosis-prone regions of the mouse aorta and in an *in vitro* model of disturbed flow. *The American Journal of Pathology,* **171**(5): 1691-1704.

Wu TY, Kayser B. 2006. High altitude adaptation in Tibetans. *High Altitude Medicine & Biology,* **7**(3): 193-208.

Xiang K, Ouzhuluobu, Peng Y, Yang ZH, Zhang XM, Cui CY, Zhang H, Li M, Zhang YF, Bianba, Gonggalanzi, Basang, Ciwangsangbu, Wu TY, Chen H, Shi H, Qi XB, Su B. 2013. Identification of a Tibetan-specific mutation in the hypoxic gene EGLN1 and its contribution to high-altitude adaptation. *Molecular Biology and Evolution,* **30**(8): 1889-1898.

Xu SH, Li SL, Yang YJ, Tan JZ, Lou HY, Jin WF, Yang L, Pan XD, Wang JC, Shen YP, Wu BL, Wang HY, Jin L. 2011. A genome-wide search for signals of high-altitude adaptation in Tibetans. *Molecular Biology and Evolution,* **28**(2): 1003-1011.

Yang DY, Peng Y, Ouzhuluobu, Bianbazhuoma, Cui CY, Bianba, Wang LB, Xiang K, He YX, Zhang H, Zhang XM, Liu JW, Shi H, Pan YY, Duojizhuoma, Dejiquzong, Cirenyangji, Baimakangzhuo, Gonggalanzi, Liu SM, Gengdeng, Wu TY, Chen H, Qi XB, Su B. 2016. *HMOX2* functions as a modifier gene for high-altitude adaptation in Tibetans. *Human Mutation,* **37**(2): 216-223.

Yi X, Liang Y, Huerta-Sanchez E, Jin X, Cuo ZXP, Pool JE, Xu X, Jiang H, Vinckenbosch N, Korneliussen TS, Zheng HC, Liu T, He WM, Li K, Luo RB, Nie XF, Wu HL, Zhao MR, Cao HZ, Zou J, Shan Y, Li SZ, Yang Q, Asan, Ni PX, Tian G, Xu JM, Liu X, Jiang T, Wu RH, Zhou GY, Tang MF, Qin JJ, Wang T, Feng SJ, Li GH, Huasang, Luosang JB, Wang W, Chen F, Wang YD, Zheng XG, Li Z, Bianba Z, Yang G, Wang XP, Tang SH, Gao GY, Chen Y, Luo Z, Gusang L, Cao Z, Zhang QH, Ouyang WH, Ren XL, Liang HQ, Zheng HS, Huang YB, Li JX, Bolund L, Kristiansen K, Li YR, Zhang Y, Zhang XQ, Li RQ, Li SG, Yang HM, Nielsen R, Wang J, Wang J. 2010. Sequencing of 50 human exomes reveals adaptation to high altitude. *Science,* **329**(5987): 75-78.

Zhang B, Day DS, Ho JW, Song LY, Cao JJ, Christodoulou D, Seidman JG, Crawford GE, Park PJ, Pu WT. 2013. A dynamic H3K27ac signature identifies VEGFA-stimulated endothelial enhancers and requires EP300 activity. *Genome Research,* **23**(6): 917-927.

Zoological Research Editorial Board

ZOOLOGICAL RESEARCH
动物学研究
Bimonthly, Since 1980

Project for Enhancing International Impact of China STM Journals

中国精品科技期刊 中国科技核心期刊 中国百强报刊

Editor-in-Chief: Yong-Gang Yao

Executive Editor-in-Chief: Wai-Yee Chan

Editors: Su-Qing Liu Long Nie

Edited by Editorial Office of Zoological Research

(Kunming Institute of Zoology, Chinese Academy of Sciences, 32 Jiaochang Donglu, Kunming, Yunnan, Post Code: 650223 Tel: +86 871 65199026 E-mail: zoores@mail.kiz.ac.cn)

Sponsored by Kunming Institute of Zoology, Chinese Academy of Sciences; China Zoological Society©

Supervised by Chinese Academy of Sciences

Published by Science Press (16 Donghuangchenggen Beijie, Beijing 100717, China)

Printed by Kunming Xiaosong Plate Making & Printing Co, Ltd

Domestic distribution by Yunnan Post and all local post offices in China

International distribution by China International Book Trading Corporation (Guoji Shudian) P.O.BOX 399, Beijing 100044, China

Advertising Business License 广告经营许可证：滇工商广字66号

Domestic Postal Issue No.: 64-20

Price: 10.00 USD/60.00 CNY Post No.: BM358

ISSN 2095-8137